2023

Investigation of Thermal Performance Enhancement and Thermo-mechanical Assessment of ITE using Single-Phase Immersion Cooling Technology

Pratik Bansode

Investigation of Thermal Performance Enhancement and Thermo-mechanical Assessment of ITE using Single-Phase Immersion Cooling Technology

Dissertation

by

PRATIK VITHOBA BANSODE

Submitted in Partial Fulfillment of the Requirements

for the Degree of Doctor of Philosophy at

The University of Texas at Arlington

AUGUST 2023

Supervising Committee:

Dr. Dereje Agonafer

Dr. Abdolhossein Haji-Sheikh

Dr. Miguel A. Amaya

Dr. Amir Ameri

Dr. Satyam Saini

Acknowledgments

Above all, I extend my heartfelt gratitude to my parents for granting me the opportunity to fulfill my educational aspirations in the United States. Their unwavering support and the numerous sacrifices they have made on my behalf have been instrumental in my journey. Throughout the various trials and successes of my life, I have been fortunate to receive constant moral and emotional support from my parents, my brother, my girlfriend Emily Laughlin, and her parents. Their encouragement has been a source of strength and inspiration. I am immensely thankful to Dr. Agonafer, who has been an invaluable academic advisor, providing me with essential guidance, mentoring, and insightful advice throughout both my Master's and Doctoral studies. His support has been crucial to my academic growth and achievements. I express my gratitude to Dr. Haji Sheikh, Dr. Miguel Amaya, Dr. Amir Ameri, and Dr. Satyam Saini for their contributions as members of my thesis committee, offering useful insights to enhance the quality of my study.

The active participation of my peers and colleagues has been crucial in shaping my experience inside the EMNSPC research group. I consider myself incredibly fortunate to have had the esteemed guidance and collaboration of Dr. Pardeep Shahi, Dr. Satyam Saini, Gautam Gupta, Rabin Bhandari, Vibin Simon, Himanshu Modi and Dr. Vivek Nair during my PhD study. Their invaluable contributions as research collaborators have played a pivotal role in shaping and advancing my research. Furthermore, I have had the opportunity to collaborate with other people who have similar interests and possess exceptional intellect as part of the EMNSPC team. I extend my sincere appreciation to Dr. Jimil Shah, who served as my mentor throughout my pursuit of a master's degree and has continued to provide significant guidance even subsequent to his graduation from UTA.

Abstract

The use of air-cooling as a thermal management technique in data centers has consistently maintained its importance, however its efficacy is limited to CPUs with lower power requirements. The expenses and energy use related to the air circulation process for high-power density racks are deemed excessively costly. The limits of air cooling have aroused concerns owing to its low specific heat capacity and poor thermal conductivity, which result in reduced effectiveness. Consequently, a substantial discourse has emerged about alternate and effective cooling methods that provide supplementary advantages, such as the recuperation of waste heat. In light of the limitations associated with conventional air-cooling approaches, several operators of data centers are embracing inventive methodologies to alleviate the consequences caused by escalating power densities. A solution gaining traction for high-power IT equipment is immersion cooling. A comparison between forced convection air cooling and single-phase liquid immersion cooling (Sp-LIC) highlights substantial advantages in the latter. The direct contact of dielectric fluids with components enables higher heat dissipation. This technique enhances IT equipment reliability by safeguarding against pollutants and harsh conditions. Furthermore, Sp-LIC reduces capital expenditure (CapEx) and energy costs by eliminating the necessity for fans and computer room air handler units.

The objective of this investigation is divided into two parts: thermal efficiency of immersed information technology equipment (ITE) and operational efficiency (overall life cycle of fluid, reliability of components, and serviceability). The thermal part of the study is further divided into 3 sections: In first section, an in-depth numerical study is performed which explores multi-parametric optimization for heat sinks in forced convection within an open compute server design when immersed in single phase immersion fluid. Optimization at constant pumping power iterates pressure drop and thermal resistance minimization as objective functions. Varying fin count and fin thickness for a constant base thickness in

aluminum heat sinks reveals the correlation between geometric parameters and objective functions. These results contribute to standard methodologies for optimizing heat sinks in immersion cooling. In the second section of the thermal study, a systematic empirical study is undertaken to examine the heat transfer and pressure loss characteristics of aluminum metal foams while immersed in a dielectric synthetic fluid. The research used metal foam specimens with core heights of 0.0127m (0.5 in), varying relative densities between 10.7 and 12.3 percent, and pores per inch (PPI) values of 5, 10, 20, and 40. The metal foams underwent exposure to several flow rates, heat fluxes and inlet fluid temperature. In the final section of the thermal study, the experimental methodology for obtaining the velocity fields using Particle Image Velocimetry (PIV) in a single-phase immersion tank is discussed. PIV is a non-intrusive optical measurement technique used to visualize and measure fluid flow velocity patterns. The velocity field data obtained from these experiments provides valuable insights into the fluid flow behavior and aids in understanding the thermal performance of the immersion cooling system.

The second part of the research aims to investigate the impact of immersion cooling on server reliability. While immersion cooling excels in thermal energy management compared to conventional air-cooling, there have been limited studies on its reliability. The assessment of material characteristics, such as modulus and glass transition temperature, has substantial significance in the mechanical engineering of electronic components. The substrate, which is an essential element of an electronic package, significantly impacts the dependability and failure mechanisms of electronics, both at the package and board levels. The use of established material compatibility tests, such as ASTM 3455, is applied with appropriate adjustments in compliance with the design recommendations for immersion-cooled IT equipment outlined by the Open Compute Project (OCP). The main objective of this research is to investigate the effects of thermal aging on the thermo-mechanical properties of various substrate cores when immersed in single-phase dielectric fluids. This research examines the effects of aging on the

substrate core by subjecting it to synthetic hydrocarbon fluid (EC100), Polyalphaolefin 6 (PAO 6), and ambient air for a duration of 720 hours (about 4 and a half weeks). The aging process is conducted at two different temperatures, namely 85°C and 125°C. The complex modulus and the glass transition temperature of the substrate core are then determined and compared before and after the aging process.

Table of Contents

List of Illustrations

List of Tables

Chapter 1 Introduction

1.1 Literature review

The global demand for energy is seeing a steady rise, as shown by British Petroleum's data. In 2019, primary energy consumption worldwide saw a notable growth of almost 5%, marking the most rapid rate of expansion seen since 2013 [1]. Despite its significant relevance and extensive use, renewable energy continues to constitute a very limited proportion within the overall energy composition. Renewable energy sources, as of 2020, provide a mere 10% of the whole world final energy consumption [2]. The acceleration of the shift from conventional to renewable energy sources has been facilitated by several key events and discoveries that have taken place worldwide. Several reasons contribute to the need for reducing carbon footprint, including increasing demands from governments and society, changing oil prices, and substantial dependence on foreign energy suppliers [3]. To mitigate their reliance on fossil fuels, several developing countries have increased their investments in renewable energy sources. Since 2004, there has been a notable rise in worldwide investment in renewable energy, with the percentage increasing from 18% to 42%. Achieving decarbonization of future energy systems would need a significant advancement in technical development in order to ensure uninterrupted functionality [2, 3].

The data center industry is characterized by a significant level of energy usage. The data center serves as a facility for storing and managing Information Technology equipment (ITE), as well as housing electrical systems, Heating, Ventilation, and Air Conditioning (HVAC) systems, and other necessary supporting equipment. Additionally, it provides essential services to ensure the security and efficiency of the equipment [4]. Based on a study conducted by the Synergy Research Group, it was found that as of the conclusion of the third quarter in 2019,

there were a total of 504 hyper-scale data centers on a worldwide scale [5]. According to another estimate, it is projected that this figure will see an annual increase of 12-14% during the subsequent five-year period [6]. The power consumption attributed to data centers accounted for around 3% of the worldwide power supply in the year 2018, and it is projected to increase at an annual growth rate of 15-20% [7].

Data centers consist of two main components that use energy: Information Technology Equipment (ITE) and cooling system equipment. Additionally, there are secondary power and auxiliary equipment involved in the energy consumption of data centers. The operation of the cooling system is necessary for continuous operation, almost around the clock. The cooling system is a significant contributor to the overall cost, accounting for 30-50% of the total expenses. It also consumes a big amount of energy, around 30% of the total power demand, which corresponds to around 90% of the total energy consumption [8, 9, 10]. One crucial aspect in enhancing the energy efficiency of data centers is the optimization of the cooling system. The Power Usage Effectiveness (PUE) is widely recognized as a recommended metric in the industry for evaluating the energy efficiency of data centers. The optimal energy efficiency of a data center is achieved when its Power Usage Effectiveness (PUE) is minimized, approaching a value of 1.0 [11].

As per the iNEMI Technology Roadmap, a critical challenge facing the micro and power-electronics industries is maintaining operating temperatures below 85°C for the heat flux generated by chips within a potentially limited area of 300 W/cm² [12]. In contrast, air-cooled data centers can effectively handle cooling demands of only up to 37 W/cm², which falls short for rapidly advancing Information and Communication Technology facilities, like big data and cloud computing [13]. Data center cooling systems fall into two categories: air-cooled and liquid-cooled. Air-cooled systems disperse server heat by circulating cooled air, while liquid-cooled systems are divided into direct and indirect cooling based on fluid interaction with heat

sources. In direct cooling, dielectric fluid makes direct contact with server components like CPUs, GPUs, and DIMMs, whereas indirect cooling involves fluid passage through cold plates attached to heat-generating components. Direct cooling further branches into single-phase immersion and two-phase immersion cooling systems. Single-Phase Liquid Immersion Cooling (Sp-LIC) is a notable liquid-cooling technology due to its advantages in terms of deployment convenience, cost-effectiveness of dielectric fluids, and the simplicity of cooling infrastructure [14]. Several existing proprietary cooling techniques have shown the effectiveness of single-phase immersion cooling in terms of achieving low Power Usage Effectiveness (PUE) values [15] as shown in figure 1.1 [16] and improving the dependability of server components [17].

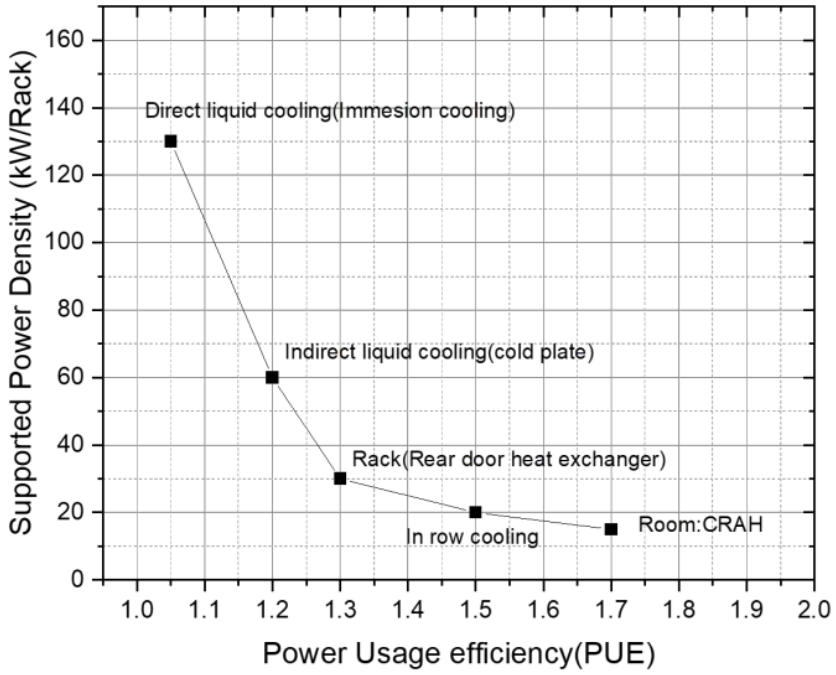

Figure 1.1: Cooling techniques for data center and supported power densities and PUEs [16]

Figure 1.2 [18] illustrates the schematic depiction of a standard single immersion system. The system is comprised of two distinct components, namely the primary loop and the secondary loop. The primary loop encompasses the path of coolant to and from the heat exchanger for the facility's cooling system. On the other hand, the secondary loop consists of

the tank, server system, pump, and heat exchanger. The process of single-phase immersion cooling involves submerging servers in a dielectric coolant. This coolant is then cycled to remove heat from the overheated electronic components. The ejected heat from the coolant is released via a heat exchanger [19]. In contrast to forced convection air cooling, single-phase liquid immersion cooling (Sp-LIC) offers notable advantages. These include increased thermal mass, reduced temperature fluctuations or hot spots, absence of electrochemical migration, and enhanced reliability due to the protection of information technology equipment from contaminants and harsh environmental conditions [20, 21]. Additional benefits of Sp-LIC include the capacity to recuperate wasted heat, mitigate carbon emissions, and diminish water use [22]. In response to the escalating energy consumption and growing intricacy in thermal management, scholars have put forward many approaches to augment the thermal efficiency of single-phase immersion cooling. One such approach involves the incorporation of nanoparticles into the fluid to amplify its thermal characteristics [22].

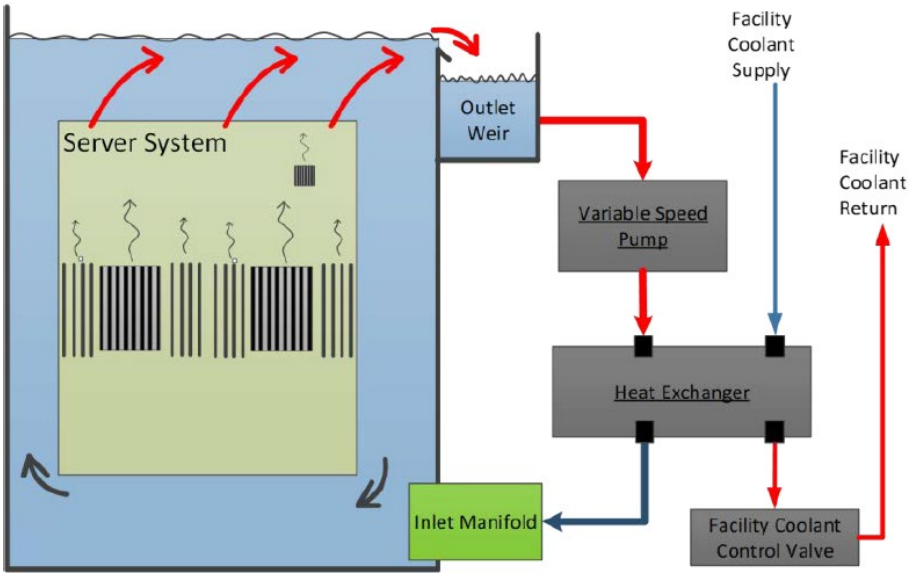

Figure 1.2: Schematic of the single-phase immersion system [18]

The use of immersion cooling has several advantages in comparison to air cooling; nonetheless, it requires meticulous consideration of thermal and non-thermal design aspects for systems that are typically air-cooled. In the context of submerging air-cooled electronics, it is

recommended to remove fans from the server, seal hard drives, resolve problems related to material compatibility, enhance heat sink design, and consider other relevant factors [23]. Numerous researchers have conducted investigations on the continual improvement of conventional air-cooled heat sinks for air-cooled servers. However, only a limited number of studies have examined the effects of altering heat sink characteristics in the context of Sp-LIC. Saini et al. [24] performed a research on heat sinks in immersion-cooled servers, using a multi-objective approach and considering several design variables for optimization purposes. The fluid used in this investigation is a synthetic hydrocarbon fluid known as EC 100. The objective of the research was to minimize heat resistance and pressure loss while ensuring a constant level of pumping power. In comparison to the baseline heat sink design, the enhanced heat sink achieved a 15% reduction in thermal resistance and a 15.3% decrease in pumping power just by modifications to the fin counts and fin thickness of the heat sink.

Several research have been undertaken to enhance the effectiveness of heat dissipation in forced convective cooling by the use of heat sinks with diverse shapes, materials, flow patterns, and other pertinent characteristics, such as metal foam heat sinks. The second half of the 20th century saw significant progress in manufacturing technology, leading to a marked rise in the occurrence of metal foams. This phenomenon may be ascribed to the ability to generate substantial quantities of superior quality foams via the use of various metal alloys. Metal foams are a kind of cellular structured material characterized by a random arrangement of linked pores, often possessing consistent dimensions and morphology. Metallic foams find extensive applications across diverse domains including multifunctional heat exchangers, cryogenics, combustion chambers, cladding on buildings, strain isolation, buffering between rigid structures and fluctuating temperature fields, geothermal operations, petroleum reservoirs, compact heat exchangers for airborne equipment, air cooled condensers, and heat sinks for power electronics.

Bayomy and Saghir [25] conducted an investigation on the thermal performance of a finned aluminum heat sink with two, three, and four channels using experimental and computational methods. The research revealed that the mean Nusselt number of heat sinks including three channels exhibited a 17% improvement compared to heat sinks with two channels, and a 30% improvement compared to heat sinks with four channels. In their study, Mancin et al. [26] performed an experimental investigation aimed at quantifying the heat transfer occurring during the passage of airflow through seven distinct samples of aluminum open-cell foam. These samples were characterized by variations in terms of PPI (pores per inch), porosity, and foam core height. The study included a broad spectrum of air mass velocities to ensure comprehensive analysis. The research findings indicate that, when the number of pores per inch (PPI) is constant, there is a positive correlation between the global heat transfer coefficient and decreasing porosity.

In a study conducted by Mancin et al. [27], the authors reported experimental data on heat transfer and pressure decrease in forced convection across four distinct aluminum foams, using the air as the flowing medium. The researchers conducted experiments on aluminum foams with varying pore densities of 5, 10, 20, and 40 pores per inch (PPI). The foams exhibited porosity levels ranging from around 0.92 to 0.93, with a foam core height of 0.02 meters. The researchers noted that, despite the 5 PPI and 40 PPI 20 mm high samples having twice the surface efficiency and almost half the heat transfer area compared to the 40 mm high samples, their global heat transfer coefficients were found to be virtually equal. Mancin et al. [28] provided an analysis of heat transfer and pressure drop characteristics for a set of five distinct copper foams. These foams were produced by a casting process and had varying pore per inch (PPI) values of 5, 10, 20, and 40. The porosity of the foams ranged from 0.905 to 0.934. The experimental results suggest that the copper foam sample with a porosity of 10 pores per inch (PPI) exhibits favorable characteristics for the development of novel thermal

management systems in electronic cooling applications, owing to its efficient heat transfer properties. In a study done by Younis and Viskanta [29], an experiment was performed with the objective of finding the volumetric heat transfer coefficient between ceramic foams, namely alumina and cordierite, and a heated air stream. The aim was achieved by using a single-blow transient method, as used by the researchers. The researchers have determined that there is a notable correlation between the volumetric heat transfer coefficient and the exponents of the Reynolds number, with respect to the mean pore diameter.

Reliability concerns may occur in situations where heat-generating components are submerged inside dielectric fluids. The failure of the whole package may be caused by small variations in the material characteristics of the components, leading to deformation, warpage, or delamination modes of failure [30]. Tushar et al. [31] conducted a study to investigate the thermo-mechanical properties of low loss printed circuit boards when subjected to immersion in mineral oil for a duration of 720 hours at temperatures of 25, 50, 75, and 105°C. The researchers discovered that the in-plane coefficient of thermal expansion (CTE) values of the post-aged samples exhibited little changes at the specified temperatures. Ramdas et al. [32] conducted research that bears resemblance to the present investigation, whereby FR-4 PCBs were subjected to immersion in EC-100 dielectric fluid. The findings indicate that the modulus has shown a drop in post-aged samples, suggesting a reduction in the stiffness of PCBs. Consequently, this decrease in stiffness contributes to a decrease in warpage. In their study, Bhandari et al. [33] examined the impact of the immersion fluid EC-100, in a single-phase state, on the mechanical characteristics of non-halogenated substrates. The immersion process lasted for a duration of 720 hours, with the substrates being exposed to ambient temperature, 50°C, and 75°C. This research involves a comparison between the modulus of the substrate while submerged and the modulus of substrates when exposed to air at corresponding

temperatures. The experiment revealed that increasing temperatures resulted in a reduction in the modulus.

1.2 Research Objective

This investigation encompasses two main objectives: firstly, the assessment of thermal efficiency in immersed Information Technology Equipment (ITE), and secondly, the evaluation of operational efficiency, including the overall life cycle of the fluid, component reliability, and serviceability.

The thermal aspect of the study is subdivided into three sections. In the initial segment, an extensive numerical analysis is conducted to explore multi-parametric optimization for heat sinks within a forced convection setup of an open compute server design when submerged in a single-phase immersion fluid. The optimization process, carried out under constant pumping power, involves minimizing pressure drop and thermal resistance as primary objectives. Through the manipulation of fin count and fin thickness while maintaining a consistent base thickness in aluminum heat sinks, the interrelation between geometric parameters and objective functions is revealed. These findings contribute to the development of standardized methodologies for optimizing heat sinks in immersion cooling.

The second section of the thermal investigation entails a methodical empirical study aimed at examining the heat transfer and pressure loss characteristics of aluminum metal foams when immersed in dielectric synthetic fluid. Prior studies have thoroughly examined the thermohydraulic characteristics of heat sinks made of metal foam, with a focus on using air and water as cooling mediums. Nevertheless, there is a significant dearth of scholarly investigations about the use of metal foam heat sinks in single-phase immersion cooling. The study employs various specimens of metal foam with core heights of 0.5 in and 0.75 in, spanning relative densities ranging from 10.7 to 12.3 percent, and differing Pores Per Inch

(PPI) values, specifically 5, 10, 20, and 40. These metal foam samples are subjected to varying flow rates, heat fluxes, and inlet fluid temperatures. The comprehensive analysis of these parameters provides insights into the behavior of heat transfer and pressure loss in the context of metal foam immersion cooling.

In the final segment of the thermal study, a comprehensive overview of the experimental methodology employed to acquire velocity field data using Particle Image Velocimetry (PIV) in a single-phase immersion tank is presented. PIV, a non-intrusive optical measurement technique, serves to visualize and quantify fluid flow velocity patterns. The velocity field data obtained from these experiments offer valuable insights into fluid flow dynamics and significantly contribute to the comprehension of the thermal performance of the immersion cooling system.

This second part of the study deals with the impact of immersion cooling on server reliability. Despite its superior thermal management over traditional air-cooling, reliability studies on immersion cooling are scarce. Assessing material traits, like modulus and glass transition temperature, holds significant importance in electronic component mechanical engineering. The substrate, a vital electronic package element, deeply influences electronics' dependability and failure mechanisms across package and board levels. Established material compatibility tests, like ASTM 3455, are adapted in accordance with Open Compute Project (OCP) immersion-cooled IT equipment guidelines. The central goal is to explore thermal aging's effects on various substrate cores immersed in single-phase dielectric fluids. Synthetic hydrocarbon fluid (EC100), Polyalphaolefin 6 (PAO 6), and ambient air subject the substrate core to a 720-hour aging process, conducted at 85°C and 125°C. Pre- and post-aging, the substrate core's complex modulus and glass transition temperature are determined and compared, unveiling aging's impact.

1.3 References

[1] BP statistical review of world energy 2018, https//www.bp. com/en/global/corporate/energy-economics/statisticalreview-of-world-energy. html (accessed 4 Sept.2018). Sustain., vol. 10, no. 3195, p. 17, 2018.

[2] H.E. Murdock, D. Gibb, T. André, Renewables 2021 Global Status Report. Paris: REN21 Secretariat, 2021

[3] Pambudi, N. A., Sarifudin, A., Firdaus, R. A., Ulfa, D. K., Gandidi, I. M., Romadhon, R., "The immersion cooling technology: Current and future development in energy saving", Alexandria Engineering Journal, Volume 61, Issue 12, 2022, Pages 9509-9527, ISSN 1110-0168, https://doi.org/10.1016/j.aej.2022.02.059.

[4] Nadjahi, C., Louahlia, H., Lemasson, S., "A review of thermal management and innovative cooling strategies for data center", Sustainable Computing: Informatics and Systems, https://doi.org/10.1016/j.suscom.2018.05.002.

[5] Weissberger, A. Synergy Research Group: Hyperscale Data Center Count >500 as of 3Q-2019. Available online: https://techblog.comsoc.org/2019/10/19/synergy-researchgroup-hyperscale-data-center-count-500-as-of-3q-2019/ (accessed on 19 October 2019).

[6] Andrae, A.S.G. Total Consumer Power Consumption Forecast. Available online: https://10times.com/nordicdigital-business-summit (accessed on 1 October 2017).

[7] Liu, C., Yu, H., "Experimental Investigations on Heat Transfer Characteristics of Direct Contact Liquid Cooling for CPU", Building 2022, https://doi.org/10.3390/buildings12070913

[8] Jin, C., Bai, X., Yang, C., Mao, W., and Xu, X., "A review of power consumption models of servers in data centers". Appl. Energy 2020, 265, 114806.

[9] Zimmermann, S.; Meijer, I.; Tiwari, K.M.; Paredes, S.; Michel, B.; Poulikakos, and D. Aquasar, “A hot watercooled data center with direct energy reuse”. Energy 2012, 43, 237–245.

[10] Shao, S., Liu, H., Zhang, H. and Tian, C., “Experimental investigation on a loop thermosyphon with evaporative condenser for free cooling of data centers”. Energy 2019, 185, 829–836.

[11] ASHRAE. PUE: A Comprehensive Examination of the Metric; ASHRAE: Atlanta, GA, USA, 2012.

[12] Agostini, B., Fabbri, M., Park, J., Wojtan, L., Thome, J., and Michel, B., “State of the art of high heat flux cooling technologies”, Heat Transf. Eng. 28 (2007) 258–281, doi: 10.1080/01457630601117799.

[13] Ellsworth, M.J., Jr. and Iyengar, M.K., “Energy Efficiency Analyses and Comparison of Air- and Water Cooled HighPerformance Servers”, Proc. of the ASME 2009 InterPACK Conf. Collocated with the ASME 2009 Summer Heat Transfer Conf. and the ASME 2009 3rd Intl. Conf. on Energy Sustainability, ASME 2009 InterPACK Conf., San Francisco, CA, pp. 907–914, July 19–23, 2009.

[14] Bansode, P., Shah, J., Gupta, G., Agonafer, D., Patel, H., Roe, D., and Tufty, R. (November 8, 2019). "Measurement of the Thermal Performance of a Custom-Build Single-Phase Immersion Cooled Server at Various High and Low Temperatures for Prolonged Time." ASME. J. Electron. Packag. March 2020; 142(1): 011010. https://doi.org/10.1115/1.4045156.

[15] Eiland, R., Fernandes, J., Vallejo, M., Agonafer, D. and Mulay, V., "Flow Rate and inlet temperature considerations for direct immersion of a single server in mineral oil," Fourteenth Intersociety Conference on Thermal and Thermomechanical Phenomena in

Electronic Systems (ITherm), 2014, pp. 706-714, doi: 10.1109/ITHERM.2014.6892350, 2014

[16] Wen, F., 2018, “Best Practice of Alibaba Datacenter-Immersion Cooling Escorts Cloud Computing,” Presented at the OCP Global Summit, San Jose, CA, p. 12, accessed Sept. 3, 2021, https://www.opencompute.org/files/Immersion-Cooling-for-Green-Computing-V1.0.pdf

[17] Shah, J. M., Padmanaban, K., Singh, H., Duraisamy Asokan, S., Saini, S., and Agonafer, D., Evaluating the Reliability of Passive Server Components for Single-Phase Immersion Cooling, ASME. J. Electron. Packag., 144(2): 021109. https://doi.org/10.1115/1.4052536, 2022

[18] Sarangi, S., McAfee, E. D., Damm, D.G., and Gullbrand, J., "Single-Phase Immersion Cooling Performance in Intel Servers with Immersion Influenced Heatsink Design," 2022 38th Semiconductor Thermal Measurement, Modeling & Management Symposium (SEMI-THERM), 2022, pp. 1-5.

[19] Shah, J., Eiland, R., Siddharth, A., and Agonafer, D., 2016, “Effects of Mineral Oil Immersion Cooling on IT Equipment Reliability and Reliability Enhancements to Data Center Operations,” 15th IEEE Intersociety Conference on Thermal and Thermomechanical Phenomena in Electronic Systems (ITherm), Las Vegas, NV, May 31– June 3, pp. 316–325

[20] Shah, J. M., Eiland, R., Rajmane, P., Siddarth, A., Agonafer, D., and Mulay, V., “Reliability Considerations for Oil Immersion-Cooled Data Centers,” ASME. J. Electron. Packag., 141(2), p. 021007.

[21] Modi, Himanshu, Pardeep Shahi, Lochan Sai Reddy Chinthaparthy, Gautam Gupta, Pratik Bansode, Vibin Shalom Simon, and Dereje Agonafer. "Experimental Investigation of the Impact of Improved Ducting and Chassis Re-Design of a Hybrid-

Cooled Server." In International Electronic Packaging Technical Conference and Exhibition, vol. 86557, p. V001T01A019. American Society of Mechanical Engineers, 2022.

[22] Niazmand, A., Murthy, P., Saini, S., Shahi, P., Bansode, P., and Agonafer, D., "Numerical Analysis of Oil Immersion Cooling of a Server Using Mineral Oil and Al2O3 Nanofluid", ASME 2020 Int. Tech. Conf. and Exhibition on Packaging and Integration of Electronic and Photonic Microsystems

[23] Saini, S., Wagh, T., Bansode, P., Shahi, P., Herring, J., Lamotte-Dawaghreh, J., Shah, J.M. and Agonafer, D., A Numerical Study on Multi-objective Design Optimization of Heatsinks for Forced and Natural Convection Cooling of Immersion Cooled Servers, Journal of Enhanced Heat Transfer. DOI: 10.1615/JEnhHeatTransf.202204380.

[24] Brink, R., et al., "Design Guidelines for Immersion-Cooled IT Equipment", Open Compute Project Advanced Cooling Solutions Immersion Workstream, accessed March 2022.

[25] A. M. Bayomy, Z. Saghir, Thermal performance of finned aluminum heat sink filled with erg aluminum foam: Experimental and numerical approach, International Journal of Energy Research 44 (2020) 4411–4425.

[26] S. Mancin, C. Zilio, A. Cavallini, L. Rossetto, Heat transfer during air flow in aluminum foams, International Journal of Heat and Mass Transfer 53 (2010) 4976–4984. https://doi.org/10.1016/j.ijheatmasstransfer.2010.05.033.

[27] S. Mancin, C. Zilio, L. Rossetto, A. Cavallini, Heat transfer performance of aluminum foams, International Journal of Heat and Mass Transfer 133 (2011). doi:10.1115/1.4003451.

[28] S. Mancin, C. Zilio, A. Diani, L. Rossetto, Experimental air heat transfer and pressure drop through copper foams, Experimental Thermal and Fluid Science 36 (2012) 224–232. https://doi.org/10.1016/j.expthermflusci.2011.09.016.

[29] L.B. Younis, R. Viskanta, Experimental determination of the volumetric heat transfer coefficient between stream of air and ceramic foam, Int. J. Heat Mass Transfer 36 (1993) 1425–1434

[30] Shah, J., Padmanaban, K., Singh, H., Duraisamy, S., Saini, S., and Agonafer, D.," Evaluating the Reliability of Passive Server Components for Single-Phase Immersion Cooling", J. Microelectron. Electron. Packag., vol. 18, no. 1. Pp. 21-28,2021.

[31] Chauhan, T., Bhandari, R., Sivaraju, K., Chowdhury, R., and Agonafer, D., "Impact of immersion cooling on thermomechanical properties of low-loss material printed circuit boards", Volume 28, Issue 7, 2021, pp. 73-90, DOI: 10.1615/JEnhHeatTransf.2021039486

[32] Ramdas, S., Rajmane, P., Chauhan, T., Misrak, A., and Agonafer, D. "Impact of Immersion Cooling on Thermo-Mechanical Properties of PCB's and Reliability of Electronic Packages", ASME 2019 International Technical Conference and Exhibition on Packaging and Integration of Electronic and Photonic Microsystems. Anaheim, California, USA. October 7–9, 2019. V001T02A011. ASME. https://doi.org/10.1115/IPACK2019-6568

[33] Bhandari, R., Lakshminarayana, AB., Sivaraju, KB., Bansode, P., Kejela, E., and Agonafer, D., "Impact of Immersion Cooling on Thermomechanical Properties of Non-Halogenated Substrate." ASME 2022 International Technical Conference and Exhibition on Packaging and Integration of Electronic and Photonic Microsystems. Garden Grove, California, USA. October 25–27, 2022. V001T10A007. ASME. https://doi.org/10.1115/IPACK2022-97423

Chapter 2 Thermal Performance Analysis of Optimized Heat Sinks for Single-Phase Immersion-Cooled Servers: A Numerical and Experimental Investigation

2.1 Introduction

The increasing prevalence of technologies such as 5G mobile communication, artificial intelligence (AI), the Internet of Things (IoT), big data, and automation has substantially amplified the requirements imposed on Internet Data Centers (IDCs). These facilities provide support for either physical or virtual servers, enabling them to do high-capacity computation, handle complex transactions, provide significant storage, and maintain a range of other functions. According to projections, the energy consumption of the information technology (IT) industry is anticipated to reach around 5% of the global energy consumption by the year 2030 [1]. The increasing energy use in data centers (DCs) has become a prominent concern on a global scale, with a recorded consumption of 205 TWh in 2018, accounting for around 1% of the total global power consumption [2]. The power densities seen in traditional data centers have the potential to be 15-100 times greater than those typically found in regular commercial buildings [3]. The increase in this particular need has noteworthy ecological implications, including a substantial rise in emissions of greenhouse gases and the excessive use of water, both via direct and indirect means [4].

The air-cooling approach has been widely used for cooling technologies in data centers (DCs) owing to its convenient installation. According to previous research [5], air-cooled systems have shown their efficacy in successfully managing cooling requirements of up to 37 W/cm2. Nevertheless, in cases when the cooling demand surpasses this level, air-cooled systems may be inadequate in fulfilling the necessary criteria. It is noteworthy that in contemporary data centers, the cooling requirement can exceed the aforementioned threshold

due to the utilization of high-performance computing applications such as big data processing, cloud computing, artificial intelligence, smart and distributed manufacturing systems, autonomous vehicles, and smart energy systems. These sophisticated applications produce substantial amounts of heat, requiring the use of cooling technologies that go beyond what air-cooled systems can provide [6]. In recent years, there has been a notable rise in energy needs and power densities of CPUs, mostly due to escalating processing requirements. As a result, conventional air-cooling techniques have encountered constraints. As a result, scholars have focused their endeavors on suggesting numerous tactics to enhance thermal performance by incorporating nanoparticles [7, 8], augment power efficiency through alternative operational methodologies for current cooling methods [9, 10], and investigate phase change cooling technologies [11, 12], in light of the escalating energy consumption and increasing intricacies linked to thermal management.

The use of immersion cooling technology has emerged as a viable alternative to traditional techniques of air-cooling and indirect cooling. Within the framework of immersion cooling, the server is fully submerged in a dielectric fluid, allowing direct contact between the IT devices, which function as the heat source, and the working fluid, which serves as the cooling medium [13]. There are two main categories of immersion cooling, namely single phase and two-phase immersion cooling. The use of two-phase immersion cooling involves the application of latent heat transfer, mainly leveraging the phase shift phenomena. This cooling method is especially suitable for managing ultra-high heat flux. Fluorocarbon refrigerants are often used in two-phase cooling systems, demonstrating a somewhat elevated global warming potential (GWP). In recent years, hydrofluoroethers, namely Novec 7000, Novec 7100, Novec 7200, and Novec 7300, have emerged as feasible substitutes for refrigerants with significant global warming potential (GWP). However, it is important to acknowledge that the HFE fluids still have a Global Warming Potential (GWP) that spans between 55 to 530 [14]. Furthermore,

the use of a condenser inside two-phase immersion cooling systems adds an additional layer of intricacy. The Single-Phase Liquid Immersion Cooling (Sp-LIC) method is a liquid-cooling technique that is well-regarded for its easy installation, cost-effectiveness in terms of expenditures related to dielectric fluid, and simplified cooling infrastructure. As a result, it is a favored option among users [15].

The cooling efficiency of a liquid immersion cooling system with natural convection was evaluated by Matsuoka et al. [16]. The system was purposefully designed to cater to high-power server boards that are often used in data centers. The study was conducted using a hybrid approach that included the use of computational fluid dynamics (CFD) software programs for modeling purposes, as well as practical tests. A range of fluids underwent tests, including silicone oil, soybean oil, and perfluorocarbon structured liquids. The best material for the heat sink and the proper circulation conditions of the coolant were determined by a combination of experimental and computational analysis undertaken by Cheng et al. [17]. The objective of this study was to investigate the thermal behavior of a single-phase immersion cooling system by modeling the flow of coolant and analyzing the corresponding temperature variations at various flow rates. In their study, Shao et al. [18] designed and implemented a system consisting of eight simulated power heaters, each resembling a GPU chipset in size. These heaters were housed inside a 4U server chassis, with a maximum simulated power of 2700 W for the GPU chassis. Three thorough experiments were conducted to assess the effectiveness of this immersion cooling system. Initially, it is essential to ascertain the primary determinant(s) for evaluating the thermal efficacy of four hydrocarbon-based dielectric coolants via the utilization of power parametric analysis, transient analysis, power cycle test, and fluid temperature profiling. The second objective pertains to the optimization of thermal performance in the immersion system, while the third objective involves assessing the ability of a 1U heat sink,

which utilizes immersion cooling, to effectively support high-density processing units operating at power levels exceeding 300 W per GPU.

The primary aim of the study done by Muneeshwaran et al. [19] was to investigate the impact of various design and operational characteristics on a system's performance while it is submerged in FC-40 dielectric fluid. The parameters encompassed in this study encompassed the arrangement of the inlet and outlet ports (T and Z configurations), the inclusion of a bypass, the range of flowrate from 1 to 3 LPM, the range of heating load from 200 to 600 W, the range of inlet fluid temperature from 15 to 35 °C, the presence of a suction fan with various configurations, and the utilization of different heat sink bases such as solid base, vapor chamber, and heat pipe base. The results revealed that the T-configuration exhibited a reduction in thermal resistance and case temperature of 12.6% and 0.5-2.8 ◦C, respectively, as compared to the Z-configuration. Shrigondekar et al. [20] did a study that included investigating the heat transfer properties of a single-phase immersion cooling system in a 1 U server. The researchers used dielectric fluid (FC40) and dielectric oil (PAO-6) for their analysis.

Several studies have been conducted by researchers to explore methods of continuously improving traditional air-cooled heat sinks for air-cooled servers. However, there is a limited amount of information available on the impacts of modifying heat sink properties in Sp-LIC. The influence of single and multi-parameters on server performance was investigated by Li et al. [21] in the context of immersion cooling. The researchers employed a single-phase immersion cooling technique to enhance the efficiency of servers. They identified seven crucial parameters, namely fin height (A), fin spacing (B), thermal conductivity (C), height ratio of baffle (D), outlet area (E), inlet flowrate (F), and inlet temperature (G), to optimize server performance. The performance indicators considered were maximum temperature and pressure loss. In their study, Saini et al. [22] conducted optimization of heat sinks for immersion-cooled servers by considering several design factors and different goals. The present study used EC

100 synthetic hydrocarbon fluid for the purposes of inquiry. The aim of the study was to minimize heat resistance and pressure loss while simultaneously preserving pumping power. By modifying just, the quantity and dimensions of the heat sink's fins, the thermal resistance was decreased by 15% and the pumping power was cut by 15.3% in the redesigned heat sink.

In their study, Sarangi et al. [23] conducted a comparison between the performance of immersion heat sink and air heat sink for a central processing unit (CPU). The CPU models used in the experiment were a 2nd Generation Cascade Lake installed in a server and a 3rd Generation Ice Lake mounted on a thermal test vehicle (TTV). The immersion heat sink and air heat sink were evaluated in the presence of PAO 6 dielectric fluid. This research aimed to conduct a comparative analysis of seven heatsinks with power capacities ranging from 165 W to 350 W for the 3rd Generation Ice Lake TTV. Additionally, two heatsinks, namely Aluminum air and copper immersion, were evaluated for the cascade lake server. According to empirical evidence, immersion heat sinks consistently exhibit a 10% higher level of efficiency compared to their air-cooled counterparts. The improvement was achieved by modifications to the fin count and thickness of the immersion heat sink, while keeping its height constant. Increasing the size of the fins and widening the distance between them in a heat sink would improve the effectiveness and natural convection flow of Sp-LIC. In this study, Herring et al. (2019) used a machine learning (ML) approach to forecast the optimization of an air-cooled heat sink for single-phase immersion-cooled servers, focusing on multi-objective and multi-design variable considerations. The evaluation of polynomial regression, random forest, and neural networks was conducted to estimate the thermal resistance and pressure drop of a heat sink, based on design inputs. Chiang and Chang (25) used the Response Surface Method (RSM) to get the ideal design parameters for pin-fin heat sinks with the aim of improving thermal performance.

The main aim of this study is to comprehensively analyze different design parameters and combinations of goal functions in order to enhance the performance of the parallel plate-

fin heat sink used in immersion cooling. The inquiry consists of two primary components. The first phase entails doing an experimental study, in which the configuration of the experimental arrangement is delineated. The experimental arrangement comprises an immersion tank and a thermal test vehicle (TTV). The second phase of the study involves the use of ANSYS Icepak software to simulate the immersion tank and thermal test vehicle (TTV). The model will be validated by comparing the simulation results with experimental data. Subsequently, heat sink optimization will be conducted. The dielectric fluid used in this investigation is POA 6, whereas the materials chosen for the heat sink are aluminum and copper. The use of OptiSLang, a specialist program for design optimization and analysis, integrated inside the ANSYS platform, was undertaken to optimize the design of a heat sink. The study focused on the optimization of heat-sink fin thickness and count, while maintaining a constant pumping power. The aim function, which encompasses thermal resistance and pressure differential across the heat sink, is established inside the Icepak program and is designed to be reduced in order to get an optimum design. The improved heat sink is then fabricated and subjected to experimental testing in order to verify the computational fluid dynamics (CFD) findings.

2.2 Experimental Methodology

Figure 2.1 illustrates the schematic design of the experimental setup used for the single-phase liquid immersion cooling system. The tank has been specifically designed to include the fundamental concept of an infinity pool. The phrase "inlet port" refers to the lower port that facilitates the entrance of fluid into the system via the use of a pump. The fluid undergoes a systematic process of being directed via a server system, after which it proceeds to flow downhill into a reservoir and eventually exits through the output port. In order to preserve the thermal conditions of the fluid being introduced, it is necessary to facilitate the circulation of such fluid through a heat exchanger. The server board consists of a thermal test vehicle (TTV) that is equipped with a 2U heat sink and dual in-line memory modules (DIMMs). The current

study does not take into account the heat load generated by the dual in-line memory module (DIMMs). The TTV device may be categorized as a CPU simulator due to its ability to provide a similar level of heat output, which is accomplished by using an external direct current (DC) power source.

Figure 2.2 illustrates the immersion tank, whereby the tank accommodates the 2U server. A plate-type heat exchanger is used for the purpose of regulating the temperature of the incoming fluid. Additionally, three thermocouples are utilized to ascertain the temperature of the fluid just before reaching the heat sink and DIMMS. The control of fluid flowrate is achieved by manipulating the power supplied to the intake pump, while the measurement of this flowrate is conducted using microflow sensors. The Keyence FDX-A1 is a device that is widely used in many industries for its advanced features and capabilities. The measurement of inlet fluid temperature (Tinlet) and outlet fluid temperature (Toutlet) is conducted using 10k thermistors with an accuracy of ±2°C. Additionally, the Keyence GPM010 pressure sensors are used to detect the inlet and outlet pressure of the tank.In order to get the experimental data, it is necessary to calibrate all the sensors and establish a connection with the data collecting system, namely the DAQ Agilent 37940A. A heater made of aluminum nitride with dimensions of 50 mm x 50 mm is used in this study. The heater has a unique groove on its surface, intentionally constructed to accept a K-type thermocouple. This thermocouple is utilized for the purpose of measuring the temperature (Ts) of the heater's surface. The calculation of the input power (Q = VI) to the heater involves the measurement of voltage (V) and current (I) using the DC power source. The thermal resistance can be calculated by

$$R_{th} = \frac{T_s - T_{inlet}}{\mathrm{Q}} \qquad (1)$$

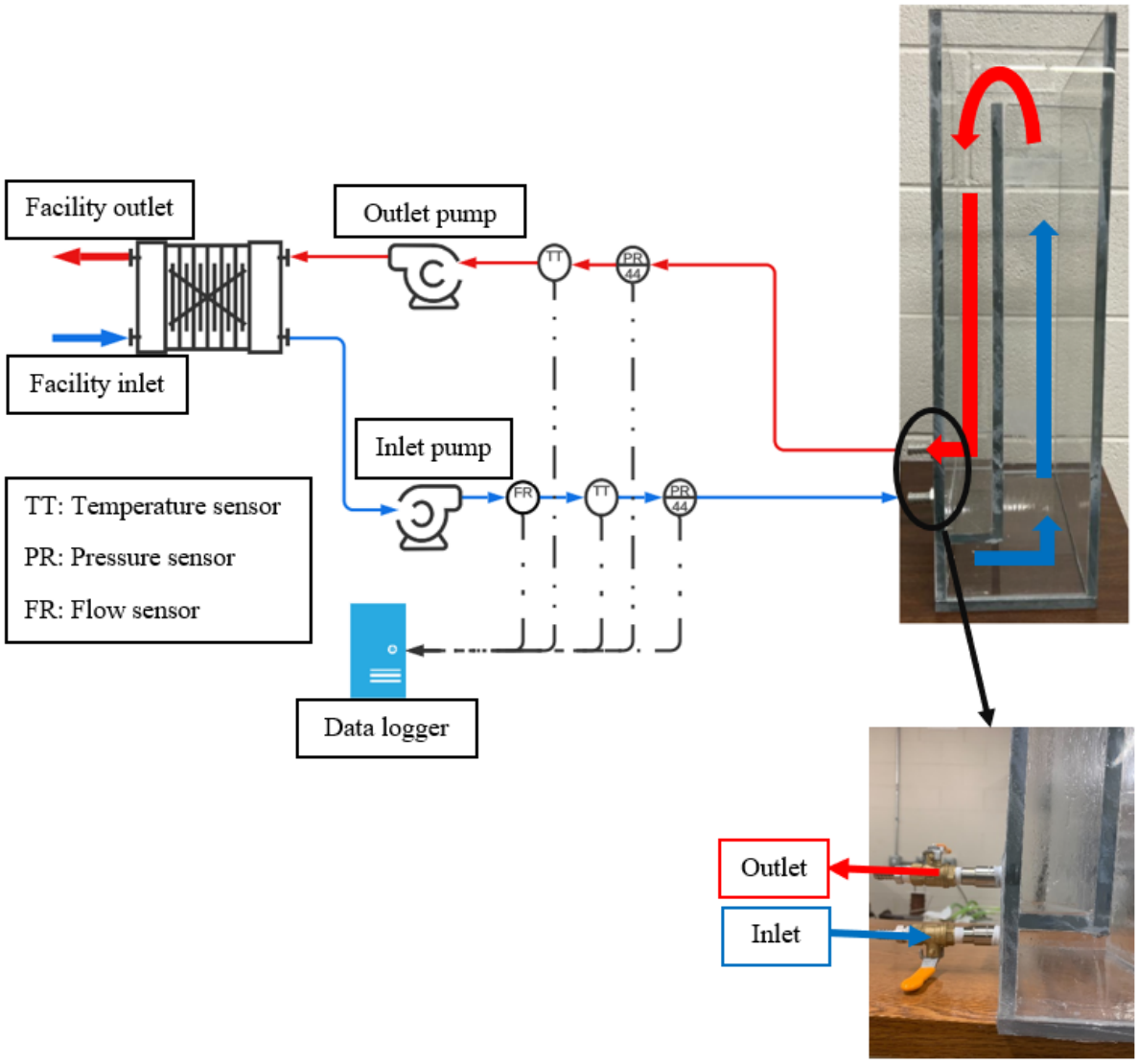

Figure 2.1: Schematic diagram of the experimental setup

The existence of mistakes in experimental measurements and methodologies is inevitable, hence requiring the implementation of an uncertainty analysis in order to determine the correctness and dependability of the obtained data. The flow sensor, pressure sensor, K type thermocouple, and 10kΩ thermistors exhibit an accuracy of ±0.3% of the measured value, ±0.3% of the measured value, ±0.1 °C, and ±0.1 °C, correspondingly. Table 1 displays the measured uncertainty values for each sensor and equipment.

Table 2.1: Experimental Uncertainty

Sensor/Equipment	Uncertainty values
Flow sensor	±0.2%
Pressure sensor	±0.3%
K type thermocouple	±0.5 °C
10kΩ thermistors	±0.5 °C
Power meter	±0.13% of the reading

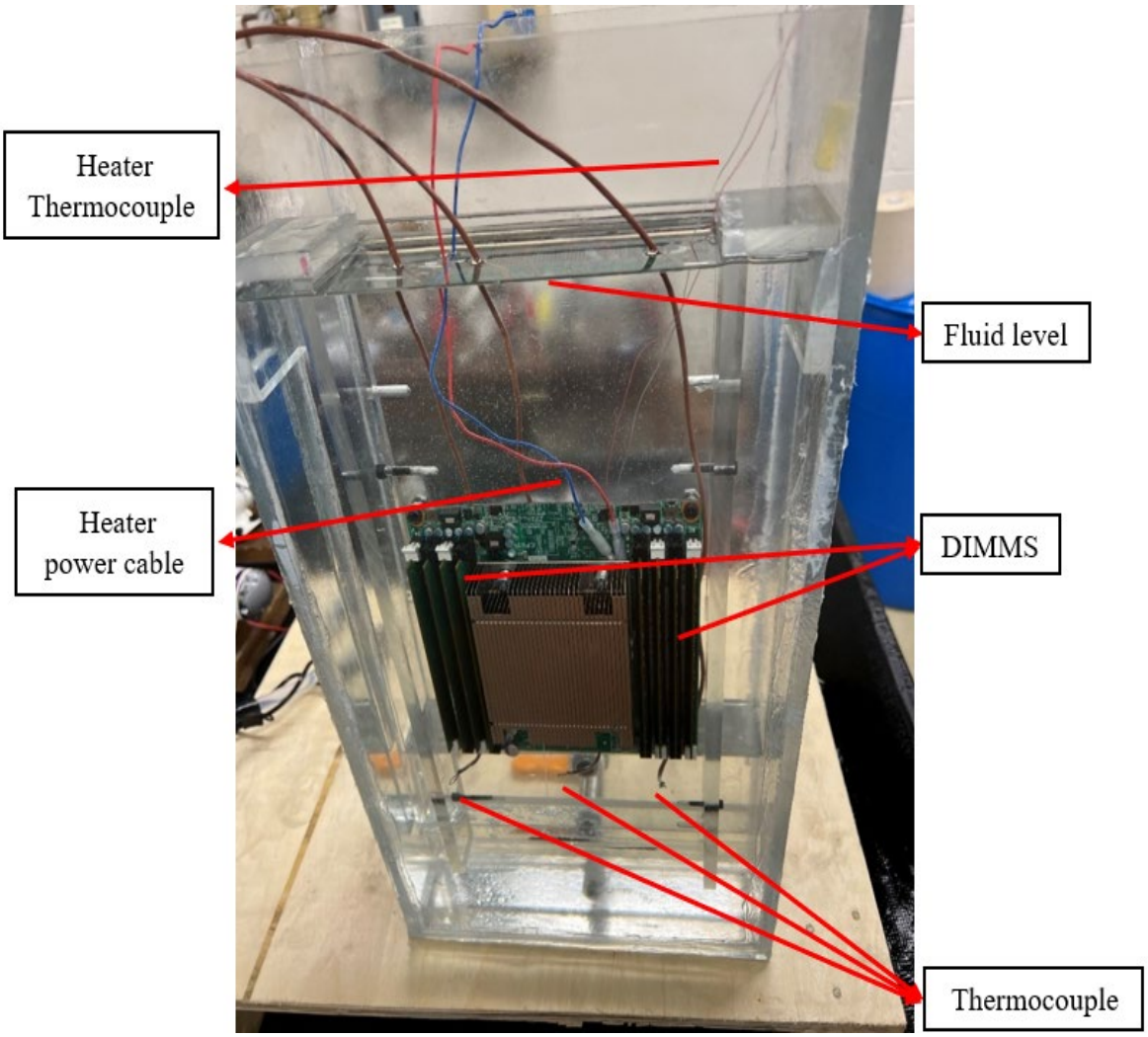

Figure 2.2: Immersion tank

The experimental uncertainty consists of test and systematic errors, and it can be estimated by [26, 27]:

$$R_\alpha = \sqrt{\left(\frac{\partial \alpha}{\partial x_1} Z_1\right)^2 + \left(\frac{\partial \alpha}{\partial x_2} Z_2\right)^2 + \ldots + \left(\frac{\partial \alpha}{\partial x_n} Z_n\right)^2} \qquad (2)$$

The parameter (α) is a function of the independent variables (x_1, x_2, …, x_n), and the associated uncertainties of the independent variables are denoted as Z_1, Z_2, …, Z_n. The thermal resistance exhibited a maximum uncertainty of 5%. The effectiveness of the single-phase immersion cooling system may be primarily impacted by several design and operational variables, including the thickness of the fins, power of the heater, and flow rate. The measurement of the variation in fin thickness is conducted subsequent to the completion of an optimization study. Therefore, a sequence of tests was undertaken to examine the influence of varying fin thicknesses and flow rates on the cooling efficiency.

2.3 Numerical Model Setup

As shown in Figure 2.3, the TTV and tank model were created in ANSYS Icepak, taking into consideration essential components involved in the heat-transfer phenomena, such as the central processor unit (CPU), heat sinks, and dual in-line memory modules (DIMMs). The thermal stack of the central processing unit (CPU) is made up of a 2D heat source embedded in a 3mm thick Aluminum nitride heater. A 0.2 mm thick Indium thermal interface material (TIM) is placed between the heat sink and heater. The thermal interface material (TIM) has a thermal conductivity of 8 W/m-K. The heat sink is 85mm x 110mm x 41mm, with a heatsink base of 5mm. The heat sink is made up of 35 fins, each measuring 0.3mm thick and 36mm tall. Table 2.2 shows the important thermophysical properties of PAO 6, whereas Table 2.3 shows the boundary conditions for both experimental and numerical investigations. The surface temperature of the heater was measured across several mesh components to ensure grid independence. As shown in Table 2.4, the present investigation used a sample size of 6.28 million elements. The CFD model was validated using experimental data collected at different flow rates, as shown in Figure 2.4. For all flow rates, the CFD findings and experimental results of the heat sink with heat pipe vary by 2%.

Table 2.2: Thermophysical Characteristics of PAO 6

Temperature [°C]	Thermal conductivity [W/m-K]	Specific Heat [J/kg K]	Density [kg/m^3]	Viscosity [cSt]	Vol expansion [1/K]	Thermal Diffusivity [m^2/s]
20	0.156	2153.37	823.1	97.814	0.0007	8.80E-08
30	0.1553	2185.77	817.1	49.116	0.0007	8.69 E-08
40	0.1546	2218.17	811.1	30.127	0.0007	8.59E-08
50	0.1539	2250.57	805.1	20.621	0.0007	8.49E-08
60	0.1532	2282.97	799.1	15.128	0.007	8.39E-08
70	0.1525	2315.37	793.1	11.642	0.0007	8.30E-08
80	0.1518	2347.77	787.1	9.279	0.0007	8.21E-08
90	0.1511	2380.17	781.1	7.596	0.0007	8.12E-08

Table 2.3: Boundary conditions

Fluid	PAO 6
Inlet temperature	40 °C
TIM	Indium
CPU power	205 W
DIMMs power	0 W

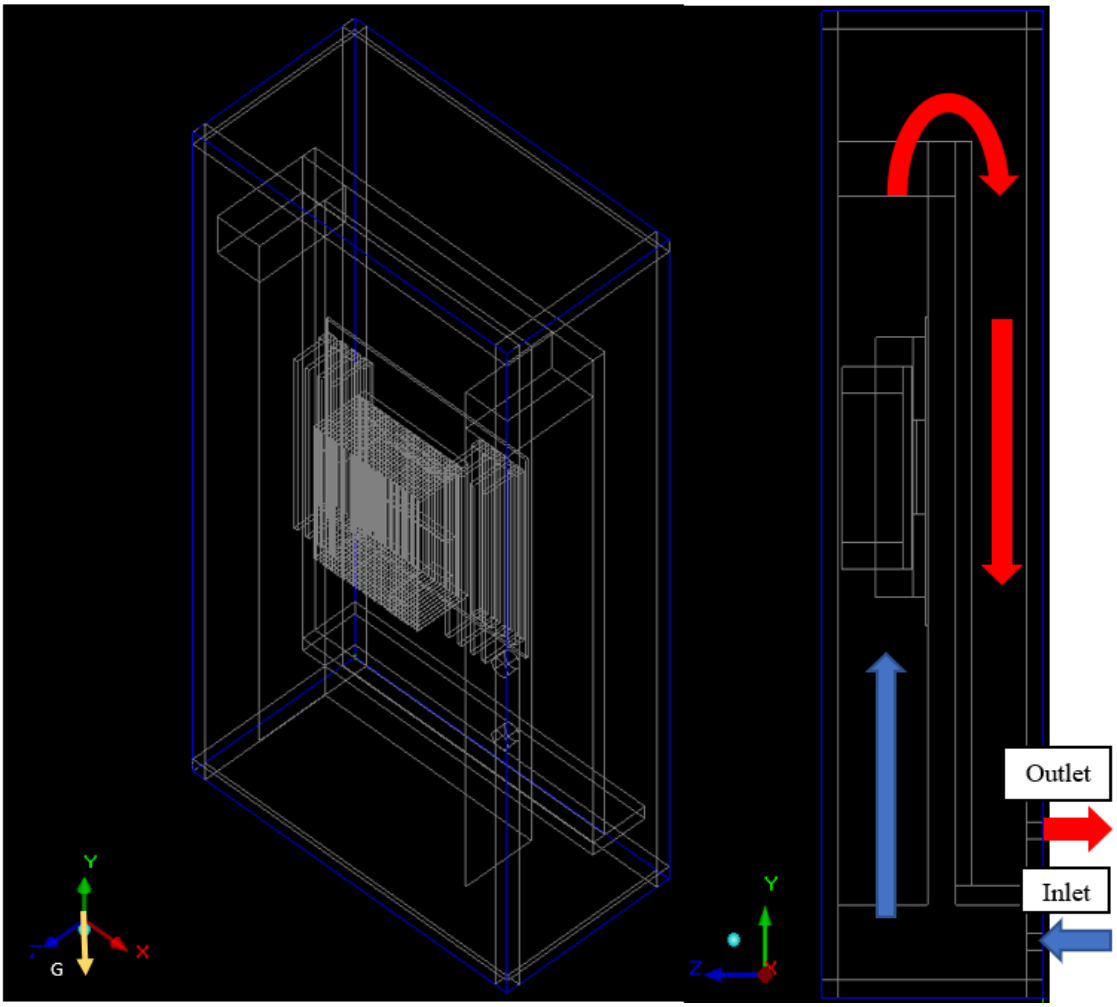

Figure 2.3: 2U immersion tank

2.3.1 Governing equations

The CFD tool employed in this study utilizes the Navier-Stokes equations, which govern the conservation of mass, momentum, species, and energy. These equations are solved to accurately predict heat transfer phenomena in laminar flow conditions. The equations as follows:

Mass conservation:

$$\frac{\partial \rho}{\partial t} + \nabla.(\rho \vec{v}) = 0 \qquad (3)$$

The above equation reduces to $\nabla.(v^{\rightarrow}) = 0$ for incompressible fluids.

Momentum Equation:

$$\frac{\partial}{\partial t}(\rho\vec{v}) + \nabla.(\rho\vec{v}\vec{v}) = -\nabla p + \nabla.(\bar{\bar{\tau}}) + \rho\vec{g} + \vec{F} \quad (4)$$

Energy Equation:

$$\frac{\partial}{\partial t}(\rho h) + \nabla.(\rho h\vec{v}) = \nabla.[(k + k_t)\nabla T] + S_h \quad (5)$$

The fluid energy equation is expressed in terms of the sensible enthalpy, denoted as h. The molecular conductivity, k, and the turbulence transport conductivity, kt, are also included in the equation. The term Sh in this context represents volumetric heat sources that are defined by the user. The energy equation for conduction within solid regions can be expressed as follows:

$$\frac{\partial}{\partial t}(\rho h) = \nabla.(k\nabla T) + S_h \quad (6)$$

Here, k is the thermal conductivity of the solid, ρ is the density, T is the temperature and Sh is the source term for volumetric heat sources.

Table 2.4: Grid independence study

Number of elements (millions)	**Heater Temperature for heat sink with heat pipe (°C)**
0.85	75.5
1.13	73.6
2.64	72.8
6.28	69.3
9.05	69.6

2.3.2 OptiSLang Setup

The current research utilizes OptiSLang as the design optimization tool. OptiSLang, as a component of ANSYS Workbench, offers the distinct benefit of enabling seamless integration with various ANSYS tools, including those pertaining to thermal analysis, structural analysis, electrical analysis, and fluid analysis. The optimization process is conducted independently using any of the ANSYS tools or modules. The design parameters and their respective optimization ranges or bounds are defined by the simulation module and then imported into OptiSLang. The software utilizes a meta-modeling technique to effectively sample the design space, specifically by employing the adaptive meta-model of optimal prognosis (AMOP). This approach incorporates a coefficient of prognosis (CoP) to approximate the quality of the model [28]. To efficiently sample the design space, OptiSLang uses a meta-modeling strategy, more especially the adaptive meta-model of optimum prognosis (AMOP). This method makes use of a coefficient of prognosis (CoP) to estimate the model's quality, assisting in the discovery of the best design options. A comprehensive depiction of the simulation model setup and its incorporation with the design optimization tool is presented in Figure 2.5 [22]. The optimization process can be controlled by defining the objective functions and constraints in both the simulation module and OptiSLang. After the completion of the optimization process, a sensitivity analysis is conducted to ascertain the impact of the selected design variables on the objective functions. Tables 2.5 and 2.6 show the baseline parameters and design variables inputs, respectively, that were used in the heat sink optimization research conducted using ANSYS Icepak and OptiSLang.

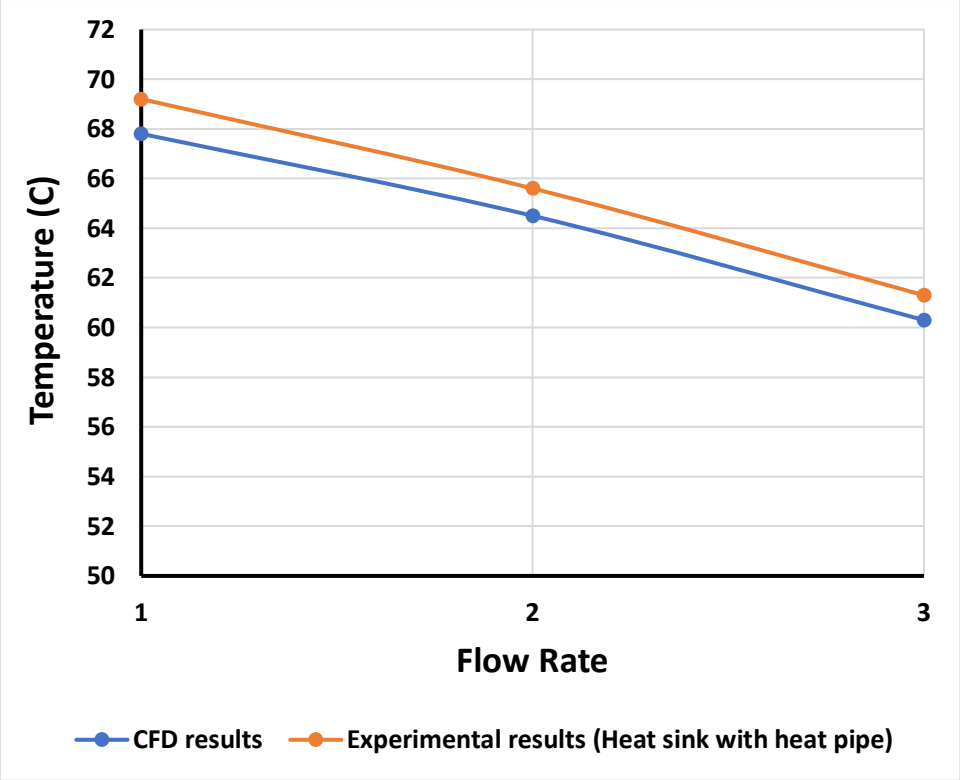

Figure 2.4: Validation of the CFD results with experimental results

Table 2.5: Baseline parameter (constant parameters)

No	Parameters	Values
1	Power	205 W
2	Fluid Flow Rate	1 lpm
3	Fluid Inlet Temperature	40 ºC
4	Heat Sink Base Height	5 mm
5	Heat Sink Base Surface Area	85 x110 mm

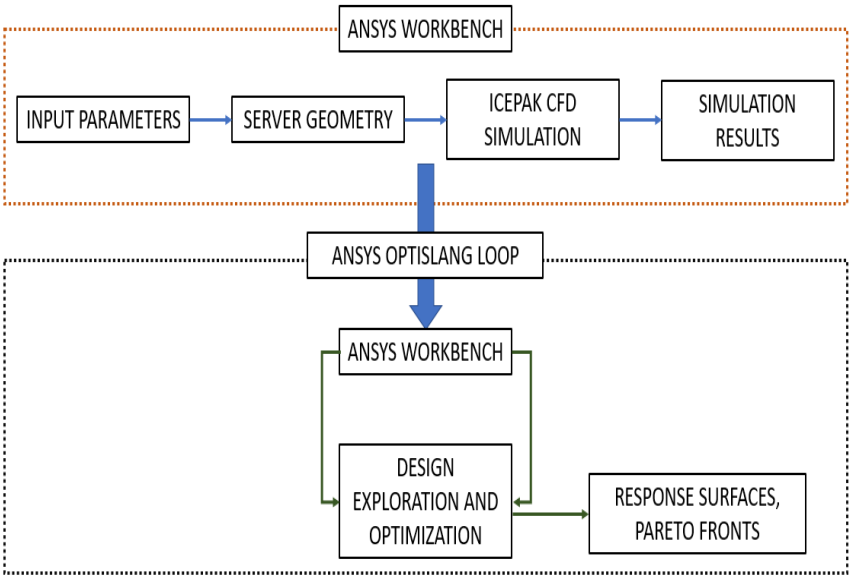

Figure 2.5: Integration of Icepak with OptiSLang on ANSYS Workbench [22]

Table 2.6: Inputs of design variables used for design exploration in OptiSLang (highlighted are baseline values of the parameters)

Constant parameter	Variable parameter	Total number of variable parameter	Total number of run	Number of iterations per run
CPU Power	Fin Thickness	0.3, 0.5, 0.7, 0.9, 1.1, 1.3, 1.5, 1.7	8 x 10	1500
DIMMs Power				
Flow rate	Number of fins	35, 33, 31, 29, 27, 25, 23, 21, 19, 17		
Inlet temperature				

After importing input parameters or design variables into OptiSLang, the program proceeds to automatically build a design of experiments (DoE). The first stage in assessing the impact of the selected design variables on the objective functions, namely thermal resistance in this research, is doing a sensitivity analysis within the context of experimental design. During the design exploration phase, which is often known as the sampling of the solution

space, the main attention is placed on the process of sampling. OptiSLang offers a range of unique sample strategies to fulfill this objective. The present research utilizes AMOP to achieve the stated purpose. Figure 2.6 illustrates the AMOP criteria included in OptiSLang, displaying the input design variable values as well as the objective function. The results obtained from this step include response surfaces, response plots, and the overall effects matrix.

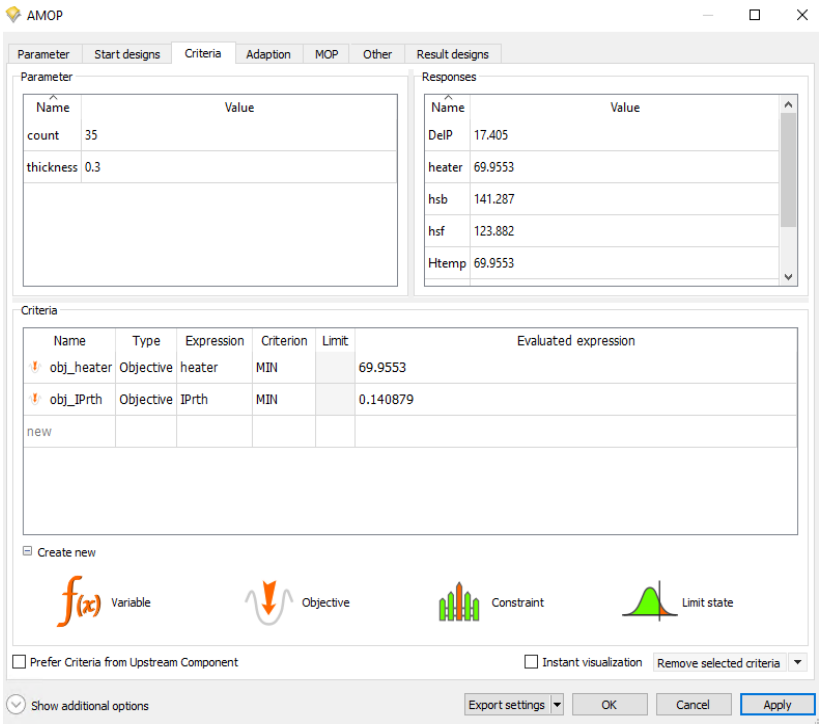

Figure 2.6: OptiSLang AMOP optimization settings for design exploration

2.3 Results

Fig. 2.7 shows the model diagnosis of AMOP prediction, and the root mean square prediction and fitting error is 2.5% and 2.05% respectively. Hence, the outcome of the AMOP was deemed satisfactory for the purpose of examining the effects of parameters and forecasting performance. The visual representation of the input design variables' dependencies in both two-dimensional (2D) and three-dimensional (3D) spaces is achieved through the utilization of linear regression-based plots and response surfaces. The total effects plots for the optimization case of the aluminum heat-sink are depicted in Figure 2.8a. The effect plot serves to quantify

the influence of each input variable on the outputs or post-processing functions. It can be seen that the thermal resistance is predominantly influenced by the thickness of the heat-sink fins and likewise, the number of fins plays a significant role in determining the pressure drop. The number of fins on the heat sink does not exhibit a substantial influence on either thermal resistance [22]. This finding challenges the previously held belief that increasing the number of fins and the corresponding surface area would enhance heat transfer. This factor contributes to the limited heat dissipation capabilities of air-cooling heat sinks when employed in immersion cooling systems. It is evident that all model outputs achieve a linear regression coefficient of prognosis (CoP) value exceeding 96%. This suggests that the sample points were generated using the design variable inputs, resulting in the creation of a highly robust model. In order to examine the combined impact of multiple design variables on the objective function, 3D response surface plots are employed. Figure 2.8b illustrates the inverse relationship between thermal resistance and the increase in fin thickness. The design point highlighted in red on the figure corresponds to the baseline thermal resistance, while the design points highlighted in blue represent heat sinks that have been optimized for thermal resistance. Figure 2.8c displays the response plots illustrating the relationship between the heat-sink fin thickness and number of fins with objective function (thermal resistance). The CoP values of 96% were obtained for all response surfaces of the objective function, indicating the accuracy of the model's approximation of the input design space.

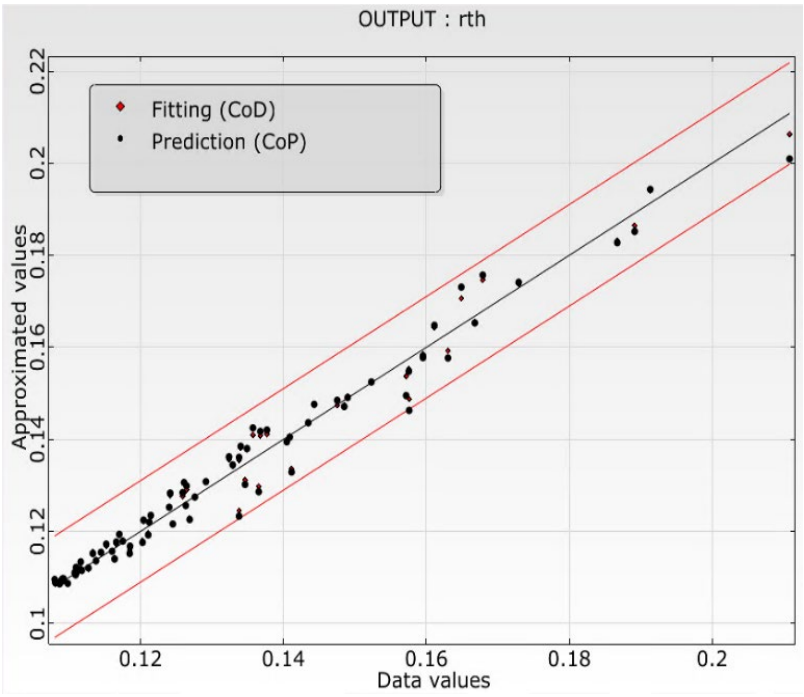

Figure 2.7: AMOP prediction model diagonsis

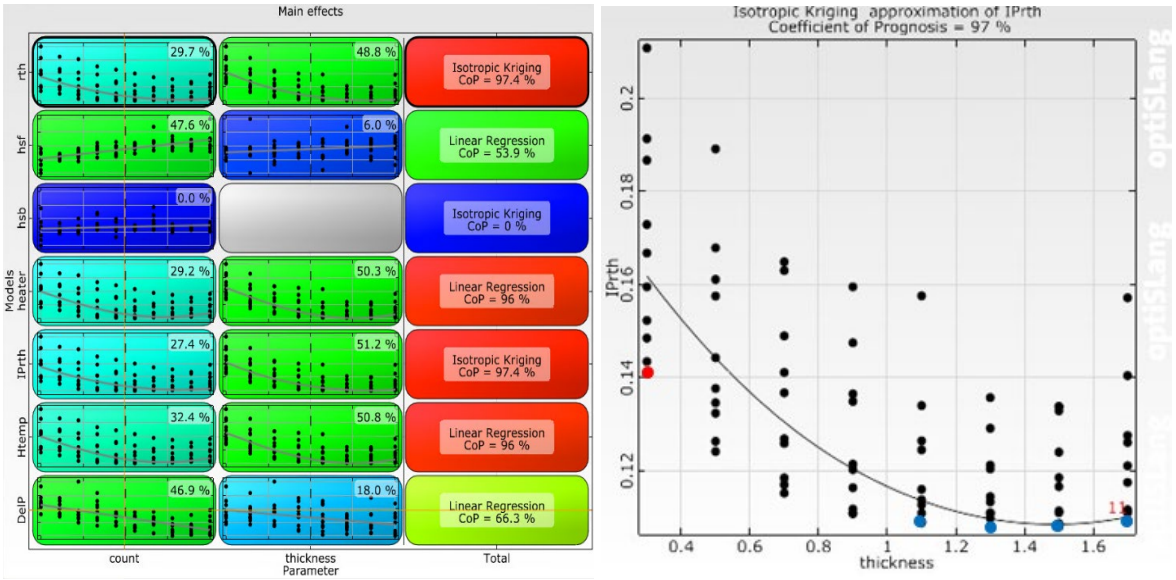

(a) **(b)**

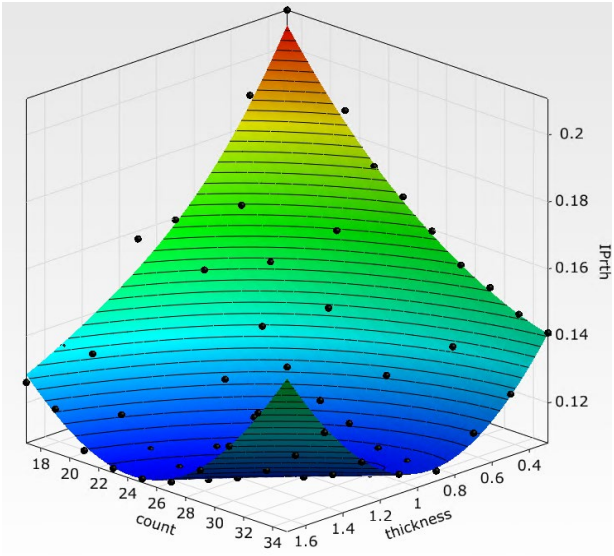

(c)

Figure 2.8: (a)Total Effect plot (b) Relation between thermal resistance and fin thickness (c) 3D response surfaces of the objective functions with varying fin thickness and fin count

After conducting a comprehensive analysis of the notable design points (DPs), it has been determined that five specific design points exhibit a reduction in thermal resistance, as shown in Table 2.7. The data shown in Table 2.7 demonstrates a notable reduction of around 16% in thermal resistance for improved heat sinks with same fin heights, in comparison to the baseline heat sink. After the identification of the optimal parameters for the heat sink, two specific heat sinks were selected for the purpose of experimental investigation. The heat sinks that were chosen for this study had fin thicknesses of 1.1mm and 1.7mm, respectively. The optimized heat sinks were then manufactured using an EDM (Electrical Discharge Machine) and material used for the heat sink is Al-6061 T6. The thermal properties of Al 6061-T6 are provided in table 2.9 [29]. The effectiveness of the optimized heat sink is comprehensively evaluated via experimental validation of the heat sink design obtained from the CFD. Figure 2.9 shows the manufactured heat sink without heat pipes which include design point 42, 13, and 55 with fin thickness 0.3mm (baseline heat sink parameter), 1.7mm and 1.1mm

respectively as mentioned in table 2.7. The experimental condition examined in this study is shown in Table 2.8.

Table 2.7: Summary of best design points showing the values of corresponding objective functions and source temperature

Design points	Number of fins	Fin thickness (mm)	Fin Spacing (mm)	Thermal resistance (W/°C)	Heater Temperature (°C)
42	35	0.3	2.22	0.145	69.3
13	21	1.7	2.5	0.118	64.4
41	23	1.3	2.55	0.119	64.3
47	25	1.5	2.02	0.118	63.9
40	27	1.5	1.75	0.118	64.0
55	29	1.1	1.93	0.119	64.5

Table 2.8: Test condition for Optimized Heat Sink

Description	Test Range
Heat sink fin thickness	1.1mm, 1.7 mm
Flow rate	1-3 LPM
Fluid inlet temperature	40 °C
Heat load	205W

Table 2.9: Thermal properties of Al-6061 T6 [29]

Thermal Properties	Metric
CTE, linear	23.6 µm/m-°C
Specific Heat Capacity	0.896 J/g-°C
Thermal Conductivity	167 W/m-K
Density	2.70 g/cc

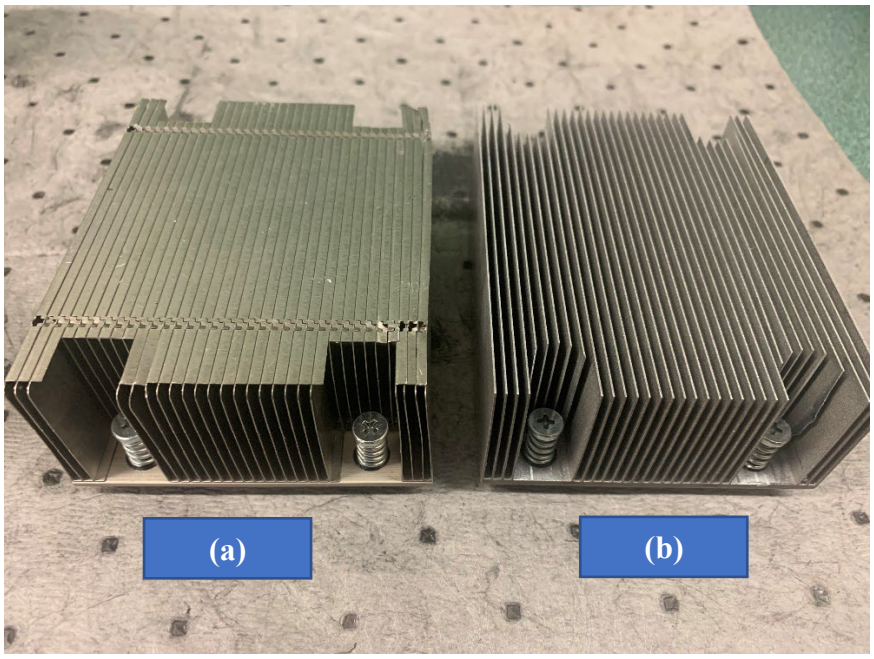

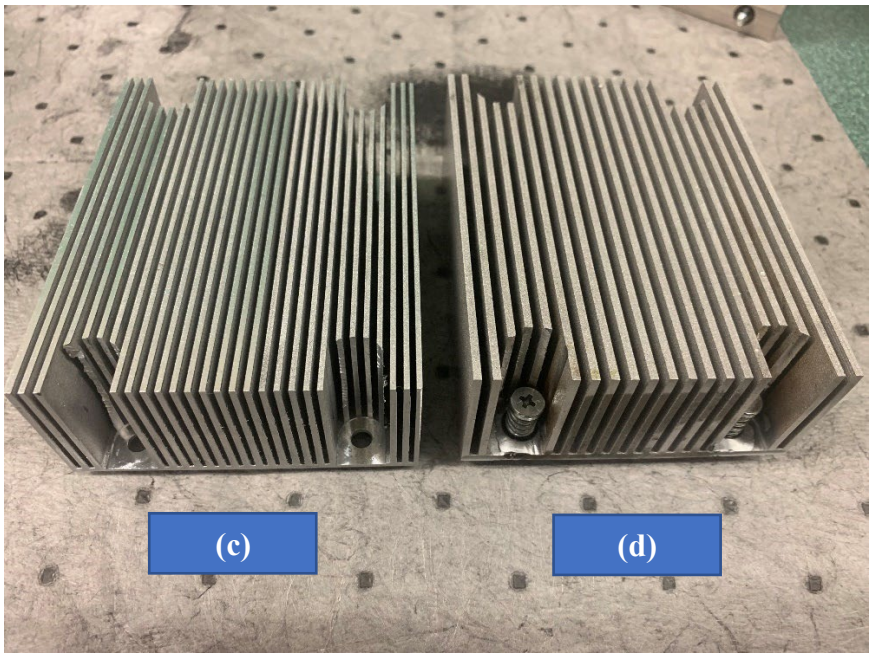

Figure 2.9: Manufactured heat sink: (a) OEM heat sink with heat pipe (b) Baseline heat sink without heat pipe, (b) Optimized heat sink with 1.1mm fin thickness, (c) Optimized heat sink with 1.7mm fin thickness

Table 2.10: Comparison of temperatures of baseline heat sink with heat pipe and manufactured optimized heat sinks without heat pipe

Flow Rate (LPM)	Baseline heat sink with heat pipe (°C)	CFD results of optimized heat sinks with heat pipe (°C)	Baseline heat sink without heat pipe (0.3 mm fin thickness) (°C)	Optimized heat sink without heat pipe (1.7 mm fin thickness) (°C)	Optimized heat sink without heat pipe (1.1 mm fin thickness) (°C)
1	69.3	62.3	80.2	73.5	74.2
2	65.4	60.3	76.3	68.8	69.4
3	62.3	58.6	74.5	66.3	67.1

The cooling performance of air-cooled heatsinks with embedded heat pipe (HPeH) was examined by Wang et al. [30]. Various configurations of embedded heat pipes have been examined, including a U-shape arrangement (referred to as Type-A), an H-shape arrangement (referred to as Type-B), and an asymmetrical U-shape arrangement (referred to as Type-C). The researchers observed that the integration of heat pipes inside the heatsink yields a significant reduction in CPU temperature, while simultaneously enhancing the uniformity of temperature distribution over the heatsink base. In terms of performance, Type-B heat pipes had the most favorable outcomes, characterized by the lowest weight-to-cooling capacity ratio. When comparing HPeH with the heat sink that does not include heat pipes, it is seen that HPeH exhibits a decrease in thermal resistance of 13-17%. The current experimental investigation

demonstrates a similar pattern, whereby the baseline heatsink without a heat pipe demonstrates an approximately 17% increase in surface temperature in comparison to the heatsink fitted with a heat pipe, as seen in Table 2.10. When comparing the experimental findings of an optimized heat sink without heat pipes to the CFD results of the optimized heat sinks, a similar pattern is seen as previously mentioned. This implies that the inclusion of a heat pipe in the experimental study will result in optimum performance that is comparable to the CFD findings.

In the data centers, the vertical dimensions of servers are often denoted by their form factor. As an example, a form factor of 1U is equivalent to a server height of 44.5mm. As mentioned earlier, immersion cooling has a significant benefit in terms of enhanced heat transfer rates when compared to conventional air-cooling methods. As a result, it becomes possible to reduce the form factor or height of the heat sink itself while efficiently dispersing an equivalent heat flow from CPUs. This allows data centers to enhance spatial utilization by integrating effective cooling techniques such as immersion cooling. In this research, the first heat sink configuration was specifically designed to accommodate a 1.5U air-cooled server. An extensive investigation was also carried out to examine the potential for decreasing the height of the heat sink, taking into account the results of optimization. In order to provide a fair comparison with the baseline design, the criteria for selection were if a heat sink of decreased height could attain lower temperatures compared to the baseline design. The findings of the optimization study indicate that the optimized design, which maintains the same CPU power, achieves reduced thermal resistance and source temperature in a more compact form factor, specifically for a heat sink height similar to that of a 1U server. This suggests that, despite a decrease in the total heat transfer area, an optimized immersion cooling heat sink exhibits improved thermal efficiency, as seen in Table 2.11. The optimal choice for the heat sink design results in a thermal resistance reduction of roughly 16% compared to the baseline design.

Table 2.11: Optimized heat sink for different fin heights (red ink: baseline heat sink parameters)

Fin height (mm)	Fin thickness (mm)	Number of fins	Fin spacing (mm)	Heater temperature (°C)	Thermal resistance (W/°C)
42	**0.3**	**35**	**2.22**	**69.3**	**0.145**
19	1.5	25	2.02	64.26	0.118
21	1.5	21	2.72	62.4	0.109
27	1.1	21	3.14	63.8	0.115
25	1.3	21	2.65	63.5	0.115

2.4 Conclusion

The rising power densities of high-performance CPUs need the implementation of effective cooling systems to meet the growing demands. The use of single-phase immersion cooling serves as an effective solution to mitigate various limitations associated with conventional air-cooling methods and competing liquid cooling technologies. In contrast to air-cooling, immersion-cooling has advantages such as increased thermal mass, a more straightforward cooling infrastructure, mitigation of concerns related to airborne pollution, and a specific suitability for the deployment of edge data centers. A comprehensive investigation was conducted to examine various optimization strategies for heat sinks in immersion-cooled servers, focusing on multi-objective and multi-design variable approaches. The geometric characteristics of the heat sink, such as the height of the fins, the thickness of the fins, and the number of fins, were subjected to variation. The objective function used for the optimization research was the minimization of thermal resistance while maintaining constant pumping

power. The findings of the optimization study reveal an evident trend in the context of single-phase immersion cooling. It suggests that thermal performance can be improved by increasing the thickness of the heat sink fins while concurrently reducing the quantity of fins. As compared to the baseline heat sink design, the optimized heat sink was able to reduce the thermal resistance by 16% and the same was verified experimentally by manufacturing the optimized heat sinks.

The outcomes of this investigation, focusing on the impact of heatsink design variables on heat transfer and pumping power, can be readily applied to optimize conventional parallel plate heat sinks intended for single-phase immersion cooling. Further avenues for exploration involve diverse heat sink fin designs and configurations, which can be subjected to optimization analysis. For instance, pin-fin heat sinks, commonly utilized in scenarios of natural convection flows, exhibit a reduced overall heat transfer surface area. By devising an optimized pin-fin geometry, it becomes feasible to simultaneously reduce pressure drop while augmenting heat transfer efficiency. Expanding the scope of this study could encompass a multi-disciplinary optimization approach. This entails considering optimization parameters spanning thermal and flow physics, integrating a cost model for the heat sink, and exploring material optimization based on the thermal profile at the heat sink's base. Such an extension would provide a holistic perspective, enriching the potential of heat sink design optimization.

2.5 References

[1] Andrae, A.S.G., and Edler, T., On Global Electricity Usage of Communication Technology: Trends to 2030. Challenges 2015, 6, 117-157. https://doi.org/10.3390/challe6010117

[2] Masanet, E., Shehabi, A., Lei, N., Smith, S., and Koomey, J., Recalibrating global data center energy-use estimates, Science 367 (2020) 984–986.

[3] Greenberg, S., Mills, E., Tschudi, B., Rumsey, P., and Myatt, B., Best Practices for Data Centers: Lessons Learned from Benchmarking 22 Data Centers, in Proc. of the ACEEE Summer Study on Energy Efficiency in Buildings, Asilomar, CA, pp. 76–87, August 3, 2006.

[4] Siddik, M.A.B., Shehabi, A., and Marston, L., The Environmental Footprint of Data Centers in the United States, Environ. Res. Lett., vol. 16, no. 6, Article ID 064017, 2021.

[5] Erden, H.S., Comprehensive energy and economic assessment of CRAH bypass method in air-cooled data centers. Sustainable Energy Technologies and Assessments, 52, p.102120, 2022.

[6] Kanbur, B., Wu, C., Fan, S., and Duan, F., System-level experimental investigations of the direct immersion cooling data center units with thermodynamic and thermoeconomic assessments, Energy J. 217 (2021), 119373.

[7] Shahi, P., Agarwal, S., Saini, S., Niazmand, A., Bansode, P., and Agonafer, D., CFD Analysis on Liquid Cooled Cold Plate Using Copper Nanoparticles, Proceedings of the ASME 2020 International Technical Conference and Exhibition on Packaging and Integration of Electronic and Photonic Microsystems. ASME 2020 International Technical Conference and Exhibition on Packaging and Integration of Electronic and Photonic Microsystems. Virtual, Online. October 27–29, 2020. V001T08A007. ASME. https://doi.org/10.1115/IPACK2020-2592, 2020

[8] Niazmand, A., Murthy, P., Saini, S., Shahi, P., Bansode, P., and Agonafer, D., Numerical Analysis of Oil Immersion Cooling of a Server Using Mineral Oil and Al2O3 Nanofluid, Proceedings of the ASME 2020 International Technical Conference and Exhibition on Packaging and Integration of Electronic and Photonic Microsystems. ASME 2020 International Technical Conference and Exhibition on Packaging and

Integration of Electronic and Photonic Microsystems. Virtual, Online. October 27–29, 2020. V001T08A009. ASME. https://doi.org/10.1115/IPACK2020-2662, 2020

[9] Shahi, P., Saini, S., Bansode, P., and Agonafer, D., A Comparative Study of Energy Savings in a Liquid-Cooled Server by Dynamic Control of Coolant Flow Rate at Server Level, in IEEE Transactions on Components, Packaging and Manufacturing Technology, vol. 11, no. 4, pp. 616-624, 2021, 10.1109/TCPMT.2021.3067045.

[10] Shahi, P., Deshmukh, A. P., Hurnekar, H. Y., Saini, S., Bansode, P., Kasukurthy, R., and Agonafer, D., Design, Development, and Characterization of a Flow Control Device for Dynamic Cooling of Liquid-Cooled Servers, ASME. J. Electron. Packag., vol 144(4): 041008. https://doi.org/10.1115/1.4052324.

[11] Niazmand, A., Chauhan, T., Saini, S., Shahi, P., Bansode, P.V., and Agonafer, D., CFD Simulation of Two-Phase Immersion Cooling Using FC-72 Dielectric Fluid, Proceedings of the ASME 2020 International Technical Conference and Exhibition on Packaging and Integration of Electronic and Photonic Microsystems. ASME 2020 International Technical Conference and Exhibition on Packaging and Integration of Electronic and Photonic Microsystems. Virtual, Online. October 27–29, 2020, V001T07A009, https://doi.org/10.1115/IPACK2020-2595.

[12] Misale, M., Bocanegra, J., and Marchitto, A., Thermo-hydraulic performance of connected single-phase natural circulation loops characterized by two different inner diameters, International Communications in Heat and Mass Transfer, Volume 125, 2021, 105309, ISSN 0735-1933, https://doi.org/10.1016/j.icheatmasstransfer.2021.105309.

[13] Bansode, P., Shah, J., Gupta, G., Agonafer, D., Patel, H., Roe, D., and Tufty, R. (November 8, 2019). "Measurement of the Thermal Performance of a Custom-Build Single-Phase Immersion Cooled Server at Various High and Low Temperatures for

Prolonged Time." ASME. J. Electron. Packag. March 2020; 142(1): 011010. https://doi.org/10.1115/1.4045156.

[14] Rodríguez, A., Rodríguez, D., Moraleda, A., Bravo, I., Moreno, E., and Notario, A., Atmospheric chemistry of HFE-7300 and HFE-7500: temperature dependent kinetics, atmospheric lifetimes, infrared spectra and global warming potentials, Atmos. Environ. 96 (2014) 145–153.

[15] P.V. Bansode, J.M. Shah, G. Gupta, D. Agonafer, H. Patel, D. Roe, R. Tufty, Measurement of the thermal performance of a single-phase immersion cooled server at elevated temperatures for prolonged time, in: Proceedings of the International Electronic Packaging Technical Conference and Exhibition, 51920, American Society of Mechanical Engineers, 2018 pp. V001T002A010.

[16] Matsuoka, M., Matsuda, K., and Kubo, H., Liquid immersion cooling technology with natural convection in data center, in: Proc. 2017 IEEE 6th Int. Conf. Cloud Networking, CloudNet 2017, Prague,Czech Republic, 2017, pp. 1–7, doi:10.1109/ CloudNet.2017.8071539

[17] Cheng, C., Chang, P., Li, H., and Hsu, F., Design of a single-phase immersion cooling system through experimental and numerical analysis, International Journal of Heat and Mass Transfer, Volume 160, 2020, 120203, ISSN 0017-9310, https://doi.org/10.1016/j.ijheatmasstransfer.2020.120203.

[18] Shao, S., Gao, T., Yang, H., Zhao, J., and Zhang, J., Evaluation of Single Phase Immersion Cooling System for High Performance Server Chassis Using Dielectric Coolants, Proceedings of the ASME 2020 International Technical Conference and Exhibition on Packaging and Integration of Electronic and Photonic Microsystems. ASME 2020 International Technical Conference and Exhibition on Packaging and

Integration of Electronic and Photonic Microsystems. Virtual, Online. October 27–29, 2020. V001T08A010. ASME. https://doi.org/10.1115/IPACK2020-2670

[19] M. Muneeshwaran, M., Lin, Y., Wang, C., Performance analysis of single-phase immersion cooling system of data center using FC-40 dielectric fluid, International Communications in Heat and Mass Transfer, Volume 145, Part B, 2023, 106843, ISSN 0735-1933, https://doi.org/10.1016/j.icheatmasstransfer.2023.106843.

[20] Shrigondekar, H., Lin, Y., and Wang, C., Investigations on performance of single-phase immersion cooling system, International Journal of Heat and Mass Transfer, 2023, 123961, ISSN 0017-9310, https://doi.org/10.1016/j.ijheatmasstransfer.2023.123961.

[21] Li, X., Xu, Z., Liu, S., Zhang, X., and Sun, H., Server performance optimization for single-phase immersion cooling data center, Applied Thermal Engineering, Volume 224, 2023, 120080, ISSN 1359-4311, https://doi.org/10.1016/j.applthermaleng.2023.120080.

[22] Saini, S., Wagh, T., Bansode, P., Shahi, P., Herring, J., Lamotte-Dawaghreh, J., Shah, J.M. and Agonafer, D., A Numerical Study on Multi-objective Design Optimization of Heatsinks for Forced and Natural Convection Cooling of Immersion Cooled Servers, Journal of Enhanced Heat Transfer. DOI: 10.1615/JEnhHeatTransf.202204380.

[23] Sarangi, S., McAfee, E. D., Damm, D.G., and Gullbrand, J., Single-Phase Immersion Cooling Performance in Intel Servers with Immersion Influenced Heatsink Design, 2022, 38th Semiconductor Thermal Measurement, Modeling & Management Symposium (SEMI-THERM), 2022, pp. 1-5.

[24] Herring, J., Smith, P., Lamotte-Dawaghreh, J., Bansode, P., Saini, S., Bhandari, R., and Agonafer, D., Machine Learning Based Heat Sink Optimization Model for

Single-Phase Immersion Cooling ASME 2022 International Technical Conference and Exhibition on Packaging and Integration of Electronic and Photonic Microsystems. Garden Grove, California, USA. October 25–27, 2022. V001T01A016. ASME. https://doi.org/10.1115/IPACK2022-97481

[25] Chiang, K., and Chang, F., Application of response surface methodology in the parametric optimization of a pin-fin type heat sink, International Communications in Heat and Mass Transfer, Volume 33, Issue 7, 2006, Pages 836-845, ISSN 0735-1933, https://doi.org/10.1016/j.icheatmasstransfer.2006.04.011

[26] Holman, J.P., Experimental Methods for Engineers, 2012.

[27] Ong, K., Tan, C., Lai, K., and Tan, K., Heat spreading and heat transfer coefficient with fin heat sink, Appl. Therm. Eng. 112 (2017) 1638–1647.

[28] Mimery, D.R., Multidisciplinary Design Optimization of Part Geometry in CAD, MS, Massachusetts Institute of Technology, USA, 2020.

[29] https://www.matweb.com/search/datasheet_print.aspx?matguid=1b8c06d0ca7c456694c7777d9e10be5b

[30] Yabo Wang, Bin Wang, Kai Zhu, Hailong Li, Wei He, Shengchun Liu, Energy saving potential of using heat pipes for CPU cooling, Applied Thermal Engineering, Volume143, https://doi.org/10.1016/j.applthermaleng.2018.07.132.

Chapter 3 Experimental Analysis of Heat Transfer and Pressure Drop in Aluminum Metal Foams Immersed in Dielectric Synthetic Fluid

3.1 Introduction

The data center and information technology sectors are subject to continuous evolution, driven by the rising power density of electronic packages. This increase in power density is primarily attributed to the growing demand for high-performance computing servers, which are utilized for various purposes such as cryptocurrency mining, cloud computing, the Internet of Things, and machine learning applications. The rise in demand is addressed by the process of scaling transistors to almost atomic dimensions, which allows for greater integration densities in packaging and subsequently leads to better power density [1]. The energy consumption attributed to the cooling of high-power density servers in data centers globally has been steadily increasing. Specifically, in 2005, the electricity consumption for this purpose accounted for 1% of the total global electricity consumption. By 2010, this figure had risen to 1.5%, indicating a 33% increase compared to the 2005 levels. Based on data provided by the Japanese Ministry of Economy, it is projected that this figure will increase by more than five times by the year 2025. The allocation of power consumption inside the data center may be categorized into different components. According to sources [2, 3], about 52 percent of the electricity is used by the IT infrastructure, while 38 percent is dedicated to the cooling system. The remaining 10 percent is allocated for supporting equipment and other related purposes. Historically, air has been conventionally used as the primary cooling agent in data centers, serving to absorb the heat produced by IT equipment. The thermal energy is transferred to the environment, where it undergoes either a process of blending with incoming ambient air or is subjected to cooling by refrigeration mechanisms. One of the primary difficulties associated with the increasing power densities of electronic components is the ongoing task of efficiently

dissipating heat from data centers. This challenge arises from the fact that air, which is often used for cooling purposes, exhibits limited effectiveness owing to its low specific heat capacity and inadequate thermal conductivity [4, 5]. Due to the drawbacks associated with conventional air-cooling technology, there has been much discourse focused on exploring alternative and more efficient cooling methods that provide additional advantages such as waste heat recovery [6, 7]. In response to the increasing power densities, a number of data center operators are using novel approaches, such as immersion cooling, to address the cooling requirements of high-power IT equipment.

In comparison to forced convection air cooling, single-phase liquid immersion cooling (Sp-LIC) has significant benefits, including increased thermal mass and enhanced heat dissipation by direct contact of dielectric fluids with each component [8]. Additionally, the improvement of dependability is facilitated by the shielding of the ITE from pollutants and severe environmental conditions. This shielding also contributes to reduced capital expenditure (CapEx) and energy expenses, since it eliminates the need for fans and computer room air handler units [9]. In contrast to direct-to-chip liquid cooling, Sp-LIC does not need a complex liquid distribution manifold design, making it a more favorable option for edge and modular data center applications [10, 11]. The complete immersion of servers in dielectric fluids offers several immediate benefits. These include the removal of server components from a harsh environment, a reduction in failures caused by fan vibrations, and the elimination of the necessity to cool peripheral components, as the coolant directly contacts the hot modules [12]. When immersing an air-cooled server in dielectric fluid, several meticulous design issues must be taken into account. These include the removal of fans, the sealing of hard drives, the design of the heat sink, and the resolution of compatibility challenges.

The second half of the 20th century saw significant progress in manufacturing technology, leading to a marked rise in the occurrence of metal foams. This phenomenon may

be ascribed to the ability to generate substantial quantities of high-quality foams using various metal alloys. Metal foams are a kind of cellular structured material characterized by a random arrangement of linked pores, often possessing consistent dimensions and morphology. Metallic foams find extensive applications in diverse domains, including multifunctional heat exchangers, cryogenics, combustion chambers, cladding on buildings, strain isolation, buffering between rigid structures and fluctuating temperature fields, geothermal operations, petroleum reservoirs, compact heat exchangers for airborne equipment, air-cooled condensers, and heat sinks for power electronics. The foam structure can be characterized by two parameters: porosity ε and pore density PPI. Porosity ε is defined as the ratio of the total void volume to the total volume occupied by the solid matrix and void volumes. Pore density, denoted as PPI, is determined by counting the number of pores within a 25.4 mm area.

Several research have been undertaken to enhance the effectiveness of heat dissipation in forced convective cooling by the use of heat sinks with diverse configurations, materials, flow patterns, and other pertinent variables [13]. Hsieh et al. [14] conducted an experimental investigation on the heat-transfer properties of heat sinks made of aluminum foam. A positive association was seen between the Nusselt number and both porosity and pore density. The researchers have reached the conclusion that there is a negative correlation between the Reynolds number and the temperatures of both the solid and gas phases of the aluminum foam. The observed occurrence may be ascribed to the increased convective heat transfer rate that is associated with higher Reynolds numbers. This material facilitates substantial heat transfer because to its considerable surface area to volume ratio, estimated to be over 1000-3000 m2/m3 [15]. In their study, Hamadouche et al. [16] conducted an empirical examination to examine the heat transfer characteristics of aluminum foam samples under conditions of turbulent forced convection. The foams were arranged in a staggered configuration inside a rectangular channel, occupying both the bottom and top walls. The study's findings indicate that the addition of

metallic foam blocks has the capacity to augment the levels of turbulent kinetic energy in the interface wall of free space, thus promoting heat transfer.

Bayomy and Saghir [17] conducted a thermal performance investigation of a finned aluminum heat sink with two, three, and four channels using experimental and computational methods. The research revealed that the mean Nusselt number of heat sinks including three channels exhibited a 17% improvement compared to heat sinks with two channels, and a 30% improvement compared to heat sinks with four channels. In their study, Mancin et al. (2018) performed an experimental investigation aimed at quantifying the heat transfer occurring during the passage of airflow through seven distinct samples of aluminum open-cell foam. These samples were characterized by variations in terms of PPI (pores per inch), porosity, and foam core height. The study included a broad spectrum of air mass velocities, allowing for a comprehensive examination of the heat transfer phenomena. The study's findings indicate that, when considering a constant number of pores per inch (PPI), there is a positive correlation between the global heat transfer coefficient and decreasing porosity. In a previous work conducted by Mancin et al. (19), the authors published experimental findings on heat transfer and pressure drop measurements in relation to forced convection of air through four distinct types of aluminum foams. The researchers conducted experiments on aluminum foams with varying pore densities of 5, 10, 20, and 40 pores per inch (PPI). The foams exhibited porosity levels ranging from around 0.92 to 0.93, with a foam core height of 0.02 meters. The researchers noted that, despite the 5 PPI and 40 PPI 20 mm high samples having twice the surface efficiency and almost half the heat transfer area compared to the 40 mm high samples, their global heat transfer coefficients were found to be virtually equal. In their study, Mancin et al. (2020) provided an analysis of heat transfer and pressure drop characteristics for a set of five distinct copper foams. These foams were produced by the casting method and had varying pore per inch (PPI) values of 5, 10, 20, and 40, with corresponding porosity levels ranging from

0.905 to 0.934. The results of the experiment suggest that the copper foam with a porosity of 10 pores per inch (PPI) has favorable characteristics for the advancement of thermal management systems in electronic cooling applications, owing to its efficient heat transfer properties. In their study, Younis and Viskanta (21) did an experimental investigation with the objective of establishing the volumetric heat transfer coefficient between ceramic foams, namely alumina and cordierite, and a heated air stream. The aim was achieved by the researchers via the use of a single-blow transient approach. The researchers have determined that there is a notable correlation between the volumetric heat transfer coefficient and the exponents of the Reynolds number, with respect to the mean pore diameter.

Numerous investigations have used water as the primary medium throughout experimental procedures. Baymony et al. [22] did a comprehensive study whereby they used both experimental and computational methods to examine the heat transfer characteristics and efficiency of aluminum parallel plate heat sinks that were infused with aluminum foam. The heat sinks were exposed to a continuous water flow under non-Darcy flow conditions, characterized by Reynolds numbers ranging from 297 to 1353. The results suggest that, for a given Reynolds number, the local Nusselt number has an inverse correlation with the boundary layer thickness and reaches a constant value in the completely developed area. The empirical study done by Fu et al. (24) aimed to analyze the heat transfer properties of a porous channel subjected to oscillatory flow. The findings of the research demonstrate that, in the case of both steady and oscillatory flows, an augmentation in the ligament Reynolds number leads to a corresponding augmentation in both the local and length averaged. Nusselt numbers. The use of a porous material with high conductivity in a channel subjected to oscillating flow gives a unique and efficient strategy for the cooling of electronic equipment. The research conducted by Li et al. (25) examined the fluid flow and heat transfer characteristics of an aluminum foam heat sink equipped with pin fins, referred to as the AFPF heat sink. Based on the findings of

the research, it has been determined that the thermal efficiency of an Active Flow and Porous Fins (AFPF) heat sink is 1.5 times greater than that of an aluminum foam heat sink, when both are subjected to identical pumping power.

Prior studies have thoroughly examined the thermohydraulic characteristics of heat sinks made of metal foam, focusing on the use of air and water as cooling mediums. Nonetheless, it is worth mentioning that there exists a significant dearth of scholarly investigations pertaining to the use of metal foam heat sinks in single-phase immersion cooling. The objective of this study is to empirically examine the heat transfer properties of an atypical heat sink composed of Aluminum metal foam, while it is submerged in a synthetic dielectric fluid known as EC100. In this study, metal foams with different Pore Per Inch (PPI) values (namely 5, 10, 20, and 40) and a relative density ranging from 10.75% to 12.3% are used for analysis. The experiment consisted of submitting the metal foams to various flow rates (0.2 lpm, 0.5 lpm, and 0.8 lpm), heat fluxes (60 kW/m^2 and 80 kW/m^2), and input temperatures (20°C, 30°C, and 40°C).

3.2 Experimental setup

The experimental configuration comprises a variety of components that have been used to investigate the phenomena of heat transfer and fluid flow in metal foams. The experimental configuration is shown in Figure 3.1(a). The thermal test vehicle, shown in Figure 3.1(c), is positioned inside a tank made of acrylic glass, as seen in Figure 3.1(b), with dimensions of 0.381m x 0.1524m x 0.1143m. The coolant used in the loop is ElectroCool (EC-100), and its characteristics are shown in table 1 [26]. The flow rate within the acrylic tank was quantified by employing Keyence clamp-on microflow sensors, specifically the Keyence FDX-A1 model, which offers a precision of ±0.3 of the reading. Simultaneously, the temperatures at the inlet and outlet of the tank were monitored using 10k thermistors with an accuracy of ±2°C.

Additionally, the pressures at these points were measured using Keyence GPM010 pressure sensors. In order to get the experimental data, it is necessary to calibrate all the sensors and establish a connection with the data collecting system, namely the DAQ Agilent 37940A. The output signals of the pressure and flow sensors have a range of 5 to 20 mA.

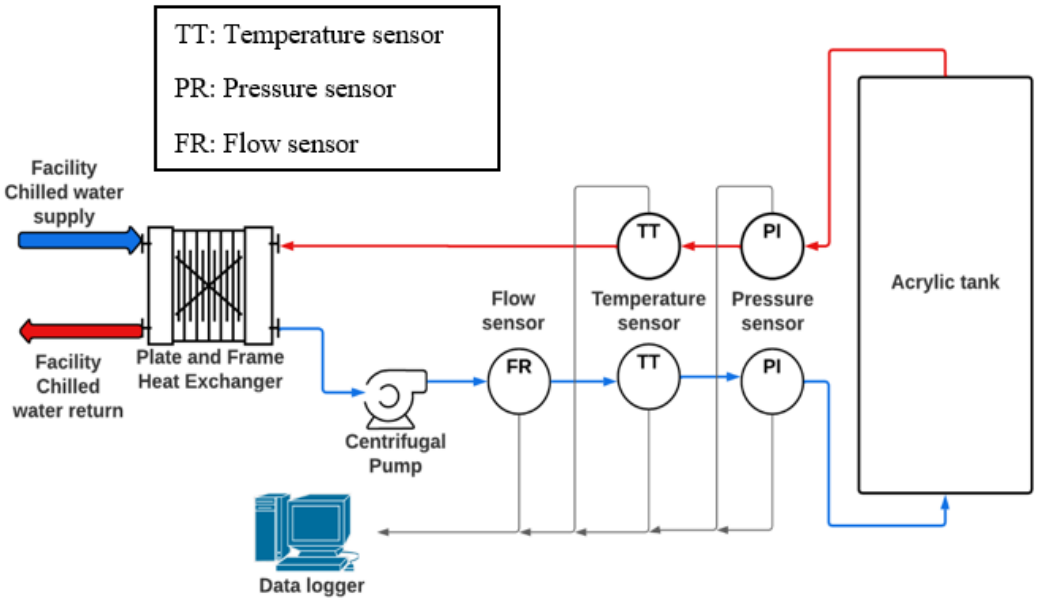

(a)

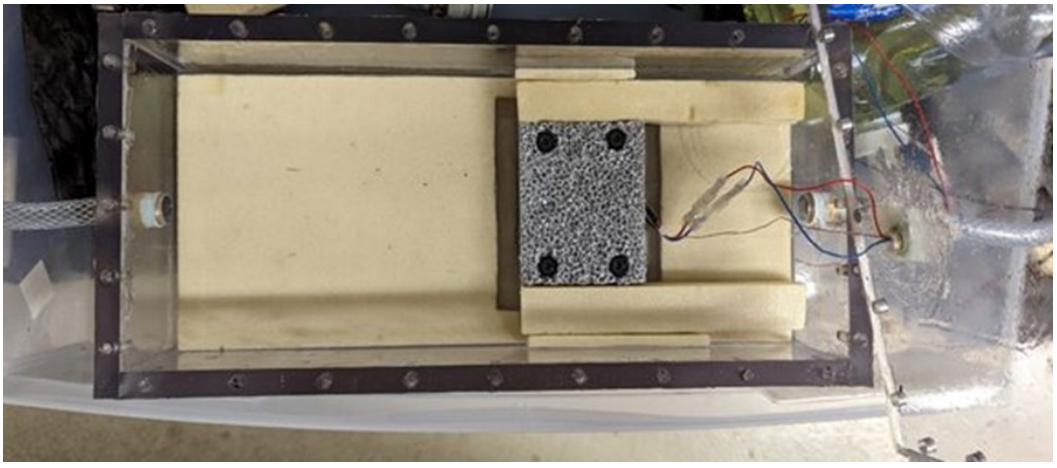

(b)

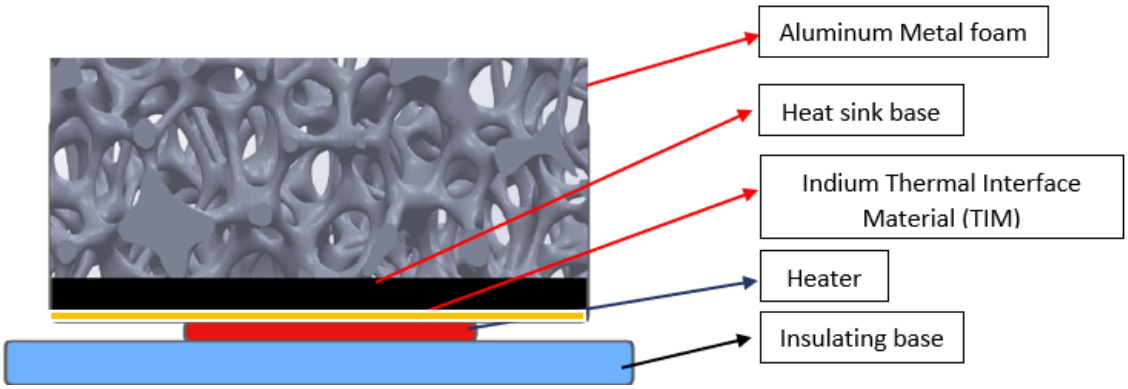

(c)

Figure 3.1: (a) Schematic of the experimental setup, (b) 5PPI metal foam with 10-12% relative density (flow direction is from left to right), (c) Thermal Test vehicle (TTV) and metal foam schematic

The experimental setup used in the study is shown in Figure 3.1(a) using a schematic design. The Thermal Test Vehicle (TTV) comprises an insulating plate composed of a half-inch acrylic substance, onto which the assembly of a ceramic heater and a metal foam heat sink was affixed. The measurements of the aluminum metal foam specimen are 76.2mm in length, 88.9mm in width, and 12.7mm in thickness. The metal foam is securely attached to an aluminum plate, which functions as a heat sink foundation, measuring 5mm in thickness. The heater is constructed using aluminum nitrite as its material and has a surface groove designed to accept a K-type thermocouple. This thermocouple, known for its precision of ±0.5 °C, is used to measure the temperature of the heater's surface. The thermal interface material (TIM) used in this scenario is indium foil, while the heat sink's spring retention mechanism experiences a torque of 0.9 N-m. The use of torque is implemented in adherence to the rules delineated in the thermal-mechanical specifications and design guide [27]. The pressure exerted on the thermal interface material was determined to be around 213.7 kilopascals. Figure 3.2(a) illustrates the metal foam given by the manufacturer, while Figure 3.2(b) showcases the machined holes inside the metal foam. These apertures are designed to assist the spring

retention mechanisms of the heater assembly. The machined metal foams with different PPIs are shown in Figure 3.3.

(a) **(b)**

Figure 3.2: (a) 5 PPI metal foam from the manufacturer, (b) Machined hole in the metal foam

Table 3.1: EC-100 Properties

Temperature (°C)	Kinematic Viscosity (cSt)	Diffusivity (cm^2/s)	Dynamic Viscosity (kg/m-sec)	Density (kg/m^3)	Thermal Conductivity (W/m/K)	Specific Heat (kJ/kg-K)
0	74.26	0.7426	0.0638	859.06	0.1404	2.0577
10	42.04	0.4204	0.03583	852.46	0.13965	2.0987
20	25.93	0.2593	0.02193	845.86	0.1389	2.1337
30	17.14	0.1714	0.01439	839.26	0.13815	2.1717
40	11.99	0.1199	0.00998	832.66	0.1374	2.209

50	8.78	0.0878	0.00725	826.06	0.13665	2.2477
60	6.68	0.0668	0.00547	819.46	0.13559	2.2857
70	5.24	0.0524	0.00426	812.86	0.13515	2.3237
80	4.22	0.0422	0.0034	806.26	0.1344	2.3617
90	3.48	0.0348	0.00278	799.66	0.13365	2.3997
100	2.92	0.0292	0.00232	739.06	0.1329	2.436

3.2.1 Sensor calibration

Precise calibration of sensors is a fundamental element in any scientific investigation. The sensors utilized in this study were calibrated through the manufacturer's prescribed technique and standard calibration methodologies. The calibration of the flow sensor was performed at different inlet temperatures using the Coriolis flow meter. The Coriolis flow meter exhibits a precision level ranging from +/- 0.1% to 0.5% of the measured quantity in both gaseous and aqueous mediums. The discrepancy observed in the readings obtained from the Coriolis flow meter and the Keyence FDX-A1 flow sensor was rectified by adjusting the span of the FDX-A1 flow sensor. The present study utilized Keyence GP-M010 pressure sensors, which underwent calibration procedures utilizing a Fluke P5510-2M Pneumatic Comparison Test Pump. The GP-M010 pressure sensor and reference pressure gauge were affixed to the left and right sides of the test pump, correspondingly. The test rig's pressure was augmented by utilizing a hand pump, while the spinning knob was employed to sustain the pressurization of the test pump. The recorded sensor and reference gauge readings were subjected to error analysis. The 10k thermistors and K-type thermocouples underwent calibration through the utilization of thermal bath equipment. The calibration protocols for all temperature sensors are outlined as follows:

1. The temperature of the bath was reduced from ambient to 5 °C and sustained for a duration of 15 minutes.

2. Following a 15-minute interval, the temperature of the bath was elevated at a rate of 5°C per minute until it reached 85°C, at which point it was sustained for an additional 15 minutes.

The data acquisition equipment (DAQ) was utilized to record temperatures from all sensors at 30-second intervals. The procedure was iterated thrice to determine the uncertainty by computing the mean of the deviations from every sensor.

3.2.2 Methodology

The purpose of this investigation was to perform heat transfer studies in order to evaluate the thermal-hydraulic efficiency of metal foam samples with varying pore per inch (PPI) values, namely 5, 10, 20, and 40. The parameters of the foam are shown in Table 3.2. The experimental parameters included the manipulation of the input fluid temperature within the range of 20°C to 40°C, the heat flux varying between 60 kW/m^2 to 80 kW/m^2, and the flow rate ranging from 0.2 LPM to 0.8 LPM. The left-to-right direction of fluid flow inside the tank is seen in Figure 3.1(c). The use of the Agilent 34972A data collection system, in conjunction with data acquisition software, enabled the continuous monitoring of temperature and the real-time reporting of data. After achieving a state of equilibrium for a specific heat flux and flow rate, in which the temperatures of the incoming and outgoing fluids remain constant, the software logs the sampling rate of temperature, flow rate, and pressure data at regular 10-second intervals throughout the entire duration of the experiment. Following each trial, the power supply to the heater was deactivated, allowing the system to complete a cooling process until the temperatures of the fluid at the input and output locations reached equilibrium. The subsequent sequence of experiments commences subsequent to the attainment of a condition

of equilibrium within the system, after which the procedure of data collecting is resumed. The experimental protocols of the investigation are detailed in Table 3.3.

Table 3.2: Characteristics of the metal foam samples, Alloy-AL 6101-T6

Length (L)	**Span (W)**	**Fin Height (H)**	**PPI**	**Relative Density (Actual)**	**Porosity Foam Area per Unit Volume (a_f)**	**Heat flux direction (k_e)**	**Porosity**	**Ligament thickness**
M	m	m		%	m^2/m^3	W/m-K	ϵ	m
0.0889	0.0762	0.0127	5	12.2%	561	8.87	0.878	6.3E-4
0.0889	0.0762	0.0127	10	12.3%	627	8.94	0.877	5.5E-4
0.0889	0.0762	0.0127	20	10.7%	818	7.78	0.893	3.8E-4
0.0889	0.0762	0.0127	40	11.2%	955	8.14	0.888	3.1E-4

Table 3.3: Experiments Performed

PPI	**Power (W)**	**Inlet temperature**	**Flow rate (lpm)**
5	150, 200	20, 30, 40	0.2, 0.5, 0.8
10			
20			
40			
Total number of experiments performed			72

3.3 Data reduction and uncertainty analysis

The overall heat transfer coefficient HTC* is calculated by equation 1. The derivation of equation 1 is provided in the appendix (section 6).

$$Q = \eta_o \times A \times \Delta T \times h = HTC^* \times A_b \times \Delta T \quad (1)$$

Where Q is the power, η_o is overall surface area efficiency, A is the total heat transfer area, A_b is the base area of the heat sink, h is the local heat transfer coefficient and

$$\Delta T = T_s - T_{avg\ fluid},\ T_{avg\ fluid} = \frac{T_{outlet\ fluid} + T_{inlet\ fluid}}{2} \quad (2)$$

T_s is the surface temperature of the heater and $T_{avg\ fluid}$ is the average temperature. The thermal resistance can be calculated by

$$R_{th} = \frac{T_s - T_{inlet\ fluid}}{\mathrm{Q}} \quad (3)$$

Considering the flow through the metal foam, the experimental pressure drop calculation can be discussed through equation 4 [28]. This is the widely accepted pressure drop gradient in a rigid porous media equation.

$$-\frac{dP}{dz}\frac{1}{u} = \frac{\mu}{K} + \frac{\rho f u}{\sqrt{K}} = A + \rho.C.u = A + B.u \quad (4)$$

where the first term A is the Darcy term which explains the linear dependency of pressure drop on flow velocity at low mass flow rates and B is the inertia constant. According to Darcy's Law, the permeability (K) of the metal foams is the measure of the flow conductance of the matrix. ρ is the density of the fluid, C is the form coefficient, u is the average velocity, and the inertia coefficient f depends on the internal structure of the foam. Fin parameter, fin efficiency, and overall surface area efficiency can be calculated by equations 5, 6, and 7 respectively.

$$m = \sqrt{\frac{HTC^* \times a_f}{k_e}} \quad (5)$$

$$\eta_f = \frac{Tanh(mH)}{mH} \quad (6)$$

$$\eta_o = 1 - \frac{A_f}{A}(1 - \eta_f) \quad (7)$$

where,

$$A = A_f + A_b - A_c \quad (8)$$

$$A_f = L \times B \times H \times a_f \quad (9)$$

$$A_c = (1 - \varepsilon)A_b \quad (10)$$

$$\varepsilon = 1 - \frac{\rho_{foam}}{\rho_{metal}} \quad (11)$$

where A_f is foam surface area, a_f is the foam area per unit volume, A is the total heat transfer area, A_b is the base area of the heat sink, A_c is the foam effective conduction area, k_e is the effective thermal conductivity. L, B, and H are the length, breadth, and height of the foam respectively and the porosity of the foam ε is provided by the manufacturer.

Uncertainty Analysis:

Errors in experimental measurements and techniques are inherent, thus, an uncertainty analysis is required to verify the correctness and dependability of the outcomes. The measured uncertainty values for each sensor and instrument are shown in table 3.4.

The uncertainty for the heat transfer coefficient is calculated by equation 12 [23].

$$\frac{\delta h}{h} = \sqrt{(\frac{\delta Q_{in}}{Q_{in}})^2 + (\frac{\delta T_s}{T_s - T_{in}})^2 + (\frac{\delta T_{in}}{T_s - T_{in}})^2} \quad (12)$$

Error assessments revealed that the heat transfer coefficient, pressure gradient, and thermal resistance have an average uncertainty of 2.5%, 0.5%, and 1% respectively.

Table 3.4: Experimental Uncertainty

Sensor/Equipment	Uncertainty values
Flow sensor	0.2%
Pressure sensor	0.5%
K type thermocouple	±1 °C
10kΩ thermistors	±1 °C
Power meter	±0.13% of the reading

3.4 Results and discussion

The experimental data are provided in the form of overall surface area efficiency, thermal resistance, local and overall heat transfer coefficient, and the pressure difference across the heat sink. The overall surface area efficiency is a critical characteristic that determines the heat transfer performance of the foams. In metal foams, temperature decays exponentially with distance from the heated base. At a dimensionless distance of roughly 0.3 from the heated base, the temperature of the foam reaches that of the ambient and as a result, the surface heat transfer area efficiency of the examined metallic foams is quite poor [28]. The overall surface efficiency in the current study is computed from equation 7, which depends on the fin parameter (m) and fin efficiency (η_f). Figure 3.7 depicts the overall surface area efficiency of various foams in relation to flow rate, and it appears that overall surface area efficiency declines as the number of pores per inch (PPI) increases and furthermore, when the flow rate increases, efficiency diminishes. When all four foam samples are compared, the overall surface area efficiency of 5 PPI and 10 PPI foam is much higher than that of 20 PPI and 40 PPI foam. The study conducted by Mancin et al. [18], and Mancin et al. [19] explained the phenomena using the classical fin-efficiency theory. The efficiency of a solid fin, as per the classical fin-efficiency theory, depends on fin thickness. According to studies [18, 19], the efficiency of a fin increases as its

thickness increases but decreases as its length increases. Applying this observation to foam heat sinks, the metal foam sample with a pore count of 5 PPI (pores per inch) has the thickest fibers compared to the 40 PPI sample, as shown in table 3.2. Consequently, the 5 PPI sample has approximately eight times fewer pores, resulting in shorter optimal fibers extending from the heat sink base plate to the top surface [18, 19]. This behavior resembles that of a solid fin, which exhibits higher efficiency in terms of surface area. The overall surface area efficiency plot indicates that this heat sink is taller than necessary, and HTC* has an asymptote, which suggests that any height more than 0.0127m will display the same HTC*.

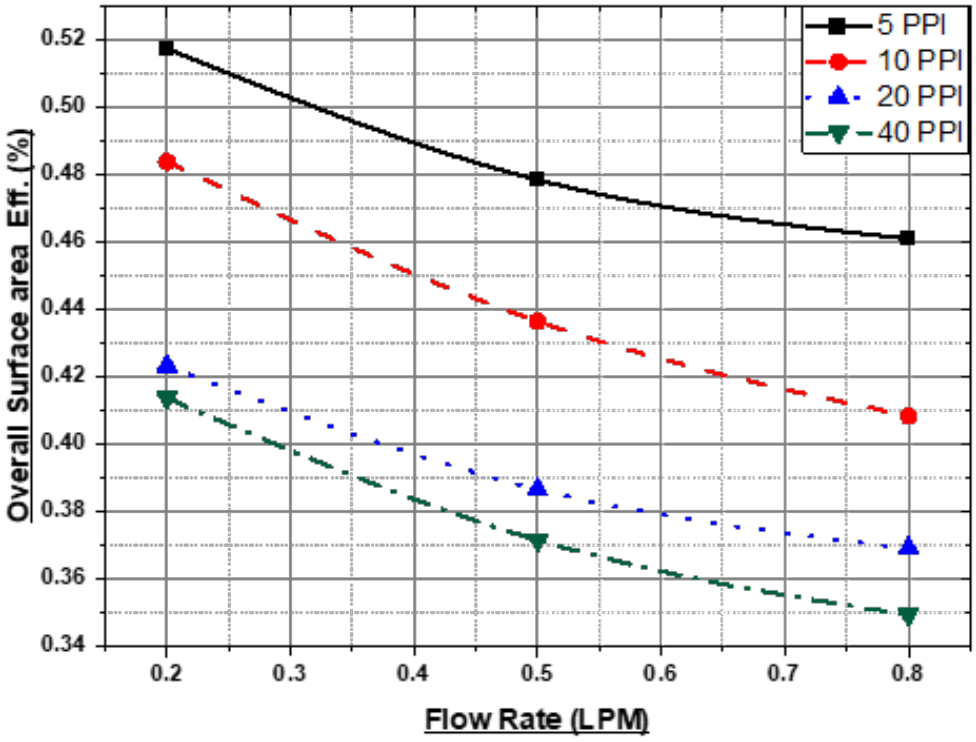

Figure 3.7: Overall surface area efficiency vs Flow rate

The convective heat transfer coefficient serves as an indicator of the thermal efficiency shown by the porous heatsink. The researchers conducted a series of experimental studies to investigate the influence of foam structure on the progression of thermal phenomena. The primary objective of this investigation was to measure the comprehensive heat transfer coefficient (HTC). This was accomplished by considering many factors, including pores per

inch (PPI), incoming fluid temperature, heat flux, and flow rate. The experimental results on the impact of flow rate on the overall and local heat transfer coefficients for different heatsinks with varying pores per inch (PPI) are shown in Figures 3.8 and 3.9. The heat fluxes used in the study were 60 kW/m^2 and 80 kW/m^2, with the input temperatures varying between 20°C and 40°C. The pore densities of all four heatsinks showed little variance. The general heat transfer coefficient (HTC*) exhibited a positive correlation with the flow rate, however, it showed a decrease of 7.14% as the fluid input temperature increased from 20°C to 40°C. Significantly, the HTC (Heat Transfer Coefficient) exhibited no discernible impact from the applied heat flux. Figure 3.9 depicts the local heat transfer coefficient for heatsinks with 5PPI and 10PPI, showcasing comparable performance across all situations at a flow rate of 0.2 LPM. Remarkably, despite possessing a lesser surface area in comparison to the 20PPI and 40PPI heatsinks, the 10PPI heatsink exhibited superior performance throughout all conducted testing. The observed effect may be ascribed to the presence of 10PPI foams, which provide ideal turbulence conditions inside their structure, hence facilitating efficient heat exchange. This assertion is substantiated by prior investigations [15, 28, and 29].

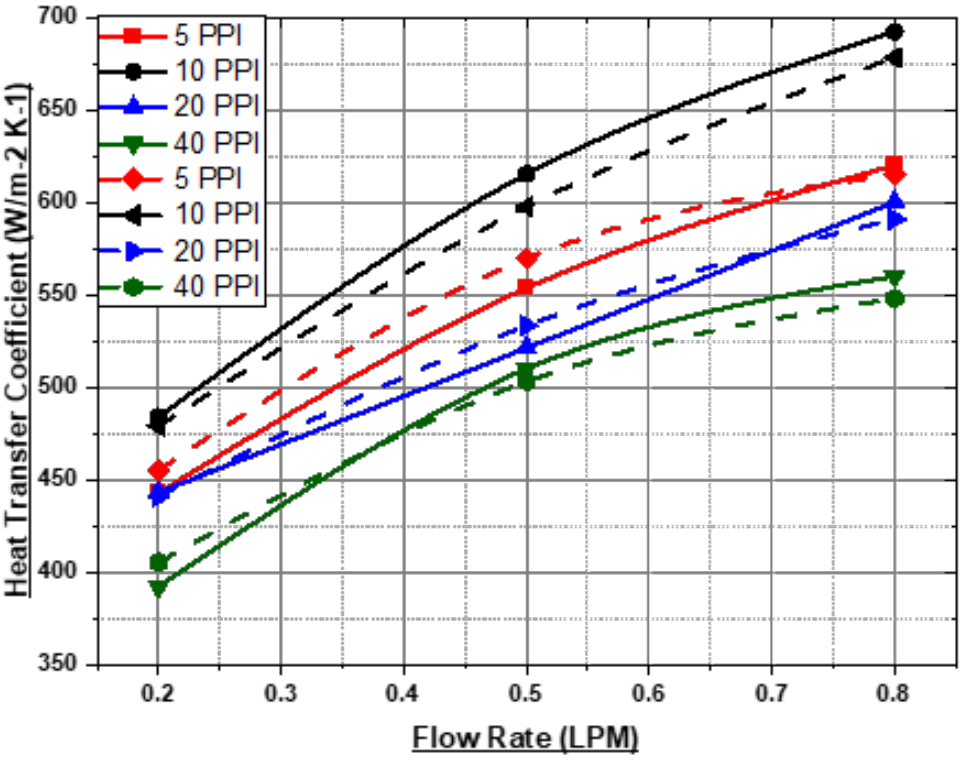
5 PPI
10 PPI
20 PPI
40 PPI
5 PPI
10 PPI
20 PPI
40 PPI
Heat Transfer Coefficient (W/m-2 K-1)
700
650
600
550
500
450
400
350
0.2
0.3
0.4
0.5
0.6
0.7
0.8
Flow Rate (LPM)

(a)

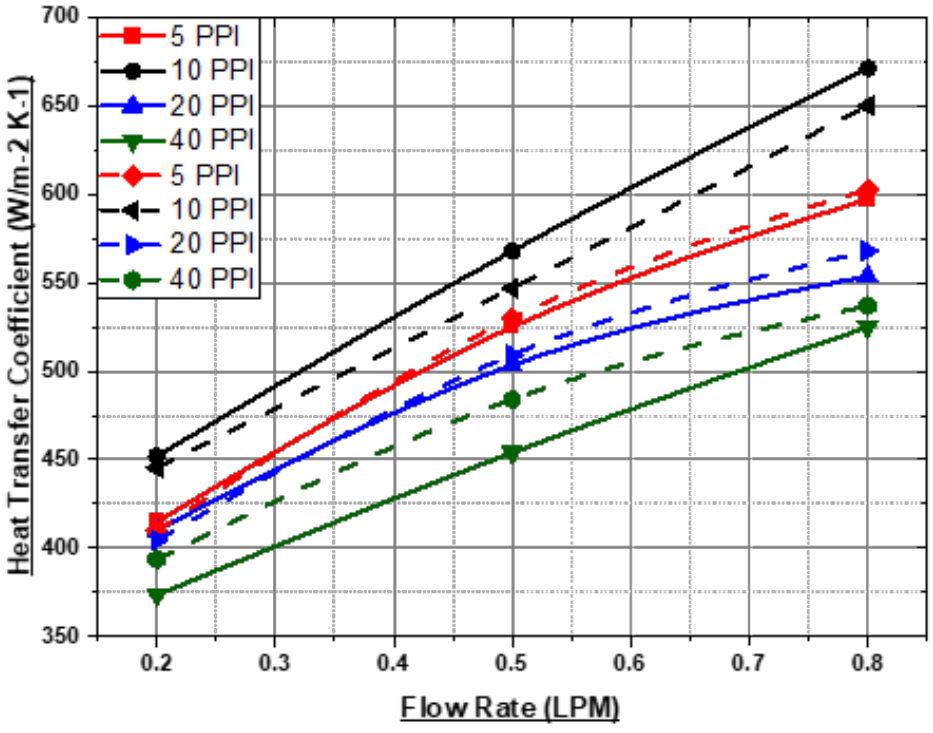
5 PPI
10 PPI
20 PPI
40 PPI
5 PPI
10 PPI
20 PPI
40 PPI
Heat Transfer Coefficient (W/m-2 K-1)
700
650
600
550
500
450
400
350
0.2
0.3
0.4
0.5
0.6
0.7
0.8
Flow Rate (LPM)

(b)

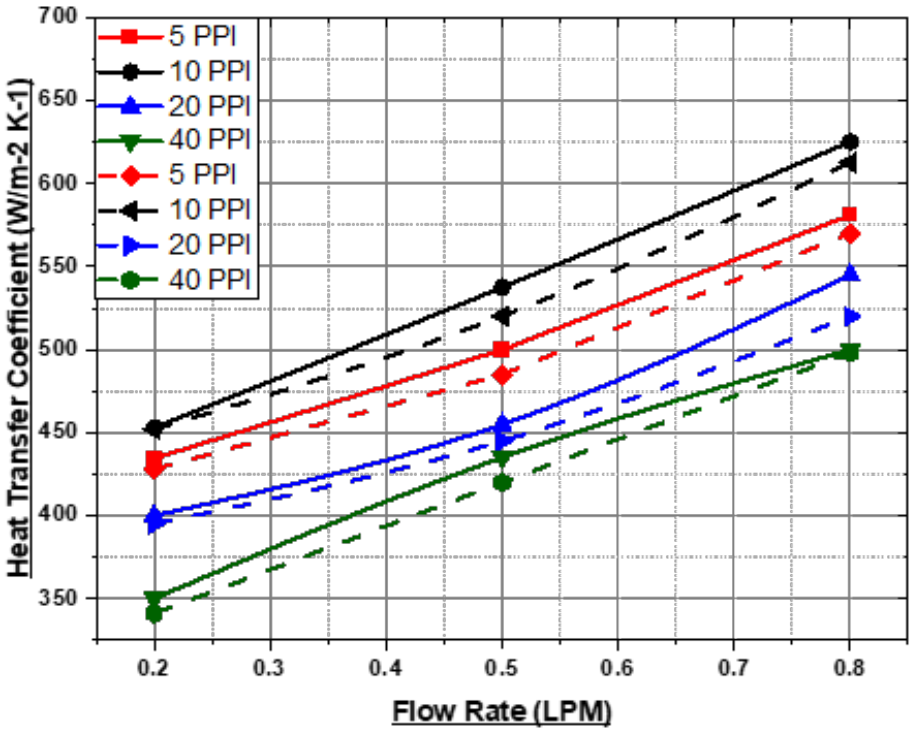

(c)

Figure 3.8: Overall Heat Transfer Coefficient (W/m^2-K) vs flow rate (LPM) for 60 kW/m^2 (Solid line) and 80 kW/m^2 (dotted line) at different fluid inlet temperatures: (a) 20°C, (b) 30°C, (c) 40°C

The analysis of the geometric data shown in Table 2.2 reveals a notable disparity in the heat transfer area between the metal foam samples with 40 pores per inch (PPI) and 5 PPI. Specifically, the former exhibits a heat transfer area that is five times more than the latter. The findings of the research indicate that the overall heat transfer coefficient consistently exceeds that of 40 PPI in all scenarios. This may be attributed to the combined effects of the local heat transfer coefficient, total heat transfer area, and overall surface efficiency, which are measured at 5 PPI. The investigation done by Mancin et al. [18] yielded comparable results. The discrepancies in the HTC (Heat Transfer Coefficient) values across different boundary conditions exhibit a marginal variation of less than 2% for heat fluxes of 60 kW/m2 and 80 kW/m2, while maintaining an input temperature of 20°C. Comparable patterns are seen for

heat fluxes of 60 kW/m^2 and 80 kW/m^2 when the intake temperatures are 30°C and 40°C, respectively. The determination of the thermal resistance of the foams is accomplished by the use of Equation 3. The connection between heat resistance and flow rate is seen in Figure 3.10. The data collected from all settings consistently indicates that foams with a density of 10 PPI display the lowest thermal resistance, whilst foams with a density of 40 PPI present the maximum thermal resistance. Moreover, it has been shown that an augmentation in the flow rate is linked to a reduction in heat resistance. The results shown in Figure 3.9 are consistent with the negative relationship between the heat transfer coefficient and thermal resistance.

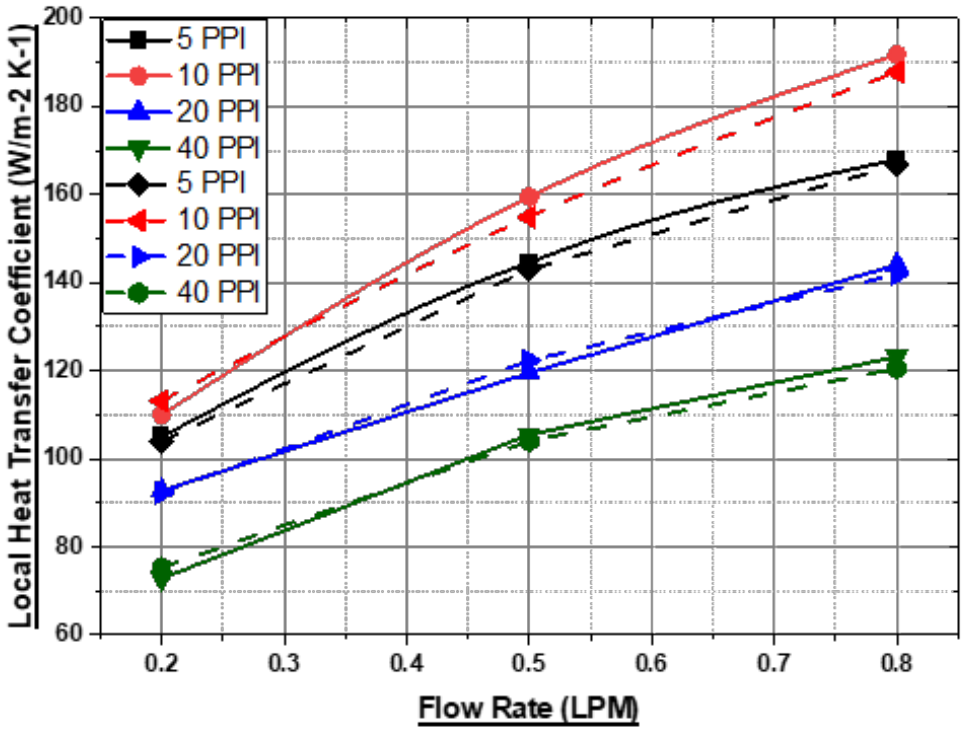

(a)

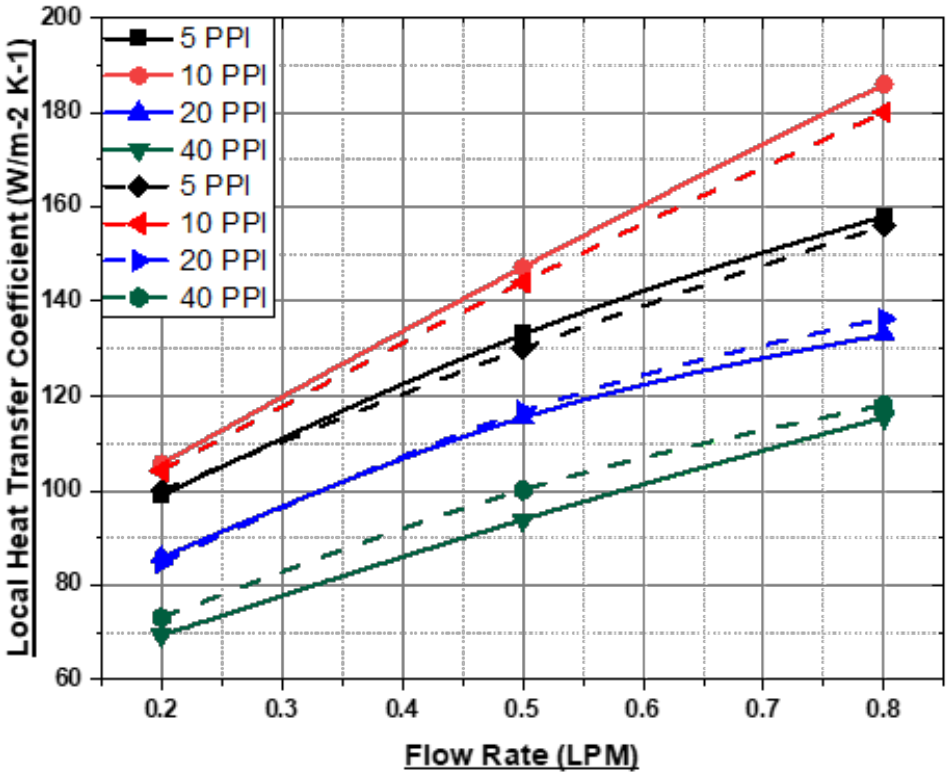
Local Heat Transfer Coefficient (W/m-2 K-1)
Flow Rate (LPM)
5 PPI
10 PPI
20 PPI
40 PPI
5 PPI
10 PPI
20 PPI
40 PPI
200
180
160
140
120
100
80
60
0.2
0.3
0.4
0.5
0.6
0.7
0.8

(b)

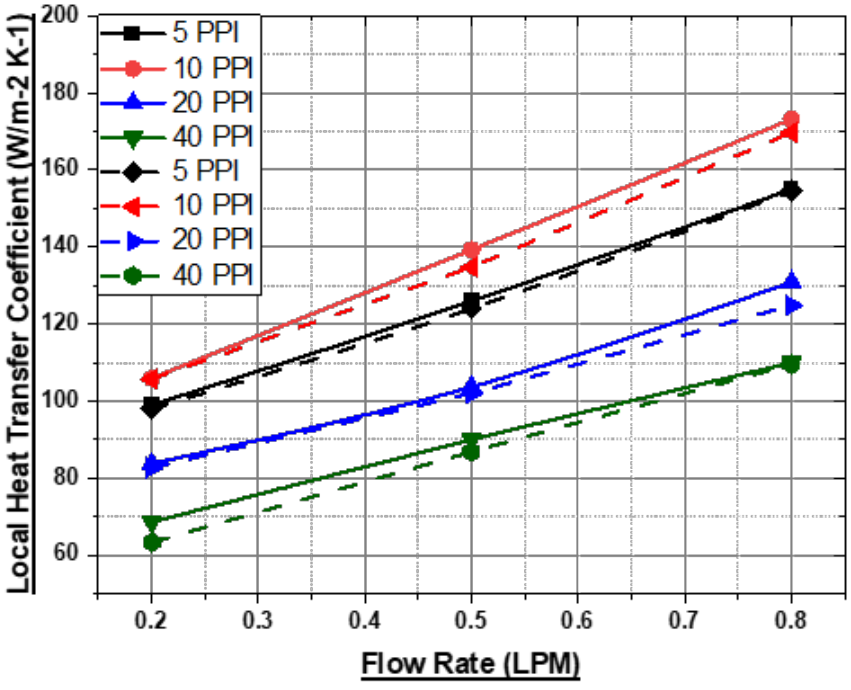
Local Heat Transfer Coefficient (W/m-2 K-1)
Flow Rate (LPM)
5 PPI
10 PPI
20 PPI
40 PPI
5 PPI
10 PPI
20 PPI
40 PPI
200
180
160
140
120
100
80
60
0.2
0.3
0.4
0.5
0.6
0.7
0.8

(c)

Figure 3.9: Local Heat Transfer Coefficient (W/m^2-K) vs flow rate (LPM) for 60 kW/m^2 (Solid line) and 80 kW/m^2 (dotted line) at different fluid inlet temperatures: (a) 20°C, (b) 30°C, (c) 40°C

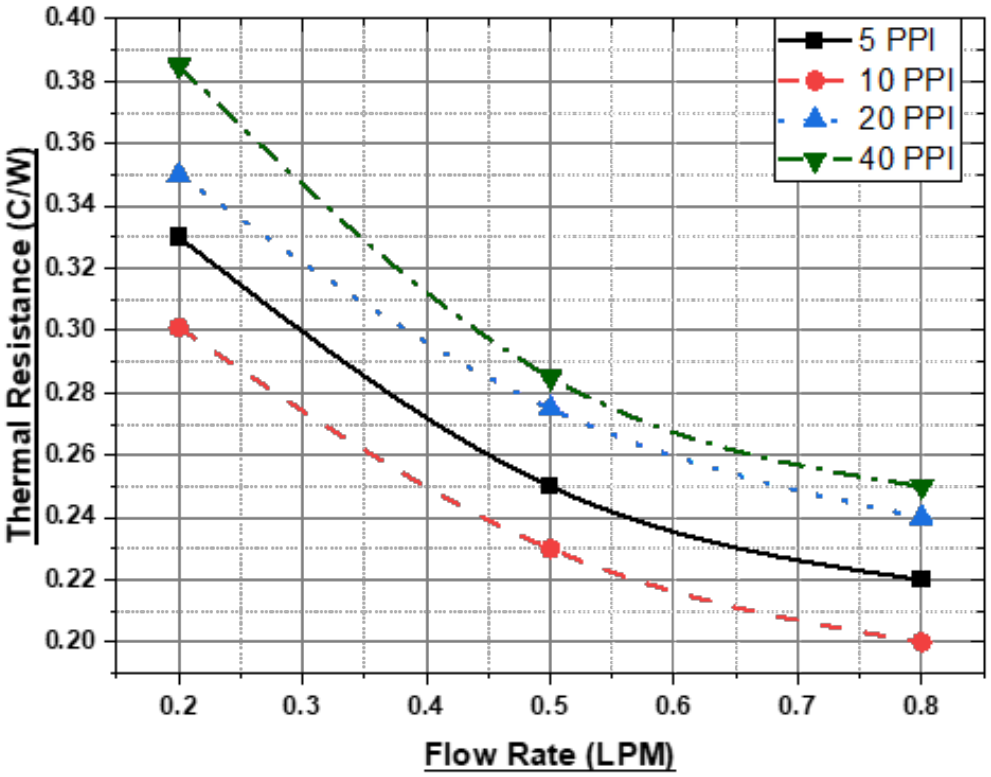

Figure 3.10: Average Thermal resistance vs Flow Rate

Figures 3.11 illustrate the pressure drop trend as a function of flow rate for heat fluxes of 60 kW/m^2 and 80 kW/m^2 for all the metal foam heat sinks at various fluid inlet temperatures. The pressure drop increases as the flow rate and PPI increases. From the pressure drop equation 4, it is possible to calculate three important parameters, the permeability K, the form coefficient C, and the inertia coefficient f. For very low speed, which is Darcy flow, the pressure gradient is linear to velocity (permeability K), and at high velocity, the separation from Darcy flow is due to form drag and turbulence, and it is proportional to the ρu^2 (inertia coefficient f). Also, the permeability (K) decreases, and the form coefficient (C) increases with increasing cell diameter or PPI, which is inversely proportional to the pressure drop gradient [30]. Experimentally the combination of this phenomenon can be seen in terms of pressure drop in

figure 3.11. 5 PPI presents the best performance as it exhibits the lowest pressure drop among all the foams, which coincides with the author's rationale explanations of the physical meaning of the permeability and inertia coefficient. The pressure drop across 40 PPI is 1.5 to 1.8 times greater than that of 5 PPI foam for both the heat fluxes and all the fluid inlet temperatures. This expected behavior can be attributed to the size and pore distribution in the metal foam.

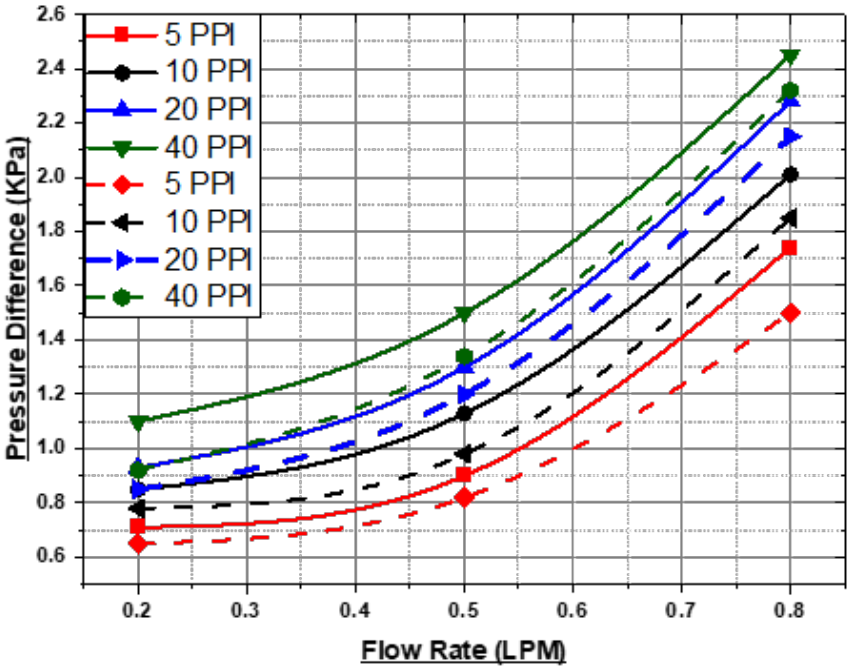

(a)

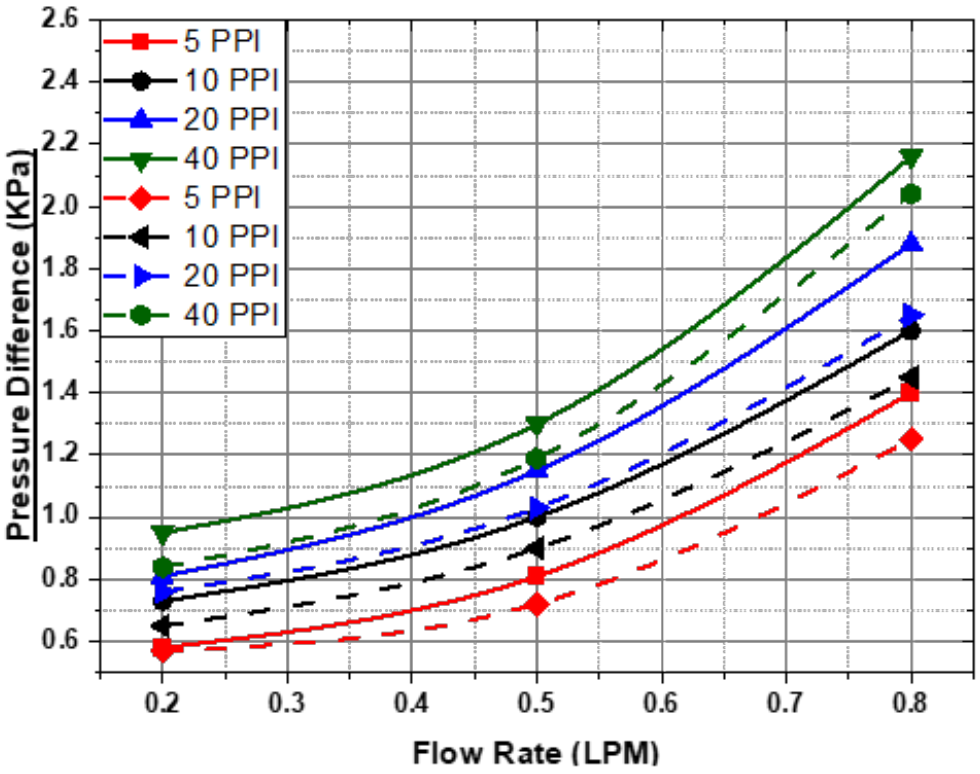
5 PPI
10 PPI
20 PPI
40 PPI
5 PPI
10 PPI
20 PPI
40 PPI
Pressure Difference (KPa)
Flow Rate (LPM)
2.6
2.4
2.2
2.0
1.8
1.6
1.4
1.2
1.0
0.8
0.6
0.2
0.3
0.4
0.5
0.6
0.7
0.8

(b)

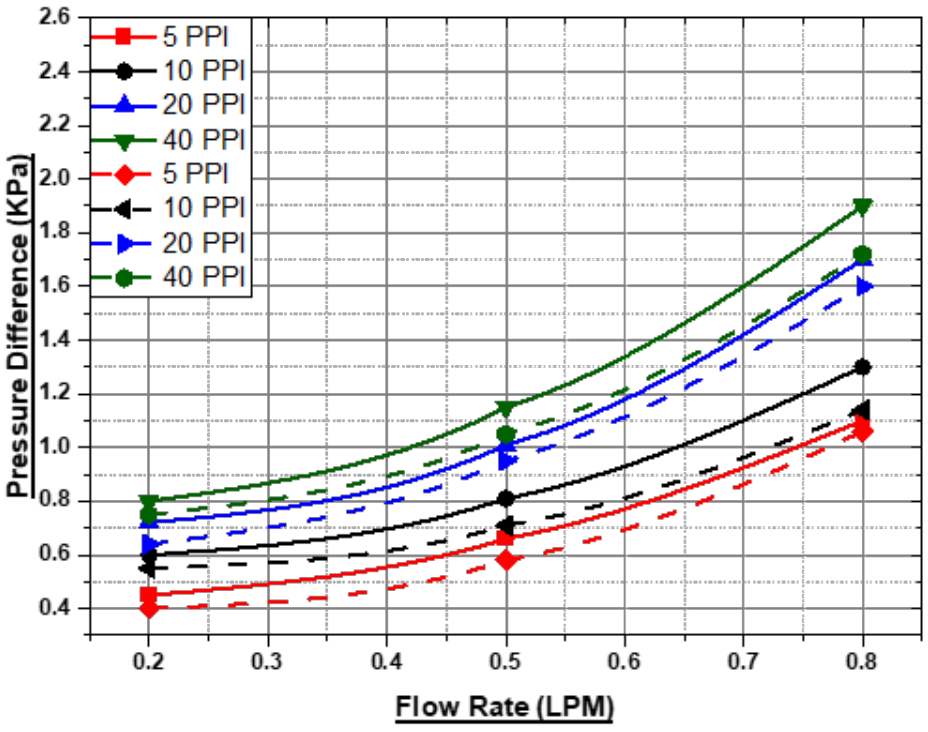
5 PPI
10 PPI
20 PPI
40 PPI
5 PPI
10 PPI
20 PPI
40 PPI
Pressure Difference (KPa)
Flow Rate (LPM)
2.6
2.4
2.2
2.0
1.8
1.6
1.4
1.2
1.0
0.8
0.6
0.4
0.2
0.3
0.4
0.5
0.6
0.7
0.8

(c)

Figure 3.11: Pressure difference (KPa) vs flow rate (LPM) for 60 kW/m^2 (Solid line) and 80 kW/m^2 (dotted line) at different fluid inlet temperatures: (a) 20°C, (b) 30°C, (c) 40°C

3.5 Conclusion

This study aimed to experimentally investigate the heat transfer and pressure drop characteristics of aluminum metal foams with different pore densities (5 PPI, 10 PPI, 20 PPI, and 40 PPI). The study maintained a nearly constant porosity and utilized foam cores with a height of 12.7 mm. The studies were conducted under two discrete heat flux situations, namely 60 kW/m² and 80 kW/m². The fluid flow rate and intake fluid temperature were manipulated within the respective ranges of 0.2-0.8 LPM and 20°C-40°C. The experimental findings were studied with respect to local and overall heat transfer coefficients, thermal resistance, overall surface area efficiency, and pressure drop. The findings of the inquiry indicate that the heat transfer coefficients, both at the overall and local levels, were shown to be unaffected by variations in the heat flux. However, it was observed that these coefficients exhibited an upward trend when the mass flow rates increased. The aluminum metal foam with a pore density of 10 PPI had superior heat transfer characteristics compared to other examined densities. It exhibited the greatest local and total heat transfer coefficients, while also displaying the lowest thermal resistance across all testing settings. Additionally, it was observed that the 5 PPI foam had the maximum surface area efficiency, whilst the 40 PPI foam displayed the lowest efficiency. The 5 PPI foam displayed the lowest pressure drop readings, whereas the 40 PPI foam revealed the maximum pressure drop. The aforementioned results underscore the prospective use of aluminum metal foams in the realm of thermal control. Nevertheless, in order to optimize these applications, a more comprehensive understanding of the heat transfer capabilities shown by these materials is required. Hence, it is recommended that forthcoming research efforts concentrate on the development of an analytical model that has the capability to effectively forecast the heat transfer coefficient and pressure drop. This

would provide a thorough evaluation and enhancement of heat sink designs that use metal foams. The implementation of such a model would make a substantial contribution towards the advancement of metal foam use in thermal management systems, thus enhancing their overall efficiency and efficacy.

3.6 Appendix

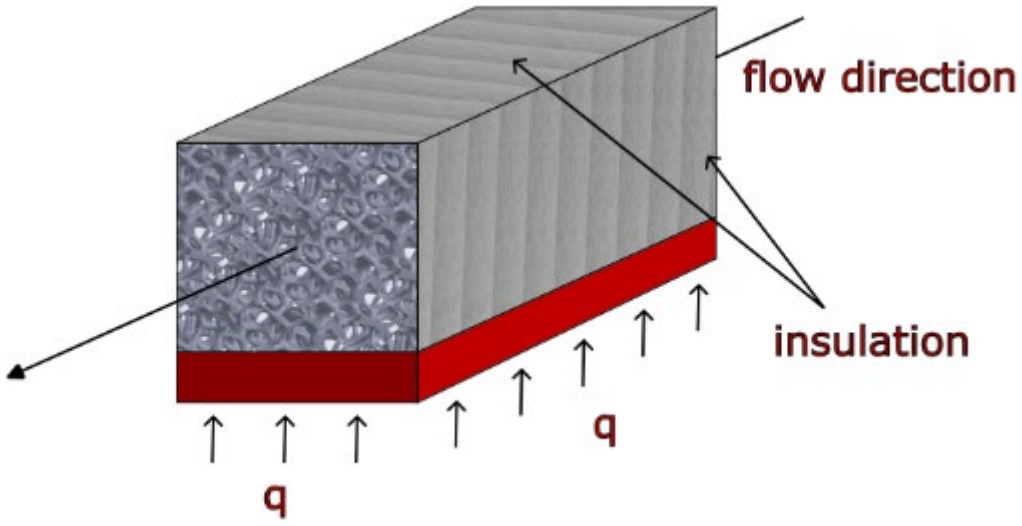

$$q_x + q_y + q_z = q_{x+dx} + q_{y+dy} + q_{z+dz} + dq_{con}$$

$$q_x = -k_x \frac{\partial T}{\partial x} dydz,$$

$$q_y = -k_y \frac{\partial T}{\partial y} dxdz$$

$$q_z = -k_z \frac{\partial T}{\partial z} dxdy$$

$$q_{x+dx} = q_x + \frac{\partial}{\partial x}\left(-k_x \frac{\partial T}{\partial x} dydz\right) dx$$

$$q_{y+dy} = q_y + \frac{\partial}{\partial y}\left(-k_y \frac{\partial T}{\partial y} dxdz\right) dy$$

$$q_{z+dz} = q_z + \frac{\partial}{\partial z}\left(-k_z \frac{\partial T}{\partial z} dxdy\right) dz$$

$$dq_{con} = hd\, A_s\, (T_s - T_f)$$

Substituting in the equation we get,

$$k_x \frac{\partial^2 T}{\partial x^2} + k_y \frac{\partial^2 T}{\partial y^2} + k_z \frac{\partial^2 T}{\partial z^2} - h\, a_s \left(T_s - T_f\right) = 0$$

$$k_x \frac{\partial^2 T}{\partial x^2} - h\, a_s \left(T_s - T_f\right) = 0$$

Let $\theta = T - T_s$

$$\frac{\partial^2 \theta}{\partial z^2} = \frac{\partial^2 T}{\partial z^2} - \frac{\partial^2 T_s}{\partial z^2}$$

$$\frac{\partial^2 \theta}{\partial z^2} - \frac{h\theta a_s}{k_s} = -\frac{\partial^2 T_f}{\partial z^2}$$

If $T_f = T_\infty$ (e.g. near the inlet), RHS of the above equation $(-\frac{\partial^2 T_f}{\partial z^2}) = 0$, $m^2 = \frac{h\theta a_s}{k_s}$

$$m = \sqrt{\frac{h\theta a_s}{k_s}}$$

3.7 Refrences

[1] T. J. Chainer, M. D. Schultz, P. R. Parida, M. A. Gaynes, Improving data center energy efficiency with advanced thermal management, IEEE Transactions on Components, Packaging, and Manufacturing Technology 7 (2017). doi:10.1109/tcpmt.2017.2661700.

[2] C. Nadjahi, H. Louahlia, S. Lemasson, A review of thermal management and innovative cooling strategies for data center, Sustainable Computing: Informatics and Systems 19 (2018) 14–28. https://doi.org/10.1016/j.suscom.2018.05.002.

[3] I.W. Kuncoro, N. A. Pambudi, M. K. Biddinika, I.Widiastuti, M. Hijriawan, K. M. Wibowo, Immersion cooling as the next technology for data center cooling: A review, Journal of Physics: Conference Series 1402 (2019) 044057. doi:10.1088/1742-6596/1402/4/044057.

[4] V. S. Simon, A. Siddarth, D. Agonafer, Artificial neural network-based prediction of control strategies for multiple air-cooling units in a raised-floor data center, 2020 19th IEEE Intersociety Conference on Thermal and Thermomechanical Phenomena in Electronic Systems (ITherm), 2020, pp. 334–340. doi:10.1109/ITherm45881.2020.9190431.

[5] S. Singh, K. Nemati, V. Simon, A. Siddarth, M. Seymour, D. Agonafer, Sensitivity analysis of a calibrated data center model to minimize the site survey effort, 2021 37th Semiconductor Thermal Measurement, Modeling Management Symposium (SEMI-THERM), 2021, pp. 50–57.

[6] L. Ardito, M. Morisio, Green it – available data and guidelines for reducing energy consumption in it systems, Sustainable Computing: Informatics and Systems 4 (2014) 24–32. https://doi.org/10.1016/j.suscom.2013.09.001.

[7] K. Ebrahimi, G. F. Jones, A. S. Fleischer, A review of data center cooling technology, operating conditions and the corresponding low-grade waste heat recovery opportunities,

Renewable and Sustainable Energy Reviews 31 (2014) 622–638. https://doi.org/10.1016/j.rser.2013.12.007.

[8] P. V. Bansode, J. M. Shah, G. Gupta, D. Agonafer, H. Patel, D. Roe, R. Tufty, Measurement of the Thermal Performance of a Custom-Build Single-Phase Immersion Cooled Server at Various High and Low Temperatures for Prolonged Time, Journal of Electronic Packaging 142 (2019). doi:10.1115/1.4045156, 011010.

[9] S. Saini, P. Shahi, P. Bansode, J. M. Shah, D. Agonafer, Simplified and Detailed Analysis of Data Center Particulate Contamination at Server and Room Level Using Computational Fluid Dynamics, Journal of electronic Packaging 144 (2022). doi:10.1115/1.4053363, 024501.

[10] P. Shahi, S. Saini, P. Bansode, D. Agonafer, A comparative study of energy savings in a liquid-cooled server by dynamic control of coolant flow rate at server level, IEEE Transactions on Components, Packaging and Manufacturing Technology 11 (2021) 616–624. doi:10.1109/TCPMT.2021.3067045.

[11] C. Tushar, B. Rabin, S. Krishna Bhavana, A. S. M. R. Chowdhury, A. Dereje, Impact of immersion cooling on thermomechanical properties of low-loss material printed circuit boards, Journal of Enhanced Heat Transfer 28 (2021) 73–90.

[12] P. Shahi, A. P. Deshmukh, H. Y. Hurnekar, S. Saini, P. Bansode, R. Kasukurthy, D. Agonafer, Design, Development, and Characterization of a Flow Control Device for Dynamic Cooling of Liquid-Cooled Servers, Journal of Electronic Packaging 144 (2021). doi:10.1115/1.4052324, 041008.

[13] A. Bhattacharya, R. L. Mahajan, Finned Metal Foam Heat Sinks for Electronics Cooling in Forced Convection, Journal of Electronic Packaging 124 (2002) 155–163. doi:10.1115/1.1464877.

[14] W. Hsieh, J. Wu, W. Shih, W. Chiu, Experimental investigation of heat-transfer characteristics of aluminum-foam heat sinks, International Journal of Heat and Mass Transfer 47 (2004) 5149–5157.

https://doi.org/10.1016/j.ijheatmasstransfer.2004.04.037.

[15] C. Zhao, Review on thermal transport in high porosity cellular metal foams with open cells, International Journal of Heat and Mass Transfer 55 (2012) 3618–3632.

https://doi.org/10.1016/j.ijheatmasstransfer.2012.03.017.

[16] Hamadouche, A., Nebbali, R., Benahmed, A., Kouidri, A., Bousri, A., Experimental investigation of convective heat transfer in an open-cell aluminum foam, Experimental Thermal and Fluid Science,

Volume 71, Pages 86-94, https://doi.org/10.1016/j.expthermflusci.2015.10.009.

[17] A. M. Bayomy, Z. Saghir, Thermal performance of finned aluminum heat sink filled with erg aluminum foam: Experimental and numerical approach, International Journal of Energy Research 44 (2020) 4411–4425.

[18] S. Mancin, C. Zilio, A. Cavallini, L. Rossetto, Heat transfer during air flow in aluminum foams, International Journal of Heat and Mass Transfer 53 (2010) 4976–4984. https://doi.org/10.1016/j.ijheatmasstransfer.2010.05.033.

[19] S. Mancin, C. Zilio, L. Rossetto, A. Cavallini, Heat transfer performance of aluminum foams, International Journal of Heat and Mass Transfer 133 (2011). doi:10.1115/1.4003451.

[20] S. Mancin, C. Zilio, A. Diani, L. Rossetto, Experimental air heat transfer and pressure drop through copper foams, Experimental Thermal and Fluid Science 36 (2012) 224–232. https://doi.org/10.1016/j.expthermflusci.2011.09.016.

[21] L.B. Younis, R. Viskanta, Experimental determination of the volumetric heat transfer coefficient between stream of air and ceramic foam, Int. J. Heat Mass Transfer 36 (1993) 1425–1434

[22] A. Bayomy, M. Saghir, T. Yousefi, Electronic cooling using water flow in aluminum metal foam heat sink: Experimental and numerical approach, International Journal of Thermal Sciences 109 (2016) 182–200. https://doi.org/10.1016/j.ijthermalsci.2016.06.007.

[23] S. Feng, F. Li, F. Zhang, and T. Lu, Natural convection in metal foam heat sinks with open slots, Experimental Thermal and Fluid Science, https://doi.org/10.1016/j.expthermflusci.2017.07.010.

[24] Fu, H. L., Leong, K. C., Huang , X. Y., and Liu, C. Y., An Experimental Study of Heat Transfer of a Porous Channel Subjected to Oscillating Flow, ASME. J. Heat Transfer. February 2001; 123(1): 162–170. https://doi.org/10.1115/1.1336510.

[25] Y. Li, L. Gong, M. Xu, Y. Joshi, Enhancing the performance of aluminum foam heat sinks through integrated pin fins, International Journal of Heat and Mass Transfer 151 (2020) 119376. https://doi.org/10.1016/j.ijheatmasstransfer.2020.119376.

[26] Electrocool® ec-100 dielectric coolant (accessed September 3, 2021). URL: https://www.engineeredfluids.com/products/electrocool.

[27] Intel Xeon Processor scable family, Thermal mechanical specifications and design guide, https://www.intel.com/content/dam/www/public/us/en/documents/guides/xeon-scalable-thermal-guide.pdf

[28] S. Mancin, C. Zilio, A. Diani, L. Rossetto, Air forced convection through metal foams: Experimental results and modeling, International Journal of Heat and Mass Transfer 62 (2013) 112–123. https://doi.org/10.1016/j.ijheatmasstransfer.2013.02.050.

[29] V.V. Calmidi, R.L. Mahajan, Forced convection in high porosity metal foams, J. Heat Transf. 122 (2000) 557–564.

[30] N. Dukhan, P. D. Quinones-Ramos, E. Cruz-Ruiz, M. V´elez-Reyes, E. P. Scott, One-dimensional heat transfer analysis in open-cell 10-ppi metal foam, International Journal of Heat and Mass Transfer 48 (2005) 5112– 5120. https://doi.org/10.1016/j.ijheatmasstransfer.2005.07.012.

[31] S. Guarino, G. Rubino, V. Tagliaferri, N. Ucciardello, Thermal behavior of open cell aluminum foams in forced air: Experimental analysis, Measurement 60 (2015) 97–103. https://doi.org/10.1016/j.measurement.2014.09.069.

[32] G. S. Beavers, E. M. Sparrow, Non-Darcy Flow Through Fibrous Porous Media, Journal of Applied Mechanics 36 (1969) 711–714. doi:10.1115/1.3564760.

4 Impact of Immersion Cooling on Thermomechanical Properties of Substrate Cores

4.1 Introduction

Data centers (DCs) play a crucial role in the collection, storage, processing, and distribution of vast quantities of data. These facilities serve many objectives, such as supporting corporate operations, providing entertainment services, and meeting other specific needs [1, 2]. By the year 2020, it is anticipated that the typical power consumption of a server equipped with a single central processing unit (CPU) would range from 140 W to 190 W. In contrast, a single processor designed for High-Performance Computing (HPC) applications is projected to surpass a power consumption of 300 W. According to a cited source [3], the dissipation of heat from information technology (IT) equipment constitutes around 50% to 60% of the total heat generated inside a data center. According to the cited source, it is projected that by the year 2025, data centers (DCs) would account for 4.5% of global power consumption. Furthermore, around 40% of this electricity use is anticipated to be allocated towards cooling systems. [4] On a global scale, it has been projected that data centers used 91 billion kilowatt-hours (kWh) of energy per year in 2013, which increased to 140 billion kWh in 2020, with further anticipated growth in 2025. According to the cited source, the outcome of this scenario would entail an annual release of carbon emissions exceeding 150 million metric tons, as well as incurring operational power expenses over $13 billion. The reduction of energy consumption is a significant priority for IT firms and policy makers due to the substantial power consumption of data centers, especially for cooling purposes [6].

Despite the considerable progress in technology seen in recent decades, the task of effectively regulating the temperature of electronics and microprocessors continues to pose substantial technical challenges. The two primary cooling challenges are the efficient

mitigation of escalating heat flow and the management of very uneven power dissipation [6]. Traditional air cooling has encountered limitations due to insufficient cooling capacity, elevated energy consumption, and substantial operating expenditures. The use of immersion cooling has several advantages, including increased thermal mass and enhanced heat dispersion, as a result of the direct contact between the dielectric fluids and all the components [7]. The use of single-phase immersion has many benefits in the context of information technology equipment (ITE). Firstly, it serves as a protective barrier against the detrimental effects of contaminants, safeguarding the ITE from potential damage. Additionally, it mitigates failures caused by vibration, therefore enhancing the overall reliability of the system. Moreover, the adoption of single-phase immersion results in reduced capital expenditure (CapEx) as it eliminates the need for complex liquid distribution manifold construction. Consequently, this simplifies the design and implementation of data center architecture [7, 14].

The immersion of heat-generating components in dielectric fluids might give rise to concerns about reliability. The failure of the whole package might be attributed to deformation, warpage, or delamination modes of failure, which can be caused by minor variations in the material characteristics of the components [8]. When supplying information on the material qualities, the majority of fluid suppliers and vendors often provide the results of the soak test. Nevertheless, the authors fail to take into account the operational dependability, namely the mechanical and electrical properties of the components that are specific to the work environment of the application [8]. Material compatibility may be categorized into two types of interactions: direct and indirect. Direct interactions refer to processes that are initiated by the fluid itself. Fluid-induced vibrations may manifest either inside the fluid itself or as a result of the fluid's interaction with a particular material component. There are six fundamental mechanisms via which direct interactions may take place in single-phase fluids: dissolution, absorption/swelling, chemical contact with material, environmental stress cracking (ESC),

fluid aging, and oxidation. The release or generation of chemicals via direct contact with IT components elicits indirect responses rather than the fluid itself [9].

Tushar et al. [10] conducted a study on the thermo-mechanical properties of low loss printed circuit boards when subjected to immersion in mineral oil for a duration of 720 hours at temperatures of 25, 50, 75, and 105°C. It was observed that the in-plane coefficient of thermal expansion (CTE) values of the post-aged samples exhibited little alterations within the specified temperature range. In a previous work conducted by Ramdas et. al [11], a similar investigation was carried out with the immersion of FR-4 PCB in EC-100 dielectric fluid. The findings indicate a reduction in modulus for the post-aged samples, implying a drop in the stiffness of the PCBs. Consequently, this decrease in stiffness contributes to a reduction in warpage. The study conducted by Bhandari et al. (2012) examined the impact of the immersion of non-halogenated substrates in a single-phase immersion fluid, namely EC-100, on their mechanical characteristics. The immersion duration lasted for a total of 720 hours, with the substrates being subjected to ambient temperature as well as elevated temperatures of 50°C and 75°C. This research aims to compare the modulus of the submerged substrate with the modulus of substrates that are exposed to air at their different temperatures. The observation revealed that increasing temperatures resulted in a reduction in the modulus. However, at a temperature of 75 °C, a fluctuating pattern was detected in both air and EC100 fluid.

The primary objective of this study is to quantitatively assess and describe the material compatibility of immersed components. According to the design requirements of the Open Compute Project (OCP) for immersion-cooled IT equipment, it is possible to use conventional material compatibility testing outlined in standards such as ASTM 3455, with some necessary modifications [9]. The current study is divided into two separate segments: The first part of the study focuses on understanding the impact of thermal aging on three distinct substrate cores immersed in a dielectric fluid used for single-phase immersion cooling, specifically in relation

to their thermo-mechanical properties. One additional objective of the study is to get comprehensive insights into the effects of thermal aging on the thermo-mechanical characteristics of the substrate core when subjected to elevated temperatures in an ambient air environment. The current investigation entails exposing the substrate cores, namely TerraGreen 400G, AstramT77, and I-Speed-S-C100, to synthetic hydrocarbon fluid (EC110), Polyalphaolefin 6 (PAO 6), and ambient air for a total time of 720 hours. This exposure will occur at two different temperatures, specifically 85°C and 125°C. The complex modulus and glass transition temperature of the substrate cores are evaluated using Dynamic Mechanical Analyzer (DMA) both before and after the aging procedure.

4.2 Materials and methods

Each of the three substrate samples had a thickness of 0.25 mm and was then trimmed to approximately 50 mm x 5 mm. A total of 24 specimens of each substrate core were prepared in anticipation of conducting Dynamic Mechanical Analysis (DMA) tests. The experiment's conditions, including the temperatures of 85°C and 125°C, as well as the durations of 720 hours or one month, were chosen based on the recommendations outlined in the OCP guidelines and ASTM 3455. Figure 4.1 presents a visual representation of the main components of DMA. The sinusoidal load is supplied to the sample via a probe in the form of stress/strain. The resulting sinusoidal stress/strain is then recorded and graphed as a function of time or temperature. The user's text does not contain any information to rewrite. Various modules of DMA, such as tension, bending, shear, and compression deformation attachments, are used to assess diverse material characteristics, which are contingent upon the shape of the sample, its modulus, and the intended purpose of the measurement. The viscoelastic characteristics, such as storage modulus and loss modulus, may be quantified using a Dynamic Mechanical Analyzer (DMA). The dynamic mechanical analyzer (DMA) used in this investigation has a temperature range spanning from roughly -150°C to 600°C. The automated liquid nitrogen (LN2) gas cooling

system is designed to administer liquid nitrogen in order to decrease the temperature of the furnace to a level lower than the ambient room temperature. Figure 4.2 showcases the configuration of the sample affixed to the tensile probe. The thermal chamber shown in Figure 4.3 contains substrate samples that are immersed in EC-100, PAO 6, and subjected to air exposure. Table 4.1 presents data on the number of samples located within each fluid.

Table 4.1: Aging of substrate samples in EC100, PAO 6 and air.

Aging Temperature	Aging Time	No. of Samples immersed in EC100	No. of Samples immersed in PAO 6	No. of samples in the air
85°C	~ 720 hours	4	4	4
125°C		4	4	4

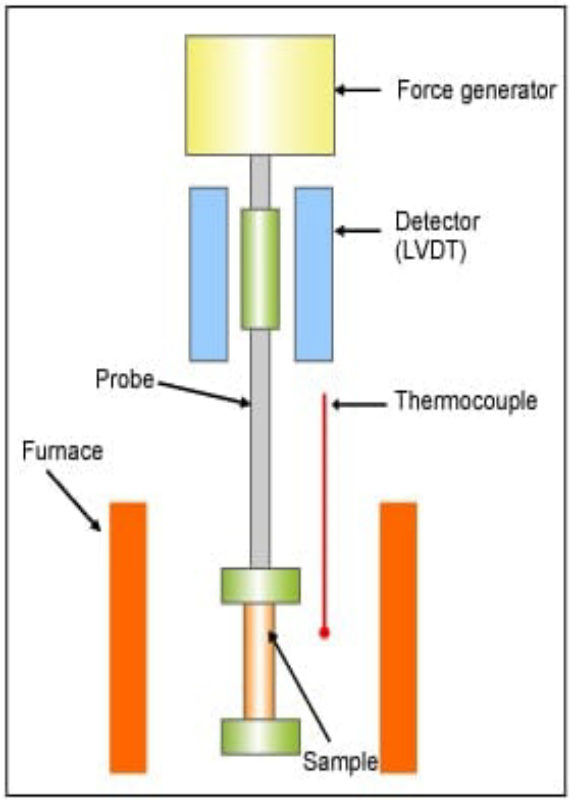

Figure 4.1: Schematic of DMA

The technique known as Dynamic Mechanical Analysis (DMA) is used to quantitatively assess the kinetic characteristics of a certain sample, including its elasticity and viscosity [10]. A range of Dynamic Mechanical Analysis (DMA) modules may be used to investigate different material properties, including as tension, bend, shear, and compression deformations. The specific module chosen depends on several criteria, including the shape of the sample, its modulus, and the purpose of the measurement. The DMA approach is used for the calculation of both the storage modulus and the loss modulus. Equations 1 and 2 provide the mathematical representation of the association between complex modulus, storage modulus, and loss modulus [12]. The estimated complex modulus may be compared to Young's modulus. The formula for calculating the complex modulus is as follows:

$$E^* = E' + iE'' \quad (1)$$

$$E^* = \sqrt{(E')^2 + (E'')^2} \quad (2)$$

$$\tan\delta = E''/E' \quad (3)$$

where,

E* =	Elastic modulus
E’ =	Storage modulus
E” =	Loss modulus
tan $\boldsymbol{\delta}$ =	Damping ratio

The sample dimensions were measured utilizing a digital caliper that possessed an accuracy of 0.02 mm. The selection of the tensile attachment for the present study was based on the projected modulus derived from the sample dimensions and the material properties. Prior to being mounted onto the DMA for testing, the samples immersed in dielectric were

appropriately cleaned using a paper towel. The DMA measurements were conducted with a fixed L amplitude of 10 μm and a force amplitude of 2000 mN for all samples. The experimental data was collected by exposing the specimens to a temperature range spanning from -35°C to 200°C, with a consistent ramp rate of 4°C per minute. Additionally, a range of frequencies, including 0.5, 1, 2, 5, and 10 Hz, were applied during the testing process. The auto LN2 gas cooling unit facilitates the dispensation of liquid nitrogen to lower the temperature of the furnace below ambient temperature [13]. A thermal equilibrium was achieved by subjecting the system to an isothermal hold at the initial temperature i.e. -35°C. This resulted in an extension of the measurement duration of the DMA to approximately 2.5 hours. Table 4.2 presents the parameters utilized for the purpose of testing.

Table 4.2: Testing parameters used in DMA

Parameters	Values
Maximum Force	2000 mN
Temperature Ramp	3°C
Sample Thickness	0.25mm~0.3mm
Sample Length	20mm
Sample Width	5 mm

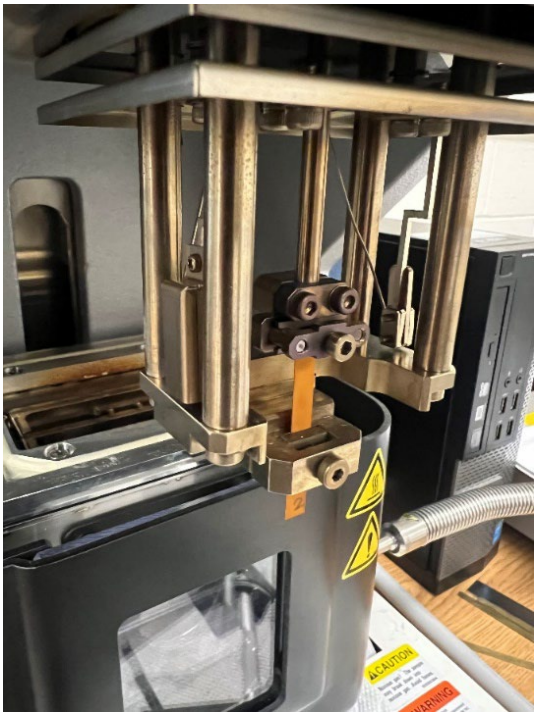

Figure 4.2: Sample mounted in the tensile attachment on DMA

Figure 4.3: Sample bottles placed in a thermal chamber

4.3 Results

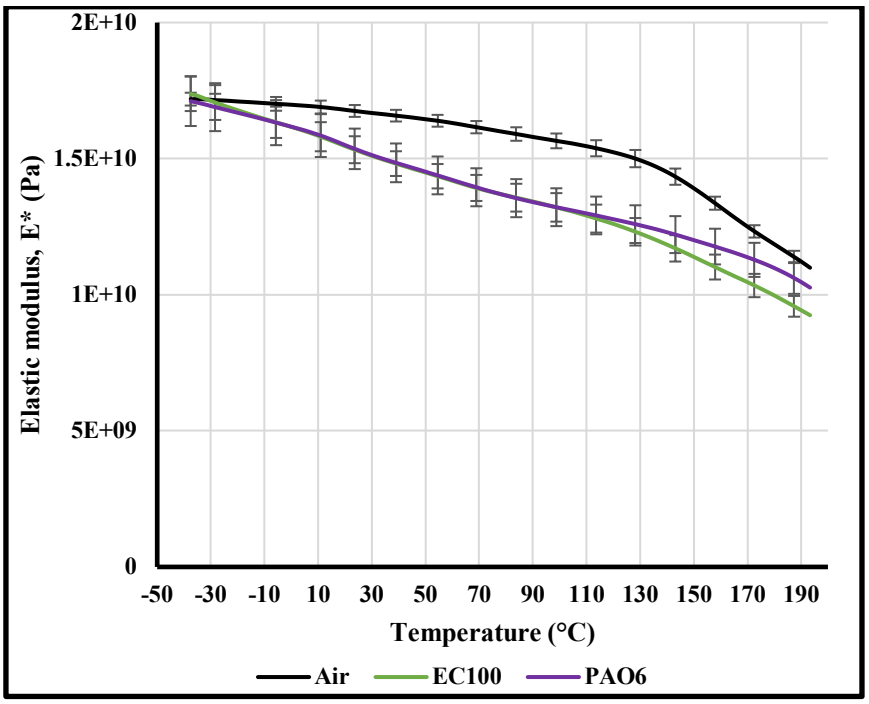

Figure 4.4: Elastic Modulus of sample TG 400G immersed in EC100, PAO6 and Air at 85°C

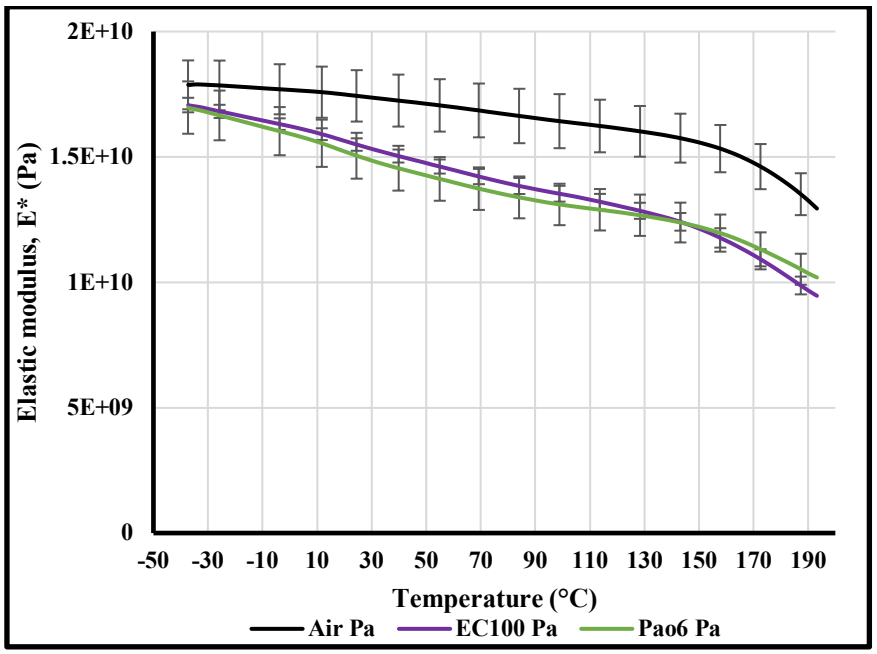

Figure 4.5: Elastic Modulus of TG400G sample immersed in EC100, PAO6 and Air at 125°C

Figure 4.4 and 4.5 shows the comparison of the comparative outcomes of Dynamic Mechanical Analysis (DMA) tests conducted on TG400G samples that were subjected to aging processes in PAO6 EC100 and air, for 85°C and 125°C temperature conditions. A minimum of four samples were tested and then averaged for each plot. A predetermined torque was applied in order to reduce the variability in clamping force during the attachment of the sample. To achieve thermal equilibrium, an isothermal hold was used at the initial temperature. The extended duration of DMA measurement was roughly 2.5 hours. The standard deviation for the findings obtained at temperatures of 85°C and 125°C is 7% and 9% respectively, across all the samples. Furthermore, the modulus values of both sample variants exhibit a decreasing trend as the temperature is raised from -35°C to 180°C in the DMA. As it can be seen the samples immersed in PAO 6 and EC 100 have lower modulus than air which means that the samples are became less stiff which means it is more flexible and they are less prone to warpage in PCB at higher or lower temperature. The glass transition temperature (Tg) of TG 400G has been determined to be 200°C based on dynamic mechanical analysis (DMA) data obtained from all samples and under different conditions.

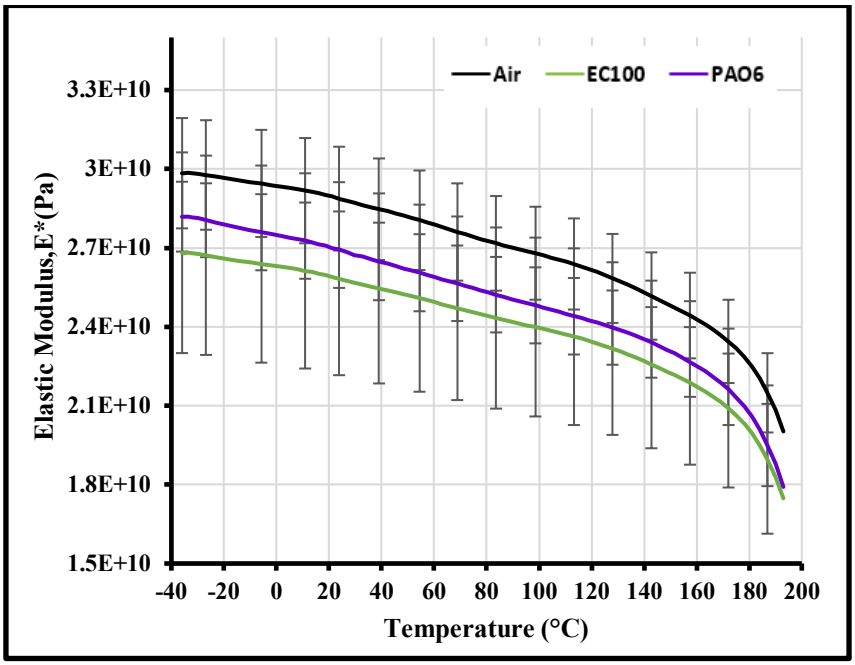

Figure 4.6: Elastic Modulus of I-Speed sample immersed in EC100, PAO6 and Air at 85°C

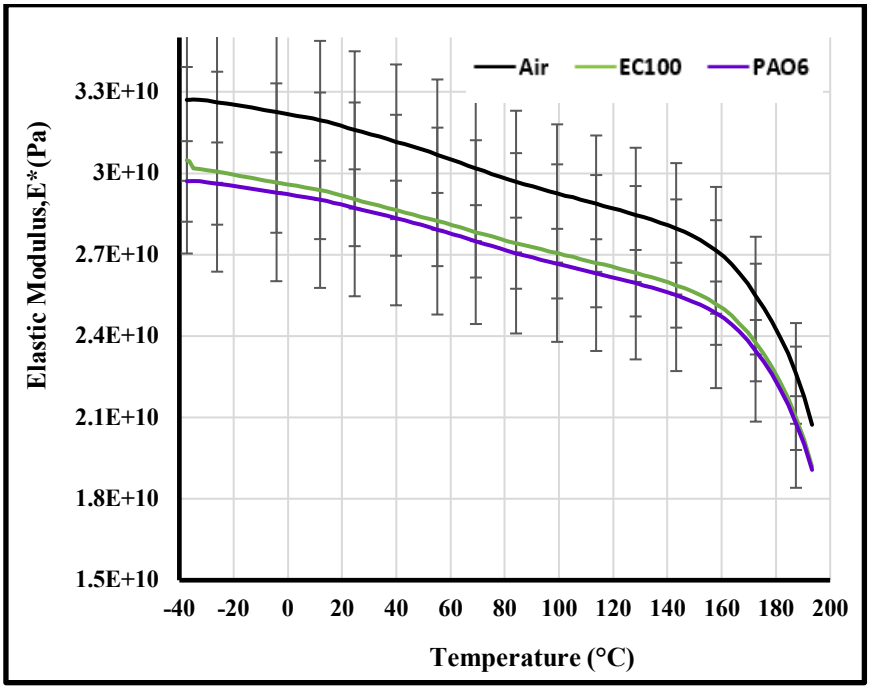

Figure 4.7: Elastic Modulus of I-Speed sample immersed in EC100, PAO6 and Air at 125°C

In a similar vein, figures 4.6 and 4.7 depict the modulus of the I-Speed sample when subjected to immersion in EC100, PAO6, and Air at temperatures of 85°C and 125°C, respectively. A total of four specimens were subjected to testing and then averaged for every plot. In order to minimize the variability in clamping force during the attachment of the sample, a predefined torque was used. In order to attain thermal equilibrium, a period of isothermal holding was used at the starting temperature. The time period of DMA measurement extended for about 2.5 hours. The presented data shows the glass transition temperature (Tg) of I-speed substrate for all the cases is 175°C derived respectively from storage modulus, loss modulus and loss tangent. Based on the data shown in figures 4.7 and 4.8, it is evident that the modulus of the substrate cores that are immersed is lower compared to the modulus of the substrate cores that

are exposed to air. This implies that the samples underwent a reduction in stiffness, resulting in increased flexibility and decreased susceptibility to warping in printed circuit boards (PCBs) exposed to both higher and lower temperatures. Similar trends can be found for the ASTRAMT77 samples as shown in figure 4.8 and 4.9. The glass transition temperature (Tg) of all the ASTRAMT77 samples is around 195°C, after which the complex modulus decreases rapidly. The modulus of elasticity of immersed samples is lower compared to that of air-exposed samples, which may be attributed to the entry of dielectric fluid into the samples, resulting in a modification of their modulus.

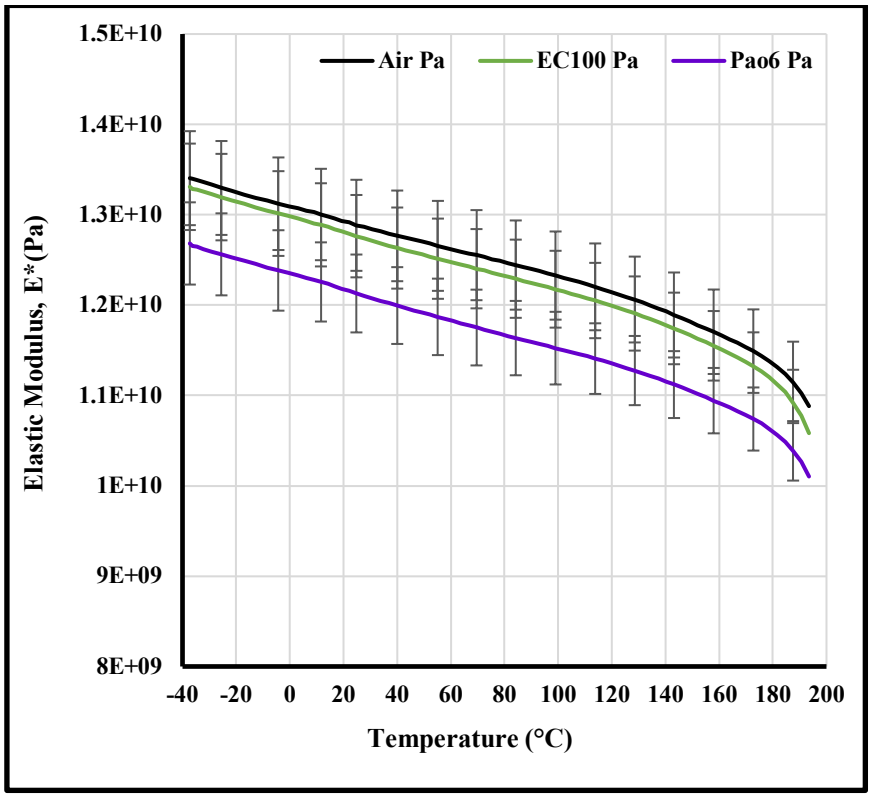

Figure 4.8: Elastic Modulus of ASTRAMT77 sample immersed in EC100, PAO6 and Air at 85°C

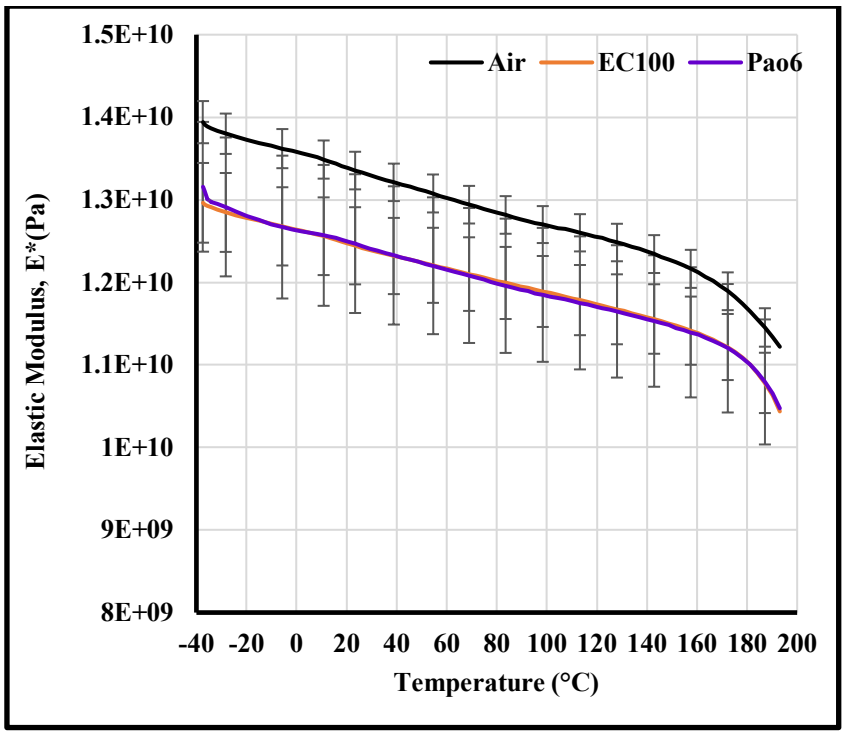

Figure 4.9: Elastic Modulus of ASTRAMT77 sample immersed in EC100, PAO6 and Air at 125°C

4.4 Conclusion

The rise in the popularity of immersion cooling may be related to the growing need for high-performance computing and the corresponding increase in power density. The issue of reliability is a persistent concern within the field of electronic packaging. The current study focuses on examining the reliability of various substrate cores. The substrates were subjected to thermal aging at two distinct temperatures, namely 85°C and 125°C. The modulus values of the aforementioned substrates were then compared to those of substrates that underwent exposure to ambient air under identical temperature conditions. As anticipated, there was a negative association seen between the modulus and increasing temperature. The modulus of elasticity of the immersed samples consistently shown lower values in comparison to the samples that were exposed to air, irrespective of the temperature. This suggests that the samples that have undergone immersion have a decrease in stiffness. As a consequence, the specimens

exhibit enhanced flexibility, leading to reduced warpage on printed circuit boards (PCBs) when subjected to elevated or lower temperatures. Furthermore, it was shown that the glass transition temperature of the substrate samples remained constant after post-aging, including exposure to air, EC100, and POA6 at temperatures of 85°C and 125°C.

4.5 References

[1] Garimella, S. V., Persoons, T., Weibel, J., and Yeh, L. T., 2013, "Technological Drivers in Data Centers and Telecom Systems: Multiscale Thermal, Electrical, and Energy Management," Appl. Energy, 107, pp. 66–80.

[2] Masanet, E., Shehabi, A., Lei, N., Smith, S., and Koomey, J., 2020, "Recalibrating Global Data Center Energy-Use Estimates," Science, 367(6481), pp. 984–986.

[3] Luo, Q., Wang, C., and Wu, C., "Study on heat transfer performance of immersion system based on SiC/white mineral oil composite nanofluids", International Journal of Thermal Sciences, Volume 187, 2023, 108203, https://doi.org/10.1016/j.ijthermalsci.2023.108203.

[4] Liu, Y.N., Wei, X.X., Xiao, J.Y., Liu, Z.J., Xu, Y., and Tian, Y., "Energy consumption and emission mitigation prediction based on data center traffic and PUE for global data centers", Global Energy Interconnection 3 (3) (2020) 272–282, https://doi.org/10.1016/j.gloei.2020.07.008.

[5] Abreu, V., Harrison, M., Gess, J., and Moita, A. S., 2018, "Two-Phase Thermosiphon Cooling Using Integrated Heat Spreaders with Copper Microstructures," Proceedings of the 17th InterSociety Conference on Thermal and Thermomechanical Phenomena in Electronic Systems, ITherm 2018, San Diego, CA, May 29–June 1.

[6] S. M. Sohel Murshed and C. A. Nieto de Castro, "A critical review of traditional and emerging techniques and fluids for electronics cooling," Renew. Sustain. Energy Rev., vol. 78, pp. 821–833, Oct. 2017, doi: 10.1016/j.rser.2017.04.112.

[7] Bansode, P. V., Shah, J. M., Gupta, G., Agonafer, D., Patel, H., Roe, D., and Tufty, R. (November 8, 2019). "Measurement of the Thermal Performance of a Custom-Build Single-Phase Immersion Cooled Server at Various High and Low Temperatures for Prolonged Time." ASME. J. Electron. Packag. March 2020; 142(1): 011010. https://doi.org/10.1115/1.4045156

[8] Shah, J., Padmanaban, K., Singh, H., Duraisamy, S., Saini, S., and Agonafer, D.," Evaluating the Reliability of Passive Server Components for Single-Phase Immersion Cooling", J. Microelectron. Electron. Packag., vol. 18, no. 1. Pp. 21-28,2021.

[9] Shivaprasad, P., Bean, J., Shah, J., Azevedo, E., Brink, R., Sengupta, S., Wirtz, K., Cooper, P., Margerison, R., Pignato, S., Diffley, P., Pooker, G., Kadhim, M., Null, V., Thomas, D., and Zhou, K., "Material Compatibility in Immersion Cooling", Open Compute Project, November 28, 2022.

[10] Chauhan, T., Bhandari, R., Sivaraju, K., Chowdhury, R., and Agonafer, D., "Impact of immersion cooling on thermomechanical properties of low-loss material printed circuit boards", Volume 28, Issue 7, 2021, pp. 73-90, DOI: 10.1615/JEnhHeatTransf.2021039486

[11] Ramdas, S., Rajmane, P., Chauhan, T., Misrak, A., and Agonafer, D. "Impact of Immersion Cooling on Thermo-Mechanical Properties of PCB's and Reliability of Electronic Packages", ASME. https://doi.org/10.1115/IPACK2019-6568

[12] Bhandari, R., Lakshminarayana, AB., Sivaraju, KB., Bansode, P., Kejela, E., and Agonafer, D., "Impact of Immersion Cooling on Thermomechanical Properties of Non-Halogenated Substrate." ASME. https://doi.org/10.1115/IPACK2022-97423

[13] Hitachi, TA7000 Series, Dynamic Mechanical Analyzer, Operation Manual, Hitachi Hi-Tech Science Corp., 2013

[14] Sivaraju, Krishna Bhavana, Pratik Bansode, Gautam Gupta, Jacob Lamotte-Dawaghreh, Satyam Saini, Vibin Simon, Joseph Herring, Saket Karajgikar, Veerendra Mulay, and Dereje Agonafer. "Comparative Study of Single-Phase Immersion Cooled Two Socket Server in Tank and Sled Configurations." In International Electronic Packaging Technical Conference and Exhibition, vol. 86557, p. V001T01A010. American Society of Mechanical Engineers, 2022.

[15] Yaragalla, Srinivasarao; Mishra, Raghvendra Kumar; Thomas, Sabu; Kalarikkal, Nandakumar; Maria, Hanna J. (11 February 2019). Carbon-Based Nanofillers and Their Rubber Nanocomposites. ISBN 9780128173428. Retrieved 2023-05-10.

[16] Shalom Simon, Vibin, Himanshu Modi, Krishna Bhavana Sivaraju, Pratik Bansode, Satyam Saini, Pardeep Shahi, Saket Karajgikar, Veerendra Mulay, and Dereje Agonafer. "Feasibility Study of Rear Door Heat Exchanger for a High Capacity Data Center." In International Electronic Packaging Technical Conference and Exhibition, vol. 86557, p. V001T01A018. American Society of Mechanical Engineers, 2022.

[17] Modi, Himanshu, Pardeep Shahi, Lochan Sai Reddy Chinthaparthy, Gautam Gupta, Pratik Bansode, Vibin Shalom Simon, and Dereje Agonafer. "Experimental Investigation of the Impact of Improved Ducting and Chassis Re-Design of a Hybrid-Cooled Server." In International Electronic Packaging Technical Conference and Exhibition, vol. 86557, p. V001T01A019. American Society of Mechanical Engineers, 2022.

5 Experimental and Numerical Investigation of Flow Visualization in Single Phase Immersion Cooling

5.1 Introduction

The ongoing patterns of diminishing electronic form factor and escalating power consumption have led to a significant rise in heat production at the component level. In light of advancements in heterogeneous integration, the need for improved thermal management at the package level has become imperative in order to ensure optimal device temperature and performance [1]. The use of liquid immersion cooling is increasingly being recognized and adopted within the industry as a viable method for effectively managing thermal conditions in advanced microelectronic devices that exhibit great performance capabilities. The increase in utilization of this methodology is propelled by numerous factors. Intel (Santa Clara, CA) presently manufactures commercially accessible high performance chipsets using 14 nm technology [2]. It is anticipated that there will be an increase in high-performance heat fluxes, reaching a projected value of 250 W/cm^2 in the near future [3]. Furthermore, it is predicted that these values may potentially escalate to as high as 1000 W/cm^2 during the following decade [4]. Heat fluxes at the die or substrate level of contemporary microprocessors may vary within the range of 30 to 70 W/cm^2 [5]. Numerous industry associations have taken advantage of the enhanced heat transfer coefficients provided by liquid immersion cooling compared to conventional air cooling systems. Additionally, they have recognized the potential for system-level energy efficiency enhancements that may be achieved via the use of this thermal management solution.

The research conducted on comprehending and forecasting the flow patterns in air-cooled thermal management systems has reached a high level of development and encompasses a wide range of studies. A comprehensive examination of the outcomes and methodologies

pertaining to the assessment of thermal performance and efficiency in data centers can be found in the work of Alkharabsheh et al. [6], specifically focusing on the modeling and forecasting aspects. Arghode and Joshi [7] conducted an experimental study to investigate the pressure drop encountered throughout a rack, which is directly associated with the fan power necessary for coolant delivery across the data center. This pressure drop also has an impact on the overall energy efficiency of the system. Arghode et al. [8] have previously used particle image velocimetry (PIV) flow visualization methods in the context of air cooling solutions for data centers, which are well acknowledged in the field. Particle Image velocimetry (PIV) is an experimental technique to accurately quantify the fluid velocity vectors within a domain of interest. The technique involves seeding a fluid with neutrally buoyant reflective particles and shining a laser sheet across a plane of interest. The laser reflects off the particles and is recorded using a camera at a certain frame rate. A correlation function is applied between two frames to calculate the direction and magnitude of each particle in the frame. The introduction of the digital camera and Nd:YaG laser miniaturized the experimental setup while allowing recording at larger timelines. At the same time, refinements in correlation techniques meant that accurate velocity profiles could be obtained across large flow regimes. The digital particle imaging velocimetry (DPIV) technique utilizes digital cameras and digitally synced laser pulses to record the flow field. It has become so ubiquitous that to say PIV is to almost always means DPIV.

The extreme accuracy of the PIV makes it an essential verification and validation tool for design and computational engineers alike. PIV systems are categorized based on the number of dimensions of observations and the flow vectors recorded. The most basic PIV is the 2-dimensional 2 component PIV (2D2C) where a 2D planar laser sheet captures the in-plane velocity vector components. To capture all the vector components in a 2D plane a stereo-PIV setup (2D3C) is required. The latest advancement in PIV is the Tomographic PIV which

captures the flow profile in a volumetric flow field (3D3C). Although there is not much literature on the Particle Image Velocimetry (PIV) analysis of dielectric fluids in both single-phase and two-phase states, some PIV investigations have been carried out on other fluids. The majority of Particle Image Velocimetry (PIV) research has focused on using water as the primary liquid cooling. Due to the conductive nature of water, it was not feasible to utilize it as the working fluid in the current flow visualization study, since the objective was to evaluate the efficacy of quenching fluid flow pathways directly onto heated items of interest [9]. The PIV methodology involves making a decision based on several factors, such as the use of shadowgraphy methods, the compatibility between particles and fluid, the desire for filtered or non-filtered approaches, and the availability of cameras. Sathe et al. [10] provide a comprehensive evaluation of Particle Image Velocimetry (PIV) methodologies designed for the measurement of single- and two-phase flow. This study used a LaVision tomographic PIV system equipped with four digital cameras for flow capture and a Quantel evergreen dual pulsed Nd:YaG laser to quantify the velocity of the fluid exiting the heat sink. The objective was to verify the computational fluid dynamics (CFD) outcomes by comparing them with the experimental findings obtained from single phase immersion cooling.

5.2 Experimental setup and methodology

The schematic design of the experimental setup used for the single-phase liquid immersion cooling system is shown in Figure 5.1. The tank has been purposefully designed to include the core principle of an infinity pool. The term "inlet port" refers to the lower port that enables the introduction of fluid into the system via the use of a pump. The fluid performs a systematic process of being guided via a server system, then falling into a reservoir and ultimately exiting out the output port. In order to regulate the temperature of the inlet fluid, the dielectric fluid (POA 6) is circulated via a heat exchanger that is connected to the chilled water supply and return line of the facility. In addition, three thermocouples are used to determine

the temperature of the fluid prior to reaching the heat sink. Fluid flowrate control is accomplished by the manipulation of power provided to the inlet pump, while the measurement of the flowrate is performed with microflow sensors. The Keyence FDX-A1 is a device that is extensively used across several sectors due to its sophisticated features and capabilities. The process of measuring the temperature of the incoming fluid (referred to as Tinlet) and the outgoing fluid (referred to as Toutlet) is carried out using 10k thermistors, which have an accuracy of ±2°C. Furthermore, the Keyence GPM010 pressure sensors are used for the purpose of detecting the pressure at both the intake and outflow of the tank.To get the experimental data, it is important to perform sensor calibration and establish a link with the data acquisition system, namely the DAQ Agilent 37940A. The server board consists of a thermal test vehicle (TTV) equipped with a 2U heat sink. However, the DIMMS were extracted, and foams were used to guide the optimal flow through the heat sink, as seen in Figure 5.2. The TTV device may be classified as a CPU simulator owing to its capacity to generate a comparable amount of thermal energy, achieved via the use of an external direct current (DC) power supply.

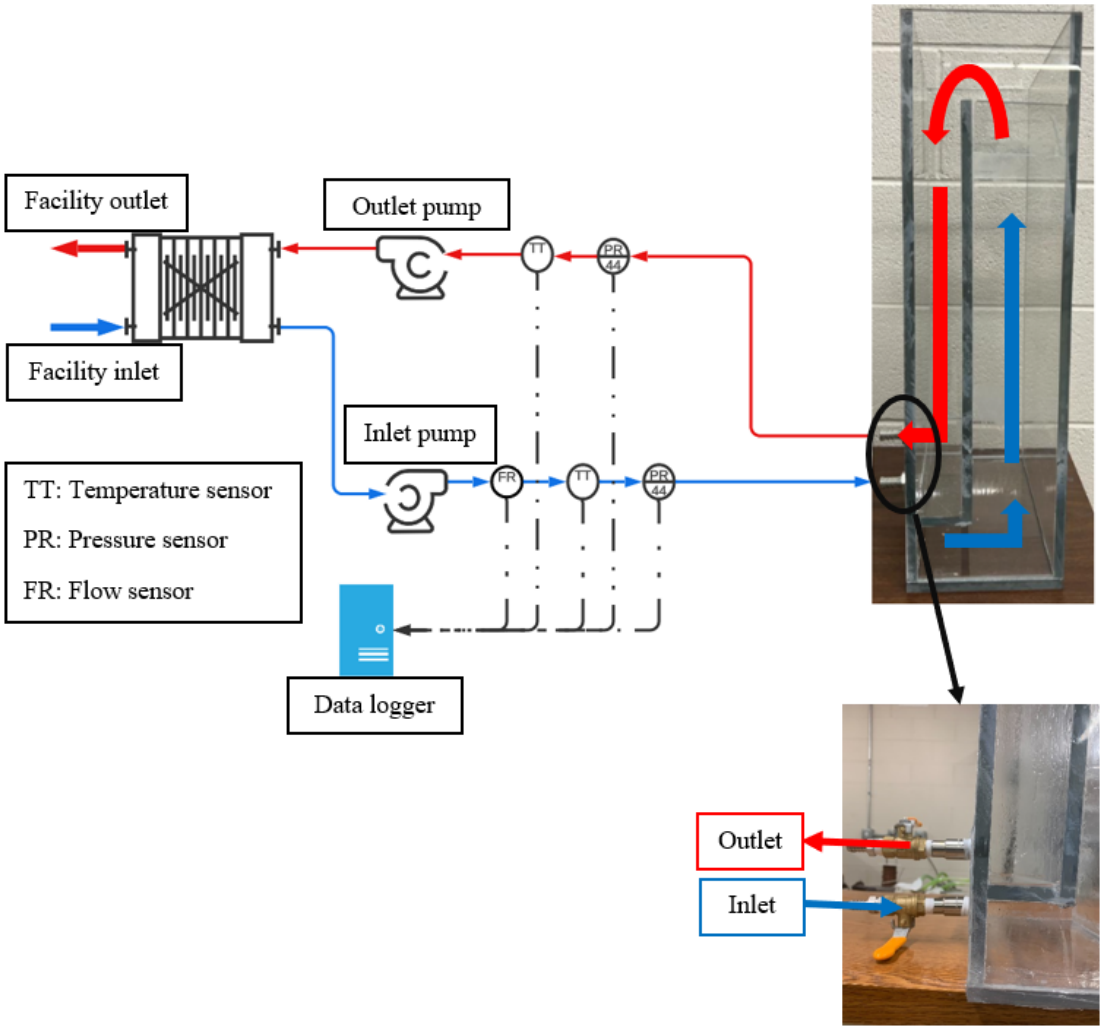

Figure 5.1: Schematic diagram of the experimental setup

In order to conduct the flow visualization, a linear imaging setup was used, as seen in figure 5.3 (a) and (b), whereby four cameras were strategically positioned in front of the tank. Four Imager CX 12 cameras with a resolution of 14080 × 2984 pixels and the capacity to record at a rate of 61 frames per second was used to capture the dispersed light from the lighted seeding particles. Each pulse was captured on distinct frames. The temporal duration between consecutive laser pulses was adjusted in order to ensure that the distance covered by the particles being tracked between photographs is distinguishable, while also preventing the particles from exiting the lighted plane during this time period. The camera captured picture pairs at a frequency of 15 Hz. The picture pairs were partitioned into distinct interrogation zones, and a cross-correlation approach was used to ascertain the movement of the particles

inside each respective interrogation area. The dimensions of the interrogation zones were established at 64 x 64 pixels. The experimental configuration incorporates a Quantel evergreen dual pulsed Nd:YaG laser, characterized by a pulse rate of 15 Hz and a single power source. The laser is equipped with a pair of lenses in order to transform the original laser sheet (2D) into a volumetric laser sheet (3D). Particle Image Velocimetry (PIV) was used as a methodology to generate velocity vector fields near the outlet of the heat sink. The study used red polyethylene microparticles with a size range of 40-47 μm and a density of 995 kg/m3, as seen in Figure 5.4 (a). The colloidal solution of PAO 6 and red polyethylene microparticles was prepared using an ultrasonic sonicator, as seen in Figure 5.4 (b). Subsequently, the colloidal solution was introduced into the tank, and first photos were captured to assess the particle density inside the tank. A comprehensive explanation of the study of experimental uncertainty may be found in section 2.2.

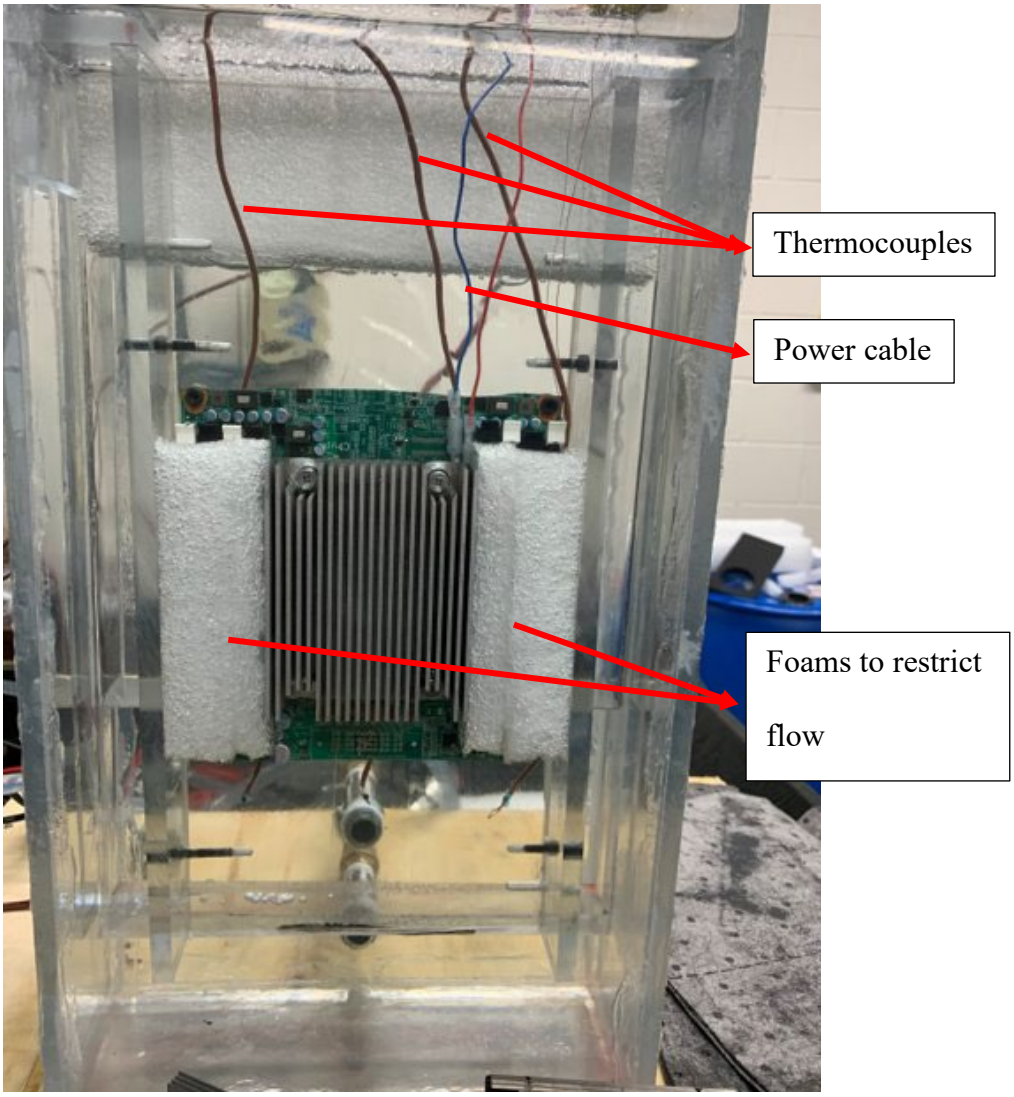

Figure 5.2: Immersion tank setup for PIV study

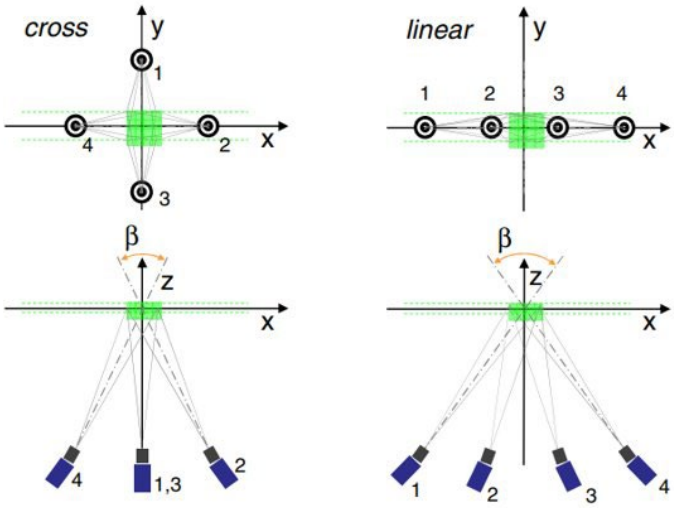

(a)

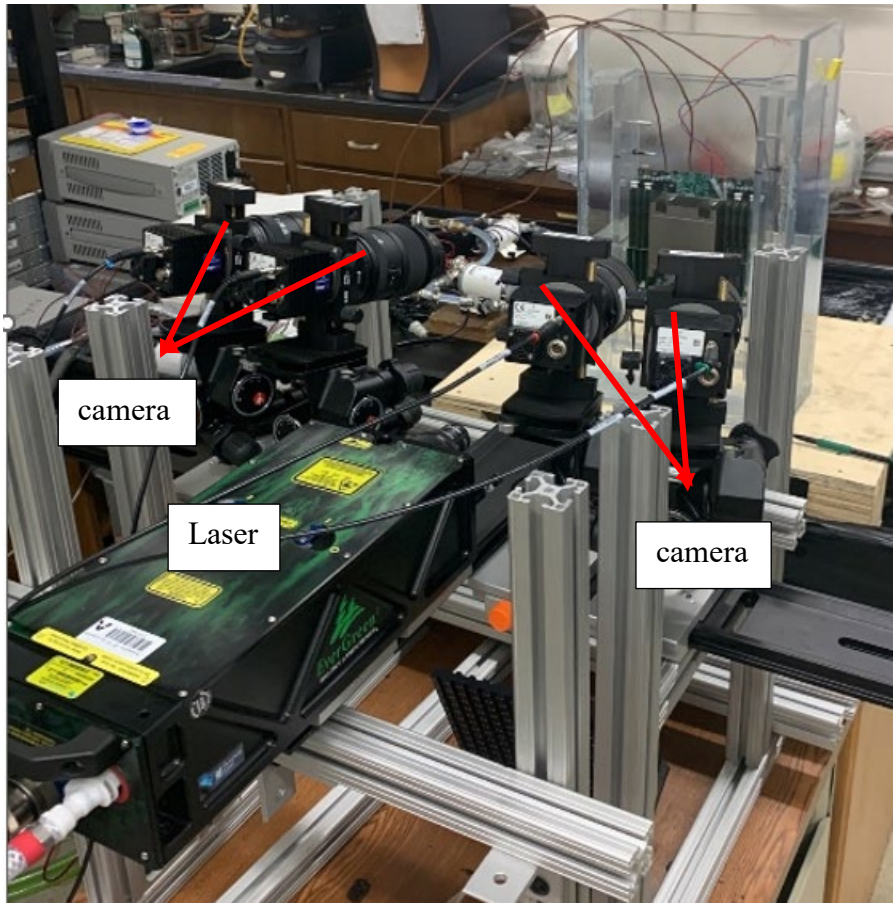

(b)

Figure 5.3: (a) Cross-like and linear imaging configurations [11], (b) experimental setup of PIV in linear imaging configuration

(a) **(b)**

Figure 5.4: (a) Seeding or Tracer particles, (b) Ultrasonic sonicator

5.3 Numerical setup

The TTV and tank model were constructed in the ANSYS Icepak software, as seen in Figure 5.6. The modeling approach included essential factors pertaining to heat transfer phenomena, such as the central processing unit (CPU), heat sinks, and the use of foams as replacements for DIMMs in order to enhance the efficiency of heat transmission via the heat sink. The thermal stack of the central processing unit (CPU) comprises a planar heat source embedded inside a heater made of Aluminum nitride, with a thickness of three millimeters. A thermal interface material (TIM) consisting of Indium, with a thickness of 0.2 mm, is situated between the heat sink and heater. The thermal interface material (TIM) has a thermal conductivity coefficient of 8 W/m-K. The heat sink has dimensions of 85mm x 110mm x 41mm, with a heatsink base of 5mm. The heat sink has a collective of 35 fins, each possessing a thickness of 0.3mm and a height of 36mm. The property of PAO6 is shown in Table 2.2,

while the boundary conditions for both the experiment and the computational fluid dynamics (CFD) study are provided in Table 2.3. The governing equations are comprehensively described in section 2.4. The grid independence analysis is shown in Figure 5.5, and in present study 6.55 million elements were used. While the validation of the computational fluid dynamics (CFD) model was conducted by comparing it with experimental data obtained at various flow rates, as seen in Figure 2.4. There is a discrepancy of 2% between the computational fluid dynamics (CFD) findings and the experimental results of the heat sink with heat pipe across all flow rates.

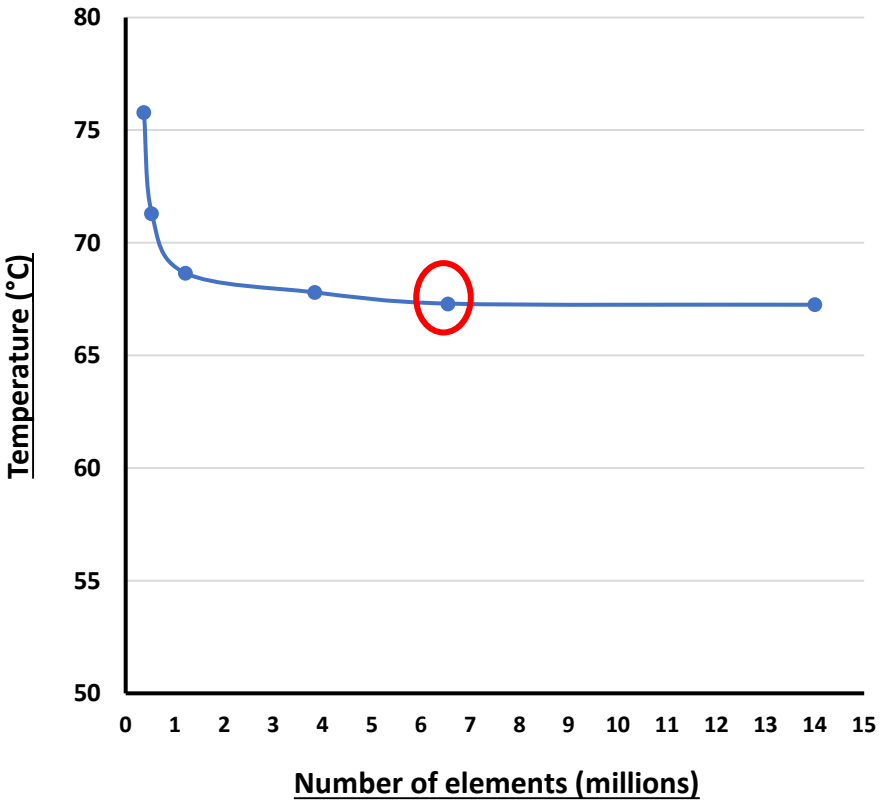

Figure 5.5: Grid independence study

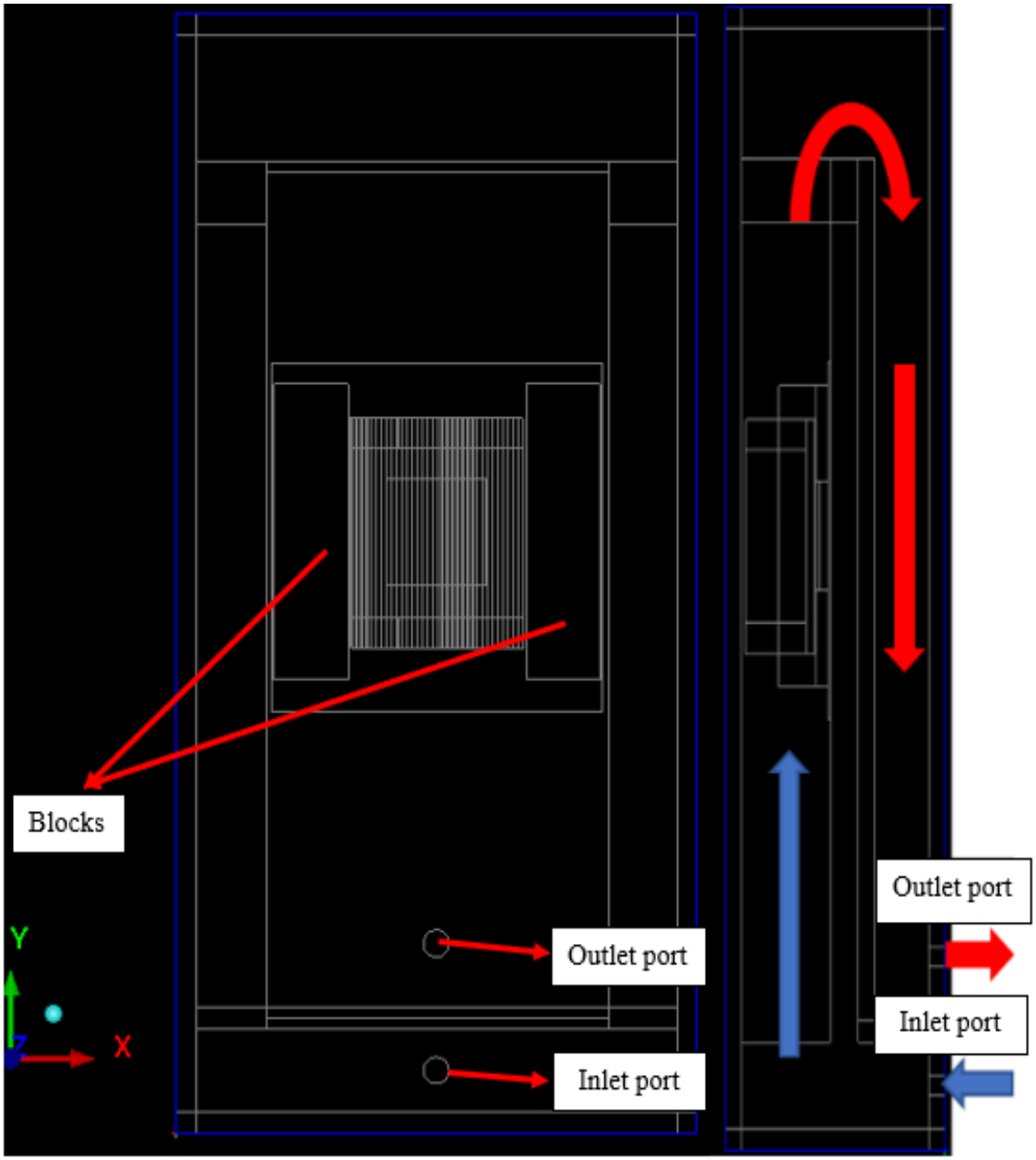

Figure 5.6: 2U immersion tank model in ANSYS Icepak

5.4 Results

The velocity contours obtained using Particle Image Velocimetry (PIV) and ANSYS Icepak are shown in Figure 5.7 and Figure 5.8, respectively. As anticipated, the fluid's velocity reaches its maximum towards the center of the heat sink owing to the presence of convection currents. In contrast to the computational fluid dynamics (CFD) models, the experimental particle image velocimetry (PIV) findings show a comparable trend, although with the presence

of additional particle recirculation caused by the non-uniform surface characteristics of the foams. The presence of completely symmetrical velocity contours may be attributed to the unaccounted effects of barriers in computational fluid dynamics (CFD), as seen in Figure 5.8. The discrepancy in velocity values obtained using Particle Image Velocimetry (PIV) and Computational Fluid Dynamics (CFD) is around 6%.

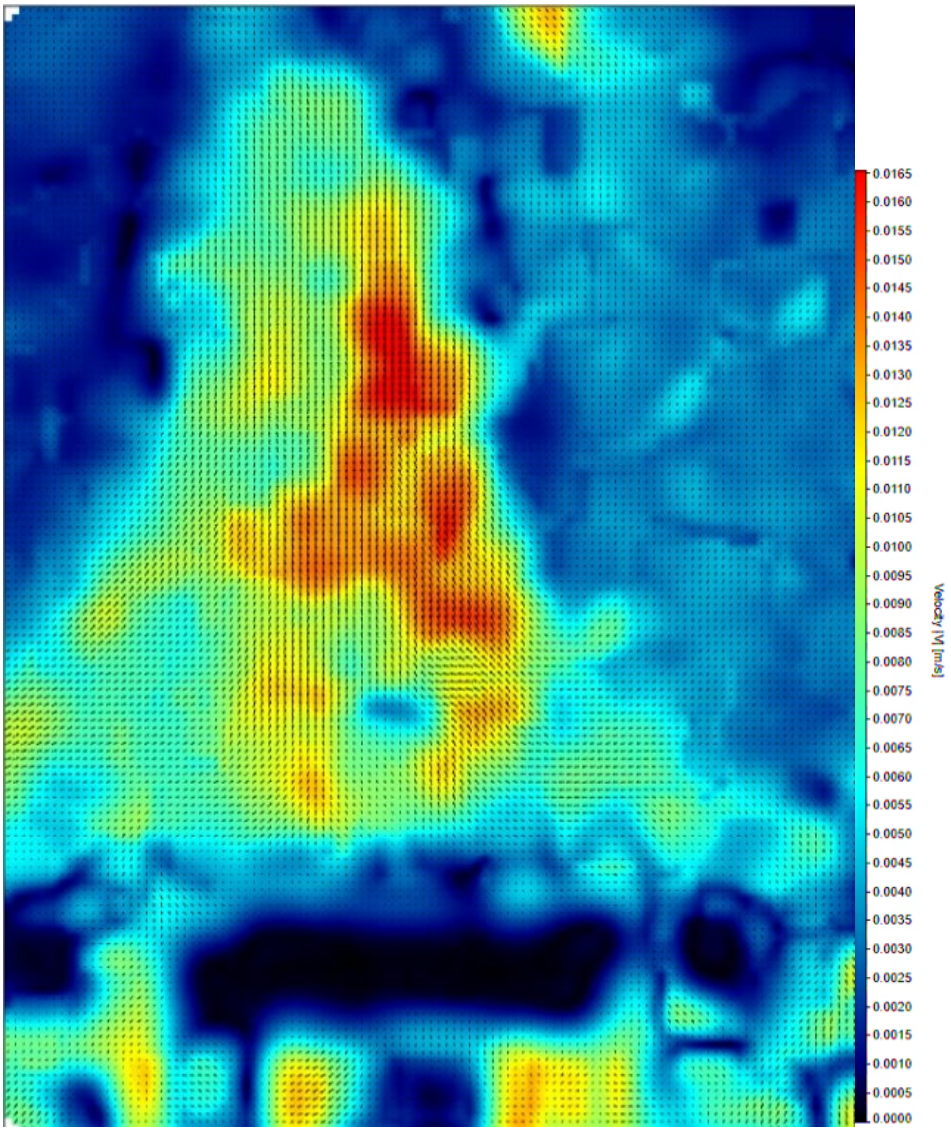

Figure 5.7: Velocity contours from PIV

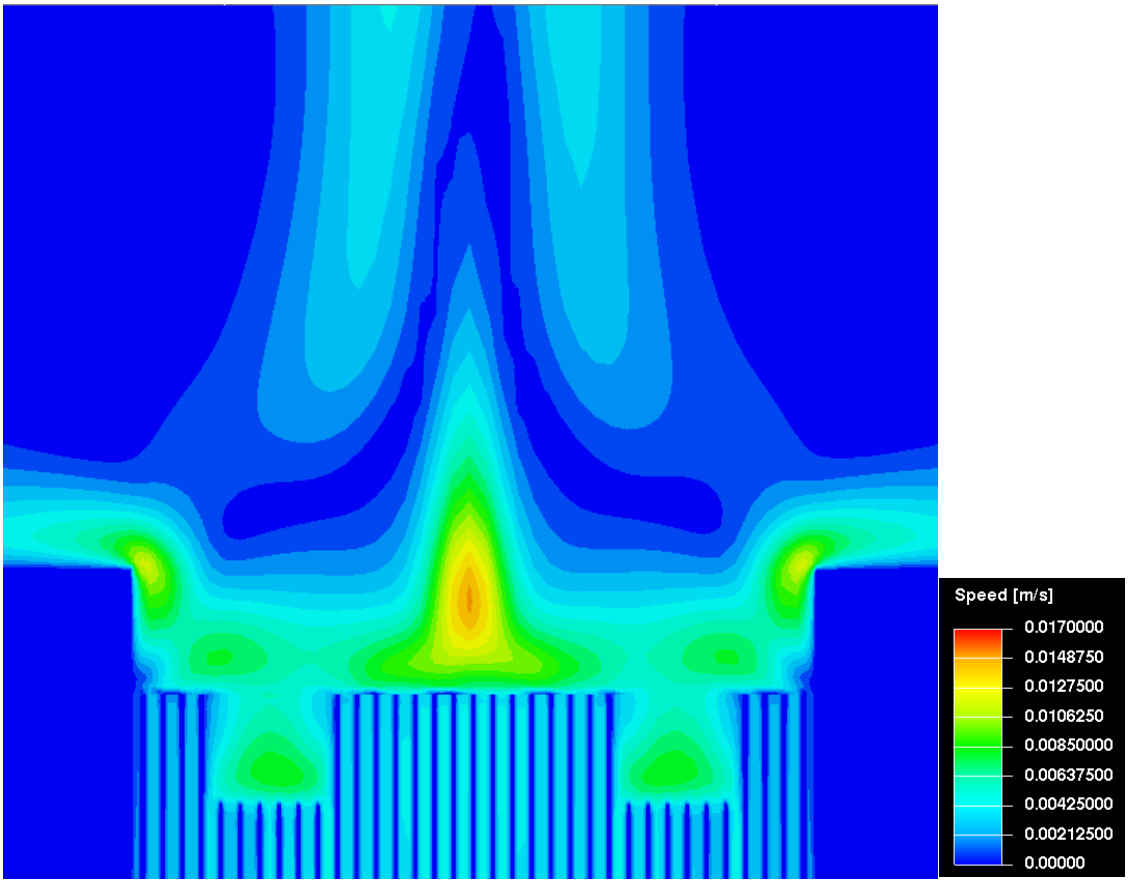

Figure 5.8: Velocity contours from ANSYS Icepak

The occurrence of fluid recirculation is clearly evident in both the empirical data and the simulated numerical model, as seen in Figures 5.9 and 5.10. In this dynamic representation, a discernible pattern arises in which fluid particles coming from both the right and left ends of the heat sink experience a notable process of convergence towards the center point of the heat sink. Exploring the particulars, the convergence of fluid particles is a direct result of the intense convection currents that are generated inside the system. The fluid acquires directional velocity as a result of the complex interaction of heat transfer processes, giving rise to these currents. As a result, fluid particles located on both sides of the heat sink exhibit this momentum, which drives them towards the central nexus of the heat sink.

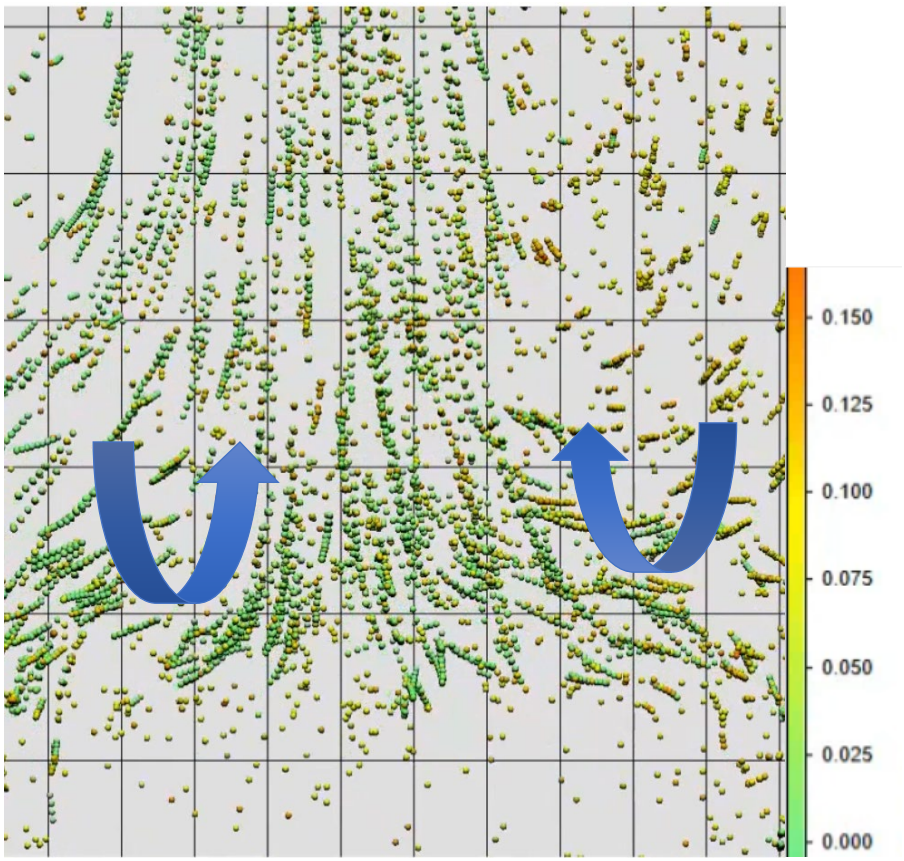

Figure 5.9: Particle movement using PIV

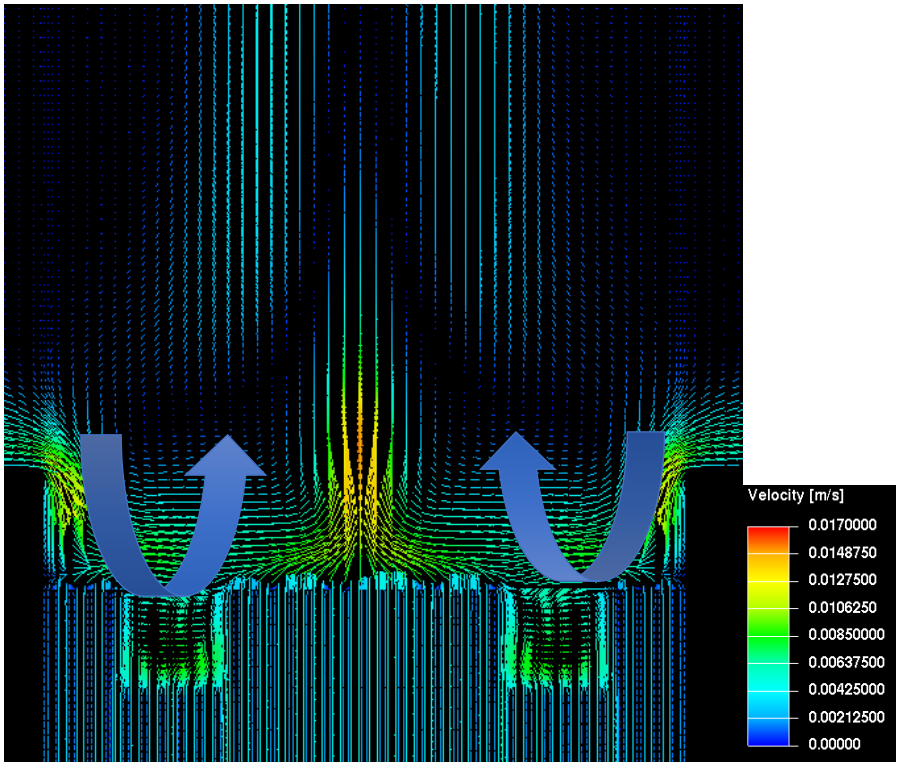

Figure 5.10: Recirculation movement by ANSYS Icepak

5.5 Conclusion

The investigation of velocity distributions using Particle Image Velocimetry (PIV) and ANSYS Icepak, has yielded noteworthy observations about the fluid dynamics in the vicinity of the heat sink. As expected, the fluid reaches its maximum velocity in the central region of the heat sink due to the dominant convection currents generated by the heat transfer mechanism. Nevertheless, notable discrepancies arise when comparing the computational fluid dynamics (CFD) models with the empirical particle image velocimetry (PIV) findings. The PIV results provide a consistent pattern that aligns with the CFD models. However, the non-uniform surface properties of the foams reveal the existence of extra particle recirculation. Furthermore, the presence of completely symmetrical velocity contours seen in the computational fluid dynamics (CFD) simulations, might perhaps be attributed to the omission of barrier effects. The observed difference of about 6% in velocity magnitudes derived from Particle Image Velocimetry (PIV) and Computational Fluid Dynamics (CFD). Moreover, the occurrence of fluid recirculation is quite notable in both empirical data and computational models. The presented dynamic model demonstrates a discernible pattern in which fluid particles coming from opposing extremities of the heat sink have a noticeable inclination to converge towards the centre point of the heat sink. The convergence seen in this phenomenon may be attributed to the significant impact of convection currents present within the system. These currents result in the fluid acquiring directional momentum as a result of the complex interactions involved in heat transfer dynamics.

5.6 References

[1] Smith. A., Bhavnani, S., and Knight, R., Flow Visualization of Turbulent Jet Impingement with Engineered Surface Modifications through Particle Image Velocimetry, 10.1109/iTherm54085.2022.9899608.

[2] Intel, 2015, “Intel 14 nm Technology,” Intel, Santa Clara, CA, accessed on Oct. 15, 2015,http://www.intel.com/content/www/us/en/silicon-innovations/intel14nm-technology.html

[3] Bar-Cohen, A., 2013, “Needs and Future Trends for Enhanced Phase Change Heat Transfer-DARPA,” International Workshop on Micro- and Nanostructures for Phase Change Heat Transfer, Dedham, MA, Apr. 22–23.

[4] Nakayama, W., 2014, “Heat in Computers: Applied Heat Transfer in Information Technology,” ASME J. Heat Transfer, 136(1), p. 013001.

[5] Suszko, A., 2015, “Enhancement of Nucleate Boiling on Rough and Dimpled Surfaces With Application to Composite Spreaders for Microprocessors Immersion Cooling,” Ph.D. dissertation, Department of Mechanical Engineering, University of New Mexico, Albuquerque, NM.

[6] Alkharabsheh, S., Fernandes, J., Gebrehiwot, B., Agonafer, D., Ghose, K., Ortega, A., Joshi, Y., and Sammakia, B., 2015, “A Brief Overview of Recent Developments in Thermal Management in Data Centers,” ASME J. Electron. Packag., 137(4), p. 040801.

[7] Arghode, V. K., and Joshi, Y., 2015, “Measurement of Air Flow Rate Sensitivity to the Differential Pressure Across a Server Rack in a Data Center,” ASME J. Electron. Packag., 137(4), p. 041002.

[8] Arghode, V. K., Kumar, P., Joshi, Y., Weiss, T., and Meyer, G., 2013, “Rack Level Modeling of Air Flow Through Perforated Tile in a Data Center,” ASME J. Electron. Packag., 135(3), p. 030902

[9] Gess, J., Bhavnani, S., and Wayne Johnson, R. (October 20, 2016). "Single- and Two-Phase Particle Image Velocimetry Characterization of Fluid Flow Within a Liquid Immersion Cooled Electronics Module." ASME. J. Electron. Packag. December 2016; 138(4): 041007. https://doi.org/10.1115/1.4034854

[10] Sathe, M. J., Thaker, I. J., Strand, T. E., and Joshi, J. B., 2010, "Advanced PIV/ LIF and Shadowgraphy System to Visualize Flow Structure in Two-Phase Bubbly Flows," Chem. Eng. Sci., 65(8), pp. 2431–2442.

[11] Tomographic PIV: principles and practice, DOI 10.1088/0957-0233/24/1/012001